

#### 4. THERMAL EVALUATION

The development of the thermal analysis of the Advanced NUHOMS® System involved consideration of several limiting decay heat loads for individual components as summarized below:

- A maximum decay heat load of 24 kW was used for the evaluation of AHSM (concrete and support steel) and 24PT1-DSC shell assembly.
- A maximum decay heat load of 14 kW and 16 kW was used for the evaluation of 24PT1-DSC basket assembly and fuel cladding.

The maximum design decay heat load for the 24PT1-DSC is 14 kW when loaded with all SC fuel assemblies and 13.706 kW when loaded with MOX fuel assemblies. The use of 24 kW and 16 kW for the scenarios discussed in this section adds margin to the 14 kW design basis thermal analyses.

## 4.1 Discussion

### 4.1.1 Overview and Purpose of Thermal Analysis

The Advanced NUHOMS® System is designed to passively reject decay heat under normal and off-normal conditions of storage, accident and loading/unloading conditions while maintaining canister temperatures and pressures within specified limits. The Advanced NUHOMS® System components considered in the thermal analysis are the concrete module (AHSM), canister (24PT1-DSC), and transfer cask.

The Advanced NUHOMS® System falls under the jurisdiction of 10CFR Part 72 when used as a component of an ISFSI. To establish the heat removal capability, several thermal design criteria are established for the Advanced NUHOMS® System. These are:

- Pressures within the 24PT1-DSC cavity are within design values considered for structural and confinement analyses.
- Maximum and minimum temperatures of the confinement structural components must not adversely affect the confinement function.
- Maintaining fuel cladding integrity during storage is a key design consideration. To minimize degradation that can occur over the storage duration, the maximum initial storage fuel cladding temperature is determined as a function of the initial fuel age using the guidelines provided by the Pacific Northwest Laboratory [4.1] for Zircalloy clad fuel and EPRI for stainless steel clad fuel [4.2]. These temperature limits are derived and reported in Section 3.5. For short term events and accident conditions, the fuel temperature limits are also derived and reported in Section 3.5.
- Thermal stresses for the AHSM, 24PT1-DSC, and transfer cask, when appropriately combined with other loads, will be maintained at acceptable levels to ensure the confinement integrity of the Advanced NUHOMS® System (see Chapters 3 and 11).

Chapter 2 presents the principal design bases for the Advanced NUHOMS® System.

The AHSMs are designed to passively cool the 24PT1-DSC primarily by buoyancy driven air flow through an opening in the base of the module, which allows ambient air to be drawn into the AHSM to cool the canister. The hot air exits through a vent in the top shield block, creating a stack effect. The AHSM is also cooled from the top and front surfaces by convection and radiation to the prevailing ambient environment.

Within the canister, the internal basket assembly contains spacer discs, support rods, and guidesleeve assemblies. The guidesleeve assembly consists of a stainless steel guidesleeve and a Boral™ poison sheet(s) held in place by a thin oversleeve. Heat transfer through the basket structure in the radial direction is achieved by conduction and radiation through the guidesleeve assemblies, spacer disc plates, and the helium cover gas. Heat transfer in the axial direction is conservatively neglected in the analysis model.

#### 4.1.2 Thermal Load Specification/Ambient Temperature

The ambient temperature ranges considered in the thermal analyses are given in Table 4.1-1. The canister and AHSM temperature response to changes in ambient conditions will be relatively slow because the AHSM thermal inertia is large. Therefore, daily average temperatures are derived to bound summer ambient conditions. For the summer ambient conditions, temperature averages are derived based on data from Reference [4.3] with the maximum temperatures from Table 4.1-1. Reference [4.3] provides factors for calculating the ambient temperature for each hour of the day based on the hottest temperature and the mean daily temperature range. The factors, together with the calculated temperatures, are given in Table 4.1-2. Conservative mean daily temperatures ranges from Reference [4.3], 20°F and 27°F temperature difference, are used for normal and off-normal conditions respectively.

For conservatism, maximum daily average ambient temperatures of 97°F and 107°F are used for thermal evaluations for normal and off-normal summer extreme ambient conditions respectively (these values bound the average temperatures calculated in Table 4.1-2). To be conservative, no averaging is done for winter extreme ambient conditions.

In general, all the thermal criteria are based on maximum temperature limits. The structural adequacy of pertinent materials at the minimum off-normal ambient temperature is addressed in Chapter 3.

The AHSM is analyzed based on a maximum heat load of 24 kW from 24 fuel assemblies with RCCAs, neutron sources, or TPAs. The 24PT1-DSC is analyzed based on a maximum heat load of 14 kW from 24 fuel assemblies with RCCAs, neutron sources, or TPAs. A peaking factor for a typical PWR fuel assembly of 1.08 based on Reference [4.4] is used in the analyses. The parameters of the fuel assembly types are given in Chapter 6. A description of the detailed analyses performed for normal conditions is provided in Section 4.4, off-normal conditions in Section 4.5, accident conditions in Section 4.6, and loading/unloading conditions in Section 4.7. A summary of the results from the analyses performed for normal, off-normal, and accident conditions, as well as maximum and minimum allowable temperatures, is provided in Table 4.1-3, Table 4.1-4, and Table 4.1-5. The thermal evaluation concludes that with these heat loads, all design criteria are satisfied for normal, off-normal, and accident conditions. The limiting heat loads used in the analysis for each component are tabulated in Table 4.1-6.

The fuel assembly type considered in the thermal analyses is given in Chapter 2.

The OS197 transfer cask was previously licensed for 24 kW [4.17], which bounds the 14 kW heat load for the 24PT1-DSC being licensed in this application. Results are therefore not repeated here for the OS197 transfer cask.

*Sections 4.8.2 and 4.8.3 address the validation of thermal analysis methodology using HEATING7 model of the 24PT1-DSC against actual test data. Section 4.8.4 provides an alternative confirmatory thermal analysis of the 24PT1-DSC.*

**Table 4.1-1**  
**Ambient Temperatures and Insolations Considered in Thermal Analysis**

|                   | Temperature<br>(°F) | Insolation<br>(Btu/hr/ft <sup>2</sup> ) |
|-------------------|---------------------|---|
| Normal            | 0 to 104°F          | 0 to 123                                |
| Long Term Average | 70°F                | 123                                     |
| Off-Normal        | -40 to 117°F        | 0 to 123                                |
| Accident          | -40 to 117°F        | 0 to 123                                |
| Fuel Building     | 50 to 120°F         | 0                                       |

**Table 4.1-2**  
**Temperature Variation for Extreme Summer Ambient Conditions**

| Time, Hour | % Daily Range <sup>(1)</sup> | Normal<br>(°F) | Off-Normal<br>(°F) |
|------------|------------------------------|----------------|--------------------|
| 1          | 87                           | 86.6           | 93.5               |
| 2          | 92                           | 85.6           | 92.2               |
| 3          | 96                           | 84.8           | 91.1               |
| 4          | 99                           | 84.2           | 90.3               |
| 5          | 100                          | 84.0           | 90.0               |
| 6          | 98                           | 84.4           | 90.5               |
| 7          | 93                           | 85.4           | 91.9               |
| 8          | 84                           | 87.2           | 94.3               |
| 9          | 71                           | 89.8           | 97.8               |
| 10         | 56                           | 92.8           | 101.9              |
| 11         | 39                           | 96.2           | 106.5              |
| 12         | 23                           | 99.4           | 110.8              |
| 13         | 11                           | 101.8          | 114.0              |
| 14         | 3                            | 103.4          | 116.2              |
| 15         | 0                            | 104.0          | 117.0              |
| 16         | 3                            | 103.4          | 116.2              |
| 17         | 10                           | 102.0          | 114.3              |
| 18         | 21                           | 99.8           | 111.3              |
| 19         | 34                           | 97.2           | 107.8              |
| 20         | 47                           | 94.6           | 104.3              |
| 21         | 58                           | 92.4           | 101.3              |
| 22         | 68                           | 90.4           | 98.6               |
| 23         | 76                           | 88.8           | 96.5               |
| 24         | 82                           | 87.6           | 94.9               |
| Averages   |                              | 92.7           | 101.8              |

- (1) Percentage of daily temperature range (see Section 4.1.2 for daily temperature range used for normal and off-normal conditions) below the maximum temperature at a given hour during the day, Reference [4.3], Chapter 26, Table 3.

**Table 4.1-3**  
**Component Minimum and Maximum Temperatures in the Advanced NUHOMS® System**  
**(Storage or Transfer Mode) for Normal Conditions**

| Component <sup>(3)</sup>           |                                     | Maximum<br>Storage<br>Mode (F°) | Maximum <sup>(1)</sup><br>Transfer<br>Mode (F°) | Minimum <sup>(2)</sup><br>(°F) | Allowable Range (°F)<br>Ref   |
|------------------------------------|-------------------------------------|---------------------------------|---|--------------------------------|---|
| AHSM Concrete                      |                                     | 219                             | N/A   | 0                              | 0 to 300 [4.5]  |
| AHSM Support Steel                 |                                     | 351                             | N/A   | 0                              | 0 to 2,600 [4.6]  |
| AHSM Heat Shield                   |                                     | 258                             | N/A   | 0                              | 0 to 2,600 [4.6]  |
| DSC Shell                          |                                     | 399                             | 439   | 0                              | 0 to 800 [4.7]  |
| DSC Top Outer Cover Plate          |                                     | 294                             | 337   | 0                              | 0 to 800 [4.7]  |
| DSC Top Inner Cover Plate          |                                     | 296                             | 337   | 0                              | 0 to 800 [4.7]  |
| DSC Top Shield Plug                |                                     | 316                             | 345   | 0                              | 0 to 700 [4.7]  |
| DSC Bottom Inner Cover Plate       |                                     | 315                             | 402   | 0                              | 0 to 800 [4.7]  |
| DSC Bottom Shield Plug             |                                     | 313                             | 400   | 0                              | 0 to 700 [4.7]  |
| DSC Bottom Outer Cover Plate       |                                     | 299                             | 393   | 0                              | 0 to 800 [4.7]  |
| DSC Spacer Disc                    |                                     | 617                             | 658   | 0                              | 0 to 700 [4.7]  |
| DSC Guidesleeve                    |                                     | 618                             | 658   | 0                              | 0 to 800 [4.7]  |
| DSC Oversleeve                     |                                     | 618                             | 658   | 0                              | 0 to 800 [4.7]  |
| DSC Support Rod/Spacer Sleeve      |                                     | 479                             | 522   | 0                              | 0 to 650 [4.7]  |
| DSC Boral™ Sheet                   |                                     | 618                             | 658   | 0                              | 0 to 850 [4.8]  |
| WE 14x14<br>SS304 Fuel<br>Cladding | 70°F long term<br>average ambient   | 604                             | 658   | 0                              | 0 to 806 <sup>(4)</sup><br>Transfer Mode<br>0 to 690<br>Storage Mode  |
|                                    | 104°F short term<br>maximum ambient | 618                             | 658   | 0                              | 0 to 806 <sup>(4)</sup>   |
| WE 14x14<br>MOX Zirc<br>Cladding   | 70°F long term<br>average ambient   | 604                             | 658   | 0                              | 0 to 1058 <sup>(4)</sup><br>Transfer Mode<br>0 to 618<br>Storage Mode |
|                                    | 104°F short term<br>maximum ambient | 618                             | 658   | 0                              | 0 to 1058 <sup>(4)</sup>  |

- (1) Temperatures provided are conservatively based on a 14 kW DSC heat load in conjunction with a DSC shell temperature based on a 24 kW transfer cask analysis.
- (2) For the minimum daily averaged temperature condition of 0°F ambient, the resulting component temperatures will approach 0°F if no credit is taken for the decay heat load.
- (3) See Table 4 1-6 for the limiting heat loads for which each component was analyzed. Maximum 24PT1-DSC heat load for this application is 14 kW. Other heat loads used in the analyses provide conservatism and may be used in future amendments. The maximum AHSM heat load for this application is 24kW.
- (4) These fuel cladding limits apply to the short term transients such as the transfer operations and 104 °F temp. transient

**Table 4.1-4**  
**Component Minimum and Maximum Temperatures in the Advanced NUHOMS® System**  
**(Storage or Transfer Mode) for Off-Normal Conditions**

| Component <sup>(4)</sup>      | Maximum <sup>(5)</sup><br>(°F) | Minimum <sup>(3)</sup><br>(°F) | Allowable Range<br>(°F) Ref |
|-------------------------------|--------------------------------|--------------------------------|-----------------------------|
| AHSM Concrete                 | 231                            | -40                            | -40 to 300 [4.5]            |
| AHSM Support Steel            | 360                            | -40                            | -40 to 2,600 [4.6]          |
| AHSM Heat Shield              | 270                            | -40                            | -40 to 2,600 [4.6]          |
| DSC Shell                     | 443                            | -40                            | -40 to 800 [4.7]            |
| DSC Top Outer Cover Plate     | 350                            | -40                            | -40 to 800 [4.7]            |
| DSC Top Inner Cover Plate     | 350                            | -40                            | -40 to 800 [4.7]            |
| DSC Top Shield Plug           | 358                            | -40                            | -40 to 700 [4.7]            |
| DSC Bottom Inner Cover Plate  | 408                            | -40                            | -40 to 800 [4.7]            |
| DSC Bottom Shield Plug        | 406                            | -40                            | -40 to 700 [4.7]            |
| DSC Bottom Outer Cover Plate  | 400                            | -40                            | -40 to 800 [4.7]            |
| DSC Spacer Disc               | 658 <sup>(2)</sup>             | -40                            | -40 to 700 [4.7]            |
| DSC Guidesleeve               | 658 <sup>(2)</sup>             | -40                            | -40 to 800 [4.7]            |
| DSC Oversleeve                | 658 <sup>(2)</sup>             | -40                            | -40 to 800 [4.7]            |
| DSC Support Rod/Spacer Sleeve | 522 <sup>(2)</sup>             | -40                            | -40 to 650 [4.7]            |
| DSC Boral™ Sheet              | 658 <sup>(2)</sup>             | -40                            | -40 to 1000 [4.8]           |
| WE 14x14 SS304 Fuel Cladding  | 658 <sup>(2)</sup>             | -40                            | -40 to 806 <sup>(1)</sup>   |
| WE 14x14 MOX Zirc Cladding    | 658 <sup>(2)</sup>             | -40                            | -40 to 1058 <sup>(1)</sup>  |

(1) The derivation of the fuel cladding temperature limits is given in Section 3.5

(2) The maximum 24PT1-DSC basket temperatures are bounded by the maximum normal case in the cask because of the required sunshade over the cask in the off-normal temperature range.

(3) For the minimum daily averaged temperature condition of -40°F ambient, the resulting component temperatures will approach -40°F if no credit is taken for the decay heat load.

(4) See Table 4.1-6 for the limiting heat loads for which each component was analyzed. Maximum 24PT1-DSC heat load for this application is 14 kW. Other heat loads used in the analyses provide conservatism and may be used in future amendments. The maximum AHSM heat load for this application is 24kW.

(5) Maximum off-normal temperature is during the transfer mode.

**Table 4.1-5**  
**Component Minimum and Maximum Temperatures in the Advanced NUHOMS® System**  
**(Storage and Transfer) for Accident Conditions**

| Component <sup>(4)</sup>      | Maximum <sup>(5)</sup><br>(°F) | Minimum <sup>(3)</sup><br>(°F) | Allowable Range<br>(°F) Ref |
|-------------------------------|--------------------------------|--------------------------------|-----------------------------|
| AHSM Concrete                 | 392 <sup>(2)</sup>             | -40                            | -40 to 350 [4.5]            |
| AHSM Support Steel            | 615                            | -40                            | -40 to 2,600 [4.6]          |
| AHSM Heat Shield              | 542                            | -40                            | -40 to 2,600 [4.6]          |
| DSC Shell                     | 646                            | -40                            | -40 to 800 [4.7]            |
| DSC Top Outer Cover Plate     | 423                            | -40                            | -40 to 800 [4.7]            |
| DSC Top Inner Cover Plate     | 424                            | -40                            | -40 to 800 [4.7]            |
| DSC Top Shield Plug           | 444                            | -40                            | -40 to 700 [4.7]            |
| DSC Bottom Inner Cover Plate  | 450                            | -40                            | -40 to 800 [4.7]            |
| DSC Bottom Shield Plug        | 448                            | -40                            | -40 to 700 [4.7]            |
| DSC Bottom Outer Cover Plate  | 434                            | -40                            | -40 to 800 [4.7]            |
| DSC Spacer Disc               | 695                            | -40                            | -40 to 700 [4.7]            |
| DSC Guidesleeve               | 696                            | -40                            | -40 to 800 [4.7]            |
| DSC Oversleeve                | 696                            | -40                            | -40 to 800 [4.7]            |
| DSC Boral™ Sheet              | 696                            | -40                            | -40 to 1000 [4.8]           |
| DSC Support Rod/Spacer Sleeve | 588                            | -40                            | -40 to 650 [4.7]            |
| WE 14x14 SS304 Fuel Cladding  | 749 <sup>(6)</sup>             | -40                            | -40 to 806 <sup>(1)</sup>   |
| WE 14x14 MOX Zirc Cladding    | 749 <sup>(6)</sup>             | -40                            | -40 to 1058 <sup>(1)</sup>  |

- (1) The derivation of the fuel cladding temperature limits is given in Section 3.5
- (2) 392°F is above the 350°F limit given in Reference [4.5] - Testing will be performed to document that concrete compressive strength will be greater than that assumed in structural analyses and that the concrete did not degrade (does not show signs of spalling, cracks and/or loss of cement bond to aggregate) due to the elevated temperature
- (3) For the minimum daily averaged temperature condition of -40°F ambient, the resulting component temperatures will approach -40°F if no credit is taken for the decay heat load
- (4) See Table 4.1-6 for the limiting heat loads for which *each component was analyzed*. Maximum 24PT1-DSC heat load for this application is 14 kW. Other heat loads used in *the analyses* provide conservatism and may be used in future amendments. The maximum AHSM heat load for this application is 24kW.
- (5) The maximum accident temperature is during a storage mode blocked vent condition.
- (6) Fuel clad temperature based on 16kW heat load while DSC basket temperatures are based on 14kW heat load



**Table 4.1-6**  
**Limiting Canister Heat Loads for DSC Components**

| Component                     | Normal<br>0 – 104 °F Ambient<br>0 – 72.6 Btu/hr/ft <sup>2</sup><br>solar | Off-Normal<br>-40 – 117 °F<br>Ambient<br>0 – 123 Btu/hr/ft <sup>2</sup><br>solar | Accident<br>-40 – 117 °F<br>Ambient<br>0 – 123 Btu/hr/ft <sup>2</sup><br>solar |
|-------------------------------|--|--|--|
| AHSM Concrete                 | 24 kW  | 24 kW  | 24 kW  |
| AHSM Support Steel            | 24 kW  | 24 kW  | 24 kW  |
| AHSM Heat Shield              | 24 kW  | 24 kW  | 24 kW  |
| DSC Shell                     | 24 kW  | 24 kW  | 16 <sup>(2)</sup> kW   |
| DSC Top Outer Cover Plate     | 24 kW  | 24 kW  | 24 kW  |
| DSC Top Inner Cover Plate     | 24 kW  | 24 kW  | 24 kW  |
| DSC Top Shield Plug           | 24 kW  | 24 kW  | 24 kW  |
| DSC Bottom Inner Cover Plate  | 24 kW  | 24 kW  | 24 kW  |
| DSC Bottom Shield Plug        | 24 kW  | 24 kW  | 24 kW  |
| DSC Bottom Outer Cover Plate  | 24 kW  | 24 kW  | 24 kW  |
| DSC Spacer Disc               | 14 kW <sup>(1)</sup>   | 16 kW  | 14 kW <sup>(2) (3)</sup>   |
| DSC Guidesleeve               | 16 kW  | 16 kW  | 14 kW <sup>(2)</sup>   |
| DSC Oversleeve                | 16 kW  | 16 kW  | 14 kW <sup>(2)</sup>   |
| DSC Boral™ Sheet              | 16 kW  | 16 kW  | 14 kW <sup>(2)</sup>   |
| DSC Support Rod/Spacer Sleeve | 16 kW  | 16 kW  | 14 kW <sup>(2)</sup>   |
| WE 14x14 SS304 Fuel Cladding  | 16 kW  | 16 kW  | 16 kW  |
| WE 14x14 MOX Zirc Cladding    | 16 kW  | 16 kW  | 16 kW  |

- (1) The vacuum drying steady state analysis are performed for a 14 kW heat load to maintain spacer disc temperatures within the maximum allowable
- (2) The DSC horizontal in cask with loss of sunshade and neutron shield analysis is conservatively based on a 16 kW DSC shell temperature imposed onto a 14 kW DSC basket analysis.
- (3) The blocked vent analysis is performed for a 14 kW heat load to maintain spacer disc temperatures within the maximum allowable.

#### 4.2 Summary of Thermal Properties of Materials

The thermal properties of materials used in the thermal analyses are reported below. The values are listed as given in the corresponding references.

a. Helium

Used for: Gaps in canister during storage mode

| Temp<br>°F | Conductivity<br>[4.10]<br>Btu/hr-ft-°F |
|------------|--|
| 0          | 0.0784                                 |
| 50         | 0.0837                                 |
| 100        | 0.0886                                 |
| 200        | 0.0980                                 |
| 300        | 0.1075                                 |
| 400        | 0.1177                                 |
| 500        | 0.1291                                 |
| 600        | 0.1403                                 |
| 700        | 0.1508                                 |
| 800        | 0.1607                                 |
| 900        | 0.1702                                 |
| 1000       | 0.1793                                 |
| 1100       | 0.1883                                 |

## b. SA-240, Type 304, ASTM A240, Type 304, 18Cr-8Ni

Used for: Guidesleeves, Oversleeves, AHSM Heat Shield, AHSM support steel, SS304 fuel rod cladding

| Temp<br>°F | Expansion<br>Coefficient [4.7]<br>1E-6 °F <sup>(1)</sup> | Conductivity<br>[4.7]<br>Btu/hr-ft-°F | Thermal<br>Diffusivity [4.7]<br>ft²/hr | Density <sup>(1)</sup><br>[4.9]<br>lbm/in³ |
|------------|--|---------------------------------------|--|--|
| 70         | --   | 8.6                                   | 0.151                                  | 0.285                                      |
| 100        | 8.55   | 8.7                                   | 0.152                                  |  |
| 150        | 8.67   | 9.0                                   | 0.154                                  |  |
| 200        | 8.79   | 9.3                                   | 0.156                                  |  |
| 250        | 8.90   | 9.6                                   | 0.158                                  |  |
| 300        | 9.00   | 9.8                                   | 0.160                                  |  |
| 350        | 9.10   | 10.1                                  | 0.162                                  |  |
| 400        | 9.19   | 10.4                                  | 0.165                                  |  |
| 450        | 9.28   | 10.6                                  | 0.167                                  |  |
| 500        | 9.37   | 10.9                                  | 0.170                                  |  |
| 550        | 9.45   | 11.1                                  | 0.172                                  |  |
| 600        | 9.53   | 11.3                                  | 0.174                                  |  |
| 650        | 9.61   | 11.6                                  | 0.177                                  |  |
| 700        | 9.69   | 11.8                                  | 0.179                                  |  |
| 750        | 9.76   | 12.0                                  | 0.181                                  |  |
| 800        | 9.82   | 12.2                                  | 0.184                                  |  |

(1) Density is assumed to be independent of temperature.

## c. SA-240, Type 316, 16Cr-12Ni-2Mo

Used for: 24PT1-DSC shell, 24PT1-DSC top outer cover, 24PT1-DSC top inner cover, 24PT1-DSC bottom inner cover, 24PT1-DSC bottom outer cover

| Temp<br>°F | Conductivity [4.7]<br>Btu/hr-ft-°F | Thermal<br>Diffusivity [4.7]<br>Ft <sup>2</sup> /hr | Density <sup>(1)</sup><br>[4.9]<br>lbm/in <sup>3</sup> |
|------------|------------------------------------|---|--|
| 70         | 7.7                                | 0.134   | 0.285  |
| 100        | 7.9                                | 0.136   |  |
| 150        | 8.2                                | 0.138   |  |
| 200        | 8.4                                | 0.141   |  |
| 250        | 8.7                                | 0.143   |  |
| 300        | 9.0                                | 0.145   |  |
| 350        | 9.2                                | 0.148   |  |
| 400        | 9.5                                | 0.151   |  |
| 450        | 9.8                                | 0.153   |  |
| 500        | 10.0                               | 0.156   |  |
| 550        | 10.3                               | 0.159   |  |
| 600        | 10.5                               | 0.162   |  |
| 650        | 10.7                               | 0.164   |  |
| 700        | 11.0                               | 0.167   |  |
| 750        | 11.2                               | 0.170   |  |
| 800        | 11.5                               | 0.173   |  |

(1) Density is assumed to be independent of temperature.

## d. SA-537, Class 2, ASTM A-36, SA-36, C-Mn-Si

Used for: Spacer discs, 24PT1-DSC top and bottom shield plugs

| Temp.<br>°F | Conductivity<br>[4.7]<br>Btu/hr-ft-°F | Thermal<br>Diffusivity [4.7]<br>ft²/hr | Density <sup>(1)</sup><br>[4.9]<br>lbm/in³ |
|-------------|---------------------------------------|--|--|
| 70          | 23.6                                  | 0.454                                  | 0.284                                      |
| 100         | 23.9                                  | 0.443                                  |  |
| 150         | 24.2                                  | 0.433                                  |  |
| 200         | 24.4                                  | 0.422                                  |  |
| 250         | 24.4                                  | 0.414                                  |  |
| 300         | 24.4                                  | 0.406                                  |  |
| 350         | 24.3                                  | 0.396                                  |  |
| 400         | 24.2                                  | 0.386                                  |  |
| 450         | 23.9                                  | 0.375                                  |  |
| 500         | 23.7                                  | 0.364                                  |  |
| 550         | 23.4                                  | 0.355                                  |  |
| 600         | 23.1                                  | 0.346                                  |  |
| 650         | 22.7                                  | 0.333                                  |  |
| 700         | 22.4                                  | 0.320                                  |  |

(1) Density is assumed to be independent of temperature.

## e. Boral™

Used for: Poison sheets

| Temp<br>°F | Conductivity<br>[4.8]<br>Btu/hr-ft-°F | Specific<br>Heat [4.8]<br>Btu/lbm-°F | Density <sup>(1)</sup><br>[4.8]<br>lbm/in³ |
|------------|---------------------------------------|--------------------------------------|--|
| 100        | 49.6                                  | 0.220                                | 0.0896                                     |
| 500        | 44.4                                  | 0.268                                |  |

(1) Density is assumed to be independent of temperature

## f. Water

Used for: Water in 24PT1-DSC cavity during loading operations

| Temp<br>°F         | Conductivity<br>[4.6]<br>(Btu/hr-ft-°F) | Specific Heat<br>[4.6]<br>(Btu/lbm-°F) | Density<br>[4.6]<br>(lbm/ft³) |
|--------------------|---|--|-------------------------------|
| 100                | 0.3633                                  | 0.998                                  | 62.00                         |
| 150                | 0.3806                                  | 1.000                                  | 61.20                         |
| 200                | 0.3916                                  | 1.005                                  | 60.10                         |
| 250 <sup>(1)</sup> | 0.3970                                  | 1.015                                  | 58.75                         |

(1) From Reference [4.12]

## g. Air

Used for: Buoyancy driven flow through the AHSM during storage. Cover gas for 24PT1-DSC during vacuum drying (see Section 4.7.1 for justification).

| Temp<br>°F | Specific<br>Heat $C_p$ [4.6]<br>Btu/lbm-°F | Density<br>$\rho$ [4.6]<br>lbm/ft <sup>3</sup> | Viscosity<br>$\mu$ ( $\times 10^{-4}$ ) [4.6]<br>lbm/sec-ft | Conductivity<br>$k$ [4.6]<br>Btu/hr-ft-°F |
|------------|--|--|---|---|
| -55        | 0.240                                      | 0.0981   | 0.0986  | 0.01168                                   |
| -46        | 0.240                                      | 0.0959   | 0.1004  | 0.01191                                   |
| -37        | 0.240                                      | 0.0939   | 0.1022  | 0.01215                                   |
| -28        | 0.240                                      | 0.0919   | 0.1039  | 0.01239                                   |
| -19        | 0.240                                      | 0.0900   | 0.1057  | 0.01263                                   |
| -10        | 0.240                                      | 0.0882   | 0.1074  | 0.01287                                   |
| 0          | 0.240                                      | 0.0865   | 0.1092  | 0.01310                                   |
| 8          | 0.240                                      | 0.0848   | 0.1109  | 0.01334                                   |
| 17         | 0.240                                      | 0.0832   | 0.1126  | 0.01357                                   |
| 26         | 0.240                                      | 0.0816   | 0.1143  | 0.01380                                   |
| 35         | 0.240                                      | 0.0802   | 0.1160  | 0.01403                                   |
| 44         | 0.240                                      | 0.0787   | 0.1176  | 0.01426                                   |
| 53         | 0.240                                      | 0.0774   | 0.1192  | 0.01448                                   |
| 62         | 0.240                                      | 0.0760   | 0.1208  | 0.01472                                   |
| 71         | 0.240                                      | 0.0747   | 0.1224  | 0.01494                                   |
| 80         | 0.240                                      | 0.0734   | 0.1241  | 0.01516                                   |
| 89         | 0.240                                      | 0.0723   | 0.1257  | 0.01539                                   |
| 98         | 0.241                                      | 0.0711   | 0.1272  | 0.01561                                   |
| 107        | 0.241                                      | 0.0700   | 0.1287  | 0.01583                                   |
| 116        | 0.241                                      | 0.0688   | 0.1303  | 0.01606                                   |
| 125        | 0.241                                      | 0.0678   | 0.1319  | 0.01627                                   |
| 134        | 0.241                                      | 0.0668   | 0.1334  | 0.01649                                   |
| 143        | 0.241                                      | 0.0658   | 0.1349  | 0.01670                                   |
| 152        | 0.241                                      | 0.0648   | 0.1364  | 0.01692                                   |
| 161        | 0.241                                      | 0.0638   | 0.1379  | 0.01713                                   |
| 170        | 0.241                                      | 0.0629   | 0.1394  | 0.01735                                   |
| 179        | 0.241                                      | 0.0621   | 0.1409  | 0.01758                                   |
| 188        | 0.241                                      | 0.0612   | 0.1423  | 0.01779                                   |
| 197        | 0.241                                      | 0.0604   | 0.1437  | 0.01800                                   |
| 206        | 0.242                                      | 0.0595   | 0.1452  | 0.01820                                   |
| 215        | 0.242                                      | 0.0587   | 0.1465  | 0.01841                                   |
| 224        | 0.242                                      | 0.0580   | 0.1479  | 0.01862                                   |
| 233        | 0.242                                      | 0.0572   | 0.1494  | 0.01883                                   |
| 242        | 0.242                                      | 0.0565   | 0.1508  | 0.01904                                   |
| 251        | 0.242                                      | 0.0558   | 0.1522  | 0.01925                                   |
| 314        | 0.2432                                     | 0.0512   | n/a   | 0.02066                                   |
| 404        | 0.2451                                     | 0.0459   | n/a   | 0.02260                                   |
| 512        | 0.2479                                     | 0.0408   | n/a   | 0.02482                                   |
| 602        | 0.2506                                     | 0.0373   | n/a   | 0.02659                                   |
| 692        | 0.2533                                     | 0.0344   | n/a   | 0.02829                                   |
| 764        | 0.2556                                     | 0.0324   | n/a   | 0.02962                                   |

## h. Concrete

Used for: AHSM concrete, basemat

| Temp<br>°F | Density [4.11]<br>(lbm/ft <sup>3</sup> ) | Specific Heat [4.11]<br>(Btu/lbm-°F) | Conductivity [4.11]<br>(Btu/hr-ft-°F) |
|------------|--|--------------------------------------|---------------------------------------|
| -75        | 145 <sup>(1)</sup>                       | 0.25                                 | 0.917                                 |
| 0          |  |                                      | 0.917                                 |
| 100        |  |                                      | 1.17                                  |
| 200        |  |                                      | 1.14                                  |
| 500        |  |                                      | 1.04                                  |
| 1000       |  |                                      | 0.80                                  |

(1) Minimum density without reinforcement specified for the concrete.

## i. Soil

Used for: Soil beneath basemat

| Temp<br>°F | Density [4.3]<br>(lb/ft <sup>3</sup> ) | Specific Heat [4.3]<br>(Btu/lb-°F) | Conductivity [4.3]<br>(Btu/hr-ft-°F) |
|------------|--|------------------------------------|--------------------------------------|
| All        | 128                                    | 0.440                              | 0.300                                |

## j. Emissivities

Used for: modeling thermal radiation

| Material                   | Nominal $\epsilon$ | Reference     |
|----------------------------|--------------------|---------------|
| Stainless Steel            | 0.40               | [4.26]        |
| 24PT1-DSC Shell surface    | 0.587              | [4.13]        |
| Carbon Steel               | 0.35               | [4.10]        |
| Electroless Nickel Coating | 0.15               | [4.14]        |
| Concrete                   | 0.9                | [4.6], [4.14] |
| Boral™ Sheet               | 0.1                | [4.8]         |

## k. PWR Fuel with helium backfill

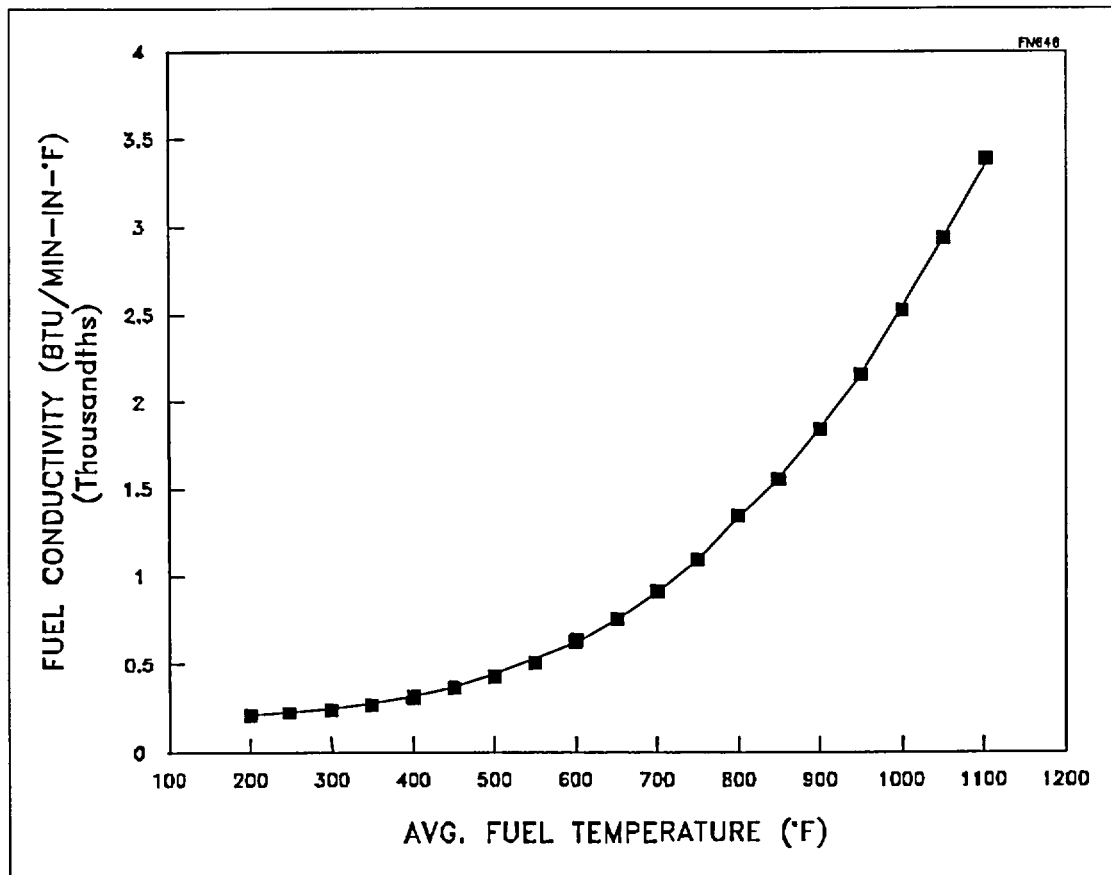
The fuel conductivity values are taken from Reference 4.17 which are based on Reference [4.15] for helium backfill cases. In Reference [4.15], extensive thermal testing was performed which showed that these effective conductivity values are conservative. The testing was performed with Zircalloy clad fuel. Because these values are based on experimental data, those effective conductivities include the effect of radiation. Zircalloy and stainless steel have similar irradiated emissivities ( $\epsilon=0.8$  for irradiated Zircalloy per Reference [4.16] and  $\epsilon=0.85$  for irradiated stainless steel per Reference [4.10]). The Zircalloy cladding and stainless steel cladding also have very similar thermal

conductivities as documented in Reference [4.16] and Section 4.2.b. Therefore, these conductivity values are applicable for both fuel types considered in this application.

| Temp<br>°F | Conductivity [4.15]<br>Btu/min-in-°F | Specific Heat [4.16]<br>Btu/lbm-°F |
|------------|--------------------------------------|------------------------------------|
| 400        | 2.22E-03                             | 0.067                              |
| 500        | 2.92E-03                             |                                    |
| 600        | 3.61E-03                             |                                    |
| 700        | 4.44E-03                             |                                    |
| 800        | 5.42E-03                             |                                    |
| 900        | 6.53E-03                             |                                    |
| 1000       | 7.64E-03                             |                                    |

#### 1. PWR Fuel in Vacuum Environment

The effective conductivity of PWR fuel in a vacuum environment was derived in Appendix B of Reference [4.17], based on test data from Reference [4.15], and is given in the figure below.



Effective Conductivity of PWR Fuel in a Vacuum Environment



### 4.3 Specifications for Components

Allowable temperature ranges for the structural materials used in the design are given in Table 4.1-3, Table 4.1-4, and Table 4.1-5. Because of the passive design of the Advanced NUHOMS® System, there is no need for rupture discs or pressure relief in the safety related components.

#### 4.4 Thermal Evaluation for Normal Conditions of Storage and Transfer

##### 4.4.1 Overview of Thermal Analysis for Normal Conditions of Storage and Transfer

This section of the SAR describes the thermal analysis of the AHSM and 24PT1-DSC. The analytical models of the AHSM, the 24PT1-DSC, and the transfer cask are described and the calculation results are summarized below. The thermophysical properties of the Advanced NUHOMS® System components used in the thermal analysis are listed in Section 4.2. The following evaluations are performed for the Advanced NUHOMS® System:

1. Thermal Analysis of the 24PT1-DSC in the AHSM (Section 4.4.2),
2. Thermal Analysis of the 24PT1-DSC in the Transfer Cask (Section 4.4.3),
3. Thermal Analysis of the 24PT1-DSC basket (Section 4.4.4).

##### 4.4.2 Thermal Model of the 24PT1-DSC Inside the AHSM

For normal condition of storage, the Advanced NUHOMS® System components are evaluated for a range of design basis ambient temperatures. The system components are evaluated for the average ambient temperatures given in Table 4.1-1. Ambient temperatures within this range are assumed to occur for a sufficient duration to cause a steady-state temperature distribution in the Advanced NUHOMS® System components. The lifetime average ambient temperature for the 40 year service life is taken as 70°F. The "stress-free" temperature for material properties is also 70°F.

The AHSM is cooled by a natural draft of air entering through the air inlet opening located in the lower front wall of the AHSM, and exiting through the air outlet opening located in the top of the AHSM. Cooler air at the prevailing ambient conditions is drawn into the AHSM. The cooler air flows from the bottom of the AHSM along the outer 24PT1-DSC surface where it is warmed by the decay heat of the spent fuel inside the 24PT1-DSC. The warmed air flows along the ceiling of the AHSM and exits through the air outlet opening. The AHSM vent geometries and flow paths for ventilation air are illustrated in Figure 4.4-1.

The AHSM roof and front wall are the primary concrete surfaces conducting heat to the outside environment. For the analytical purpose of calculating maximum temperatures, an AHSM centered in a group of AHSMs, each loaded with a 24PT1-DSC, is assumed. Rows of modules are assumed to exist back to back for this model. For the analytical purpose of calculating maximum concrete temperature gradients, an AHSM alone, with no adjacent modules or rear shield wall, is assumed.

A metal heat shield is placed around the upper half of the 24PT1-DSC to shield the AHSM concrete surfaces above and to the side of the 24PT1-DSC from thermal radiation effects. The location and geometry of the heat shield is shown in Figure 4.4-6 and on the AHSM drawings contained in Chapter 1. The heat shield protects the AHSM surfaces above and to the side of the 24PT1-DSC from direct thermal radiation emanating from the 24PT1-DSC surface and significantly increases the combined surface area for convection cooling inside the AHSM. The

concrete surfaces above and to the side of the 24PT1-DSC are subjected to thermal radiation from the back side of the heat shield. However, the radiation is emanated at substantially lower temperatures than the direct thermal radiation from the 24PT1-DSC surface.

#### 4.4.2.1 AHSM Stack Effect Calculations

The methodology used is the same as Reference [4.17]. The temperature difference ( $\Delta T$ ), and the height difference ( $\Delta h$ ) between the AHSM vent inlet and outlet creates a "stack effect" to drive air through the AHSM. The ventilation air has sufficient velocity to provide adequate cooling for the 24PT1-DSC so that the spent fuel cladding temperature remains below acceptable limits. The ventilation flow paths inside the AHSM are designed so that the pressure difference due to the stack effect ( $\Delta P_s$ ) is greater than the pressure losses due to friction, vent area changes, and flow direction changes ( $\Delta P_f$ ). Equations are derived from Reference [4.25] to describe the stack effect.

The pressure loss due to friction is calculated by summing the individual friction losses through the air inlet opening, the air outlet opening, and the flow paths through the AHSM.

$$\sum_i \frac{k_i}{n_i^2 \cdot A_i^2}$$

Where:

$k_i$  - loss coefficient

$A_i$  - flow area

$n_i$  - number of divergent paths

Standard loss coefficients for entrances, exits, screens, elbows, slots, friction, flow over curved enclosures, flow between parallel plates, flowpath expansions and contractions are taken from References [4.18] and [4.3]. The total pressure drop due to the flow losses is determined by:

$$\Delta P_f = \frac{\dot{m}^2}{2 \cdot \bar{\rho}} \cdot \sum_i \frac{k_i}{n_i^2 \cdot A_i^2} \quad (4.4-1)$$

Where:

$\dot{m}$  = Mass flow rate (lbm/sec)

$\bar{\rho}$  = Average density (lbm/ft<sup>3</sup>)

$n_i$  = number of divergent flow paths

The total pressure drop from the stack effect is calculated as follows:

$$\Delta P_s = g \Delta h \rho_0 \left( 1 - \frac{T_{amb}}{T_s} \right) \quad (4.4-2)$$

Where:

- $\Delta P_s$  = Pressure difference due to stack effect (lbf/ft<sup>2</sup>)
- $\Delta h$  = Stack Height (ft.)
- $g$  = Acceleration due to Gravity (ft/min<sup>2</sup>)
- $\rho_0$  = Density of air at ambient condition (lbm/ft<sup>3</sup>)
- $T_{amb}$  = Ambient temperature (°R)
- $T_s$  = Stack average temperature (°R)

The above equations are solved iteratively to determine values of  $T_s$  and  $\dot{m}$  at specific values of

$\sum_i \frac{k_i}{n_i^2 \cdot A_i^2}$  for  $\Delta P_i \leq \Delta P_s$ . The flow rate calculation accounts for flow separation around the circumference of the 24PT1-DSC which then consolidates and flows through the top shield block to the outlet vent. Using the calculated values of  $\dot{m}$ , the AHSM bulk air temperatures surrounding the 24PT1-DSC are determined assuming isotropic heat flow from the 24PT1-DSC surface so that the temperature of the air increases linearly across the circumference of the canister shell surface. It is conservatively assumed that 100% of the decay heat is removed by convection to the bulk air surrounding the 24PT1-DSC. The resulting differential temperatures are shown in Table 4.4-1 for a range of ambient conditions.

The resulting bulk air temperatures for the range of ambient conditions are used in the subsequent AHSM analyses to calculate the temperatures throughout the AHSM and 24PT1-DSC shell. In the AHSM HEATING7 model, the Boundary Type 1 (surface-to-boundary) is used to describe the natural circulation heat transfer between the 24PT1-DSC and the adjacent cooling air at the bulk air temperatures.

#### 4.4.2.2 Model Description

The HEATING7 thermal model of the AHSM is depicted in Figure 4.4-2 through Figure 4.4-5. The model represents the symmetric right half of an AHSM and 24PT1-DSC cross section.

For the design and qualification of the AHSM components, a decay heat of 24 kW per canister is used.

For the design and qualification of the 24PT1-DSC and the determination of fuel cladding integrity over the design life, a bounding decay heat of 0.581 kW/assembly and bounding RCCA decay heat of 0.002 kW/assembly (resulting in a total of 14 kW/canister) is used. These values were presented in Chapter 2 to bound the fuel types being considered in this SAR. Some of the 24PT1-DSC analyses are conservatively done for 16 kW per canister (0.667 kW per fuel assembly) which bounds the design heat load of 14 kW per canister.

The HEATING7 analytical model of the AHSM is one-half of a single AHSM unit. Symmetry or an insulated boundary is applied along the vertical centerline of the AHSM model shown in Figure 4.4-2 through Figure 4.4-4. The HEATING7 model includes regions for the concrete, top shield block, base block, and basemat of the AHSM. The soil below the ISFSI basemat is modeled as a seven foot thick region with a constant temperature boundary at the lower edge of this region. Sufficient nodal refinement is used in the AHSM analytical model to obtain accurate temperature distributions through the thickness of the AHSM base and storage units.

The thermal analysis of a typical AHSM is performed for a loaded 24PT1-DSC located in the interior of a multiple module array with a 24PT1-DSC present in the two adjacent AHSMs. The AHSM top and front surfaces are modeled as exposed to the prevailing ambient conditions in this model. The side and back surfaces are modeled as being adiabatic in order to simulate the adjacent modules. An additional model was constructed for the specific purpose of calculating the maximum concrete gradients. For this model, the thermal analysis is performed for a free standing AHSM, with the top and front, as well as the back and side surfaces, exposed to the prevailing ambient conditions.

For summer ambient conditions, a solar heat flux of 123 BTU/hr-ft<sup>2</sup> is applied to the top surface for normal summer ambient conditions, which is based on conservative averaging of data in Reference [4.5]. Solar heat loads are conservatively neglected for the AHSM thermal analysis for normal winter ambient conditions. The solar heat loads are listed in Table 4.1-1.

The 24PT1-DSC cylindrical shell is approximated in the AHSM thermal model as a rectangle, as shown in Figure 4.4-5. The approximation using rectangular regions is necessary since HEATING7 restricts the user to one geometry type in the same analytical model. To improve the approximation, the modeled 24PT1-DSC regions have the same surface area as the outer surface of the 24PT1-DSC cylindrical shell. The analytical model of the AHSM includes regions for the metal heat shield located between the top and sides of the 24PT1-DSC, and the AHSM, as shown in Figure 4.4-5. The surface area of the heat shield was also approximately maintained in the model.

The analytical model also includes regions to model the air gaps between the 24PT1-DSC, heat shield, and the AHSM.

The heat generation in the canister used in the AHSM thermal model is given in Table 4.4-2 for 24, 16, and 14 kW heat load in the canister. The heat generation is distributed over the entire internal cavity volume of the 24PT1-DSC, the model geometry is shown in Figure 4.4-5. Use of the entire 24PT1-DSC cavity volume and exclusion of an axial peaking factor for the AHSM thermal analysis is based on the test data contained in Reference [4.21]. The reference test data for cylindrical casks show that the measured surface temperature profiles are relatively flat over the entire length, indicating that the heat flux is nearly uniform over the surface and axial peaking is not affecting the surface temperature distribution. One reason for the relatively flat temperature profiles is the high thermal conductivity of the 24PT1-DSC shell material. The resulting heat generation is therefore more representative of the manner in which heat is actually rejected to the AHSM air space by the 24PT1-DSC. The active fuel length of 120 inches and the peaking factor of 1.08 are conservatively used in the thermal analysis of the 24PT1-DSC internals presented in Section 4.4.4 for the evaluation of local effects such as the peak fuel clad temperature. The outer

surface of the 24PT1-DSC shell dissipates heat to the AHSM through both convection and radiation. The air surrounding the 24PT1-DSC is modeled as a gap filled with gas (air), thus providing a mechanism for heat transfer from all AHSM interior surfaces and the 24PT1-DSC outer surface. Due to a limitation in the HEATING7 code, conduction in the air gap could not be included, however, this is a minor effect.

Convection heat transfer from the 24PT1-DSC and AHSM surfaces is modeled by defining analytical functions for the bulk air temperatures along the surfaces of the 24PT1-DSC, heat shield, and concrete using the calculated air temperature rises given in Table 4.4-1. A linear rise in the air temperature around the periphery of the 24PT1-DSC is assumed. The maximum temperature of the air from Table 4.4-1 is assumed at the top of the 24PT1-DSC and throughout the top shield block, which is conservative. These temperatures are also used to calculate the heat transfer coefficients along the 24PT1-DSC, heat shield, and concrete surfaces. With the air temperatures and the equations for the heat transfer coefficients described below, the HEATING7 program calculates the temperatures of the 24PT1-DSC exterior surface and the AHSM interior and exterior surfaces.

The majority of the spent fuel assembly decay heat is removed from the 24PT1-DSC outer surface through convection. Since the heat shield and the concrete surrounding the 24PT1-DSC are curved, both sides of the metal heat shield and the AHSM concrete surfaces surrounding the 24PT1-DSC are cooled by air with a heat transfer coefficient of  $h_{cyl}$ . Horizontal slab surfaces with convection on their lower surface, such as the AHSM top shield block lower surface, are cooled by natural convection with a heat transfer coefficient of  $h_{ceil}$ . Horizontal surfaces with convection on their upper surfaces, such as the AHSM top shield block outer surface, are cooled by natural convection with a heat transfer coefficient of  $h_{plate}$ . Vertical, flat surfaces are cooled by natural convection with a heat transfer coefficient of  $h_{wall}$ .

Radiation heat transfer is modeled between the 24PT1-DSC outer surface and heat shield, between the 24PT1-DSC outer surface and the basemat and lower shield block, and between the heat shield and the AHSM concrete surfaces. The external surface of the AHSM top shield block is cooled by external air with a heat transfer coefficient of  $h_{plate}$ , and by radiation cooling to ambient air. The formulas used for the calculation of the heat transfer coefficients for natural convection are as follows all in BTU/(hr-ft<sup>2</sup>°F) [4.22]:

$$h_{cyl} = 0.18 (\Delta T)^{1/3} \quad (4.4-3)$$

$$h_{ceil} = 0.12 (\Delta T/L)^{1/4} \quad (4.4-4)$$

$$h_{plate} = 0.22 (\Delta T)^{1/3} \quad (4.4-5)$$

$$h_{wall} = 0.19 (\Delta T)^{1/3} \quad (4.4-6)$$

Where:

$$\Delta T = T_{surface} - T_{air} \text{ (°F)}$$

$$L = \text{conservatively defined characteristic length of surface (ft)}$$

The heat transfer coefficients are updated by HEATING7 following each iteration using the resulting average temperature of the corresponding surface node. A sufficient number of

iterations are performed until the temperatures differ by less than 0.1% from the previous temperature calculated in two consecutive iterations indicating that stable convergence is achieved. The remaining thermal-hydraulic parameters used in the AHSM heat transfer calculations are given in Section 4.4.3.

The results of the HEATING7 analysis for the AHSM are in the form of temperature distribution profiles. The resulting temperature profiles show the steady state temperature distribution of the 24PT1-DSC shell assembly at various locations throughout the AHSM.

The calculated AHSM concrete temperatures are used in the structural analysis for long term thermal loads which occur during normal operating conditions. The AHSM thermal analysis results are also used to obtain steady state temperature distributions for the outer surface of the 24PT1-DSC for the range of design basis ambient conditions. These steady state surface temperatures are used as a temperature boundary condition for the 24PT1-DSC model, described in Section 4.4.4.

#### 4.4.2.3 Description of Cases Evaluated for the AHSM

The AHSM thermal analyses are performed for the design basis normal ambient air temperatures defined in Section 4.1. These include a total of three cases with ambient air entering and/or surrounding the AHSM at the temperatures listed in Table 4.4-1, noting that a daily average of the maximum summer ambient condition was used in accordance with Section 4.1.

Temperature distributions of the concrete are used to determine thermal stresses in the structure for all three normal cases.

The AHSM thermal model also includes the 24PT1-DSC shell, top and bottom plates and shield plugs, as shown in Figure 4.4-2 and Figure 4.4-5. The temperature profiles generated for the top and bottom cover plates and shield plugs, as well as the cylindrical shell are used to determine thermal stresses within these components. The normal cases which are considered are listed in Table 4.4-8.

#### 4.4.2.4 AHSM Thermal Model Results

The results of the AHSM thermal analysis are shown in Table 4.4-3 for the heat shield, support steel and concrete for a heat load of 24 kW. The maximum temperatures are compared to their material limits in Table 4.1-3 for normal operation. The 24PT1-DSC shell results for lower decay heats of 16 and 14 kW, which are used to generate the 24PT1-DSC basket temperature profiles, are given in Table 4.4-4.

The maximum temperature results for the 24PT1-DSC shell assembly are given in Table 4.4-5 for a heat load of 24 kW. Maximum temperatures of the 24PT1-DSC shell assembly are verified to be within their material limits, as defined in the ASME B&PV Code [4.7] in Table 4.1-3 (data provided in this table are the enveloping temperatures for the storage and transfer cases).

#### 4.4.3 Thermal Model of 24PT1-DSC in the Transfer Cask

##### 4.4.3.1 Model Description

The transfer cask analysis for the OS197 transfer cask has already been performed for 24 kW [4.17]. For the current fuel types and heat loads considered, the same model is utilized with the ambient conditions consistent with Table 4.1-1. This model is an axisymmetric two dimensional model which includes the cask and the 24PT1-DSC shell assembly. The 24PT1-DSC cavity is modeled as a homogenous region. The 24PT1-DSC shell assembly dimensions are nearly identical to those used in the previous analysis. The cover plates and shell assembly in the old model are stainless steel, type 304, as opposed to stainless steel, type 316 for the 24PT1-DSC design. But based on Section 4.4.3, the difference in thermal conductivity of these two materials is very small and would have a negligible impact on the results.

##### 4.4.3.2 Description of Cases Evaluated for the 24PT1-DSC Inside OS197 Transfer Cask

The transfer cask normal thermal analyses are performed for the range of design basis ambient air temperatures defined in Section 4.1 for normal conditions. The transfer cask thermal analysis is not performed for the design life average temperature since this case is needed only for the storage in the AHSM to ensure the integrity of the fuel cladding and is enveloped by the other normal cases. In accordance with NUREG-1536 [4.5], the short term fuel cladding temperature limit applies to all transfer cask operations.

The thermal stress analysis of the 24PT1-DSC shell assembly is based on the temperature results from the previous analysis of the OS197 cask and shell assembly with 24 kW heat load [4.17]. Three dimensional temperature profiles of the 24PT1-DSC shell and top and bottom cover plates and shield plugs are used from the prior results of the OS197 transfer cask analysis with 24 kW heat load for use in thermal stress calculations. The cases which are used to determine thermal stresses for normal conditions are listed in Table 4.4-8.

New cases are performed only in order to provide 24PT1-DSC shell temperature boundary conditions for the 24PT1-DSC basket thermal model. A single temperature for the 24PT1-DSC shell is extracted from the results of the transfer cask thermal analysis for use in the 24PT1-DSC basket thermal analysis.

##### 4.4.3.3 Transfer Cask Thermal Model Results

The maximum temperature results for the shell assembly during transfer operations are presented in Table 4.4-5. These results are for 24 kW heat load, and are from the previous thermal analysis of the OS197 transfer cask [4.17]. These results are used in the structural analysis described in Chapter 3. The maximum temperature of the 24PT1-DSC shell for 16 kW decay heat, which bounds the design basis decay heat of 14 kW, is given in Table 4.4-4. These temperatures are used as boundary conditions in the 24PT1-DSC basket thermal analysis presented in Section 4.4.5.



#### 4.4.4 24PT1-DSC Basket Thermal Model







#### 4.4.4.2 Description of Cases Evaluated for the 24PT1-DSC

The 24PT1-DSC and fuel assembly heat transfer analyses with the 24PT1-DSC inside the AHSM or OS197 transfer cask are performed for the normal ambient air temperature cases defined in Table 4.1-1. A total of five normal cases corresponding to the same conditions described in Section 4.4.2.3 for the AHSM and Section 4.4.3.2 for the transfer cask are performed. The 70°F case is not performed for the transfer cask since it is enveloped by the other cases.

Temperature profiles for the spacer disc are used to determine thermal stresses shown in Chapter 3. The normal cases which are considered are listed in Table 4.4-8 24PT1-DSC Thermal Model Results

The results obtained from the HEATING7 analysis are in the form of temperature profiles for the 24PT1-DSC cross-sections. From these analysis results, maximum 24PT1-DSC structural component temperatures are extracted and summarized in Table 4.4-6. The maximum fuel cladding temperature results are summarized in Table 4.4-7. The basket components and fuel cladding maximum temperatures are compared against their limits in Table 4.1-3. The results demonstrate that there is a very low probability of cladding failure during storage. Cladding damage due to creep failure is addressed in Section 3.5.

#### 4.4.5 Test Model

The detailed, conservative evaluations described above for the AHSM, OS197 transfer cask, and 24PT1-DSC ensure that the Advanced NUHOMS® System is capable of dissipating the design basis heat load. The conservative approach precludes the necessity to perform thermal testing.

#### 4.4.6 Maximum Temperatures

The maximum temperatures for the AHSM and canister structural components are listed in Table 4.4-3, Table 4.4-4, Table 4.4-5, and Table 4.4-6 for the full range of operating conditions. The maximum fuel cladding temperatures are listed in Table 4.4-7 for the full range of operating conditions.

#### 4.4.7 Minimum Temperatures

For the minimum daily averaged temperature condition of -40°F ambient, the resulting component temperatures will approach -40°F if no credit is taken for the decay heat load. Since the AHSM and 24PT1-DSC materials, including confinement structures and welds, continue to function at this temperature (structural materials are stainless steel, or carbon steel with  $T_{NDT}$  of  $\leq -80^\circ\text{F}$  specified), the minimum temperature condition has no adverse effect on the performance of the Advanced NUHOMS® System during storage. See Chapter 12 for lifting controls applicable to a loaded transfer cask/24PT1-DSC as a function of temperature and location.

#### 4.4.8 Maximum Internal Pressure

Based on the results of the 24PT1-DSC thermal analysis, the maximum initial pressure of the helium fill gas during loading operations, and the characteristics of the fuel assemblies being

stored, a conservative prediction of the maximum gas pressure within the 24PT1-DSC cavity during normal conditions is calculated. The criteria for normal conditions, which is the basis for structural evaluations, is given in Chapter 3.

The characteristics of the fuel assemblies are given in Table 4.4-9.

The SC fuel payload results in the maximum 24PT1-DSC pressure based on the following comparison of parameters for SC and MOX fuel:

- The SC fuel rod fill pressure is over 20 times that of the MOX fuel (330 psia vs. 15 psia, per Table 4.4-9).
- The SC fuel rod void volume is larger than that of the MOX fuel (therefore, a larger quantity of rod fill gas is at the higher SC fuel fill pressure).
- MOX fuel fission gas generation is less than 50% of that of the SC fuel (Table 4.4-9) and the rate of fission gas generation during fuel decay is very small (less than 1% of the fission gas shown in Table 4.4-9 is generated during the 20 year decay of the fuel).
- The cladding strength of the zircalloy MOX fuel cladding is higher than that of the SC fuel (per Table 3.5-5 and analysis in Section 3.5.3).

Based on the parameters discussed above, it is clear that the WE 14x14 SC fuel is the bounding fuel assembly for the pressure analysis. The WE 14x14 SC fuel is therefore used in the pressure calculations. The parameters in Table 4.4-9 are used to determine the amount of fuel rod fill gas and fission gas moles for 24 WE 14x14 SC fuel assemblies.

The characteristics of the control components are given in Table 4.4-10. Based on the parameters given, the neutron source is the only potential contributor to the overall 24PT1-DSC cavity pressure.

The limiting pressures occur when there are 24 RCCA's in place within the 24PT1-DSC cavity. This is because the RCCA's are the largest control component considered for the design, which reduces the available free volume in the 24PT1-DSC cavity and results in increased pressures. From Table 4.4-10, the neutron source assembly is the only component which contributes to pressure within the 24PT1-DSC cavity. Therefore, for analytical purposes, a maximum of 4 neutron source assemblies are assumed to be loaded together with 24 RCCAs. This scenario is not possible since only one NFAH can be loaded per fuel assembly, but the approach provides a conservative simplification for the analysis. In addition, to further reduce the available volume, the maximum quantity of 4 damaged fuel assemblies is assumed in the analysis. The damaged fuel assemblies have essentially the same potential fuel rod fill and fission gas, but are enclosed within a separate can, which is shown in the drawings in Chapter 1. This separate can further reduces the free volume within the 24PT1-DSC cavity. The total free volume within the 24PT1-DSC cavity for this condition was calculated to be 360,000 in<sup>3</sup>.

Based on the basket temperature results in Table 4.4-6 and the fuel cladding temperature results of Table 4.4-7, the maximum pressure in the 24PT1-DSC cavity for normal conditions will occur

while it is in the transfer cask during the maximum summer ambient condition. The average temperature of the helium is calculated from the results for this case by isolating the helium nodes at the hottest two-dimensional cross section of the thermal model and averaging the nodal temperatures based on area. The resulting maximum average helium temperature for the normal case is given in Table 4.4-11.

The helium pressure during the backfill operation is limited to a maximum of 3 psig (1.5 psig $\pm$ 1.5 psi) according to Chapter 12. For this condition, a uniform helium temperature of 215°F is assumed, which is approximately equal to the saturation temperature of water at the level of the center of the active fuel region when the 24PT1-DSC cavity is filled with water. This assumption is conservative for the following reasons; (1) the calculations are done for 16 kW heat load which is greater than the 14 kW design basis heat load, (2) the canister and fuel assemblies have ample time during the decontamination, welding, blowdown, and vacuum drying described in Chapter 8 to heatup as evidenced by the vacuum drying analysis results shown in Figure 4.7-1. The quantity of helium fill gas can then be calculated using the ideal gas equation.

For normal conditions, 1% failure of the fuel rods and control components is assumed. For the ruptured rods, 100% release of the fuel rod fill gas and 30% release of the fission gas is assumed, based on guidance in Reference [4.5]. Based on this guidance the maximum normal pressure is calculated using the ideal gas law and is presented in Table 4.4-11.

#### 4.4.9 Maximum Thermal Stresses

The maximum thermal stresses during normal conditions of storage are presented in Chapter 3 for the 24PT1-DSC basket and shell assemblies respectively. The AHSM thermal stresses are also presented in Chapter 3. The cases which were evaluated for the AHSM and 24PT1-DSC are listed in Table 4.4-8. The effects of maximum temperatures on fuel cladding (including evaluation of fuel cladding hoop stress) are addressed in Section 3.5.

#### 4.4.10 Evaluation of System Performance for Normal Conditions of Storage and Transfer

The thermal analysis for normal storage and transfer concludes that the Advanced NUHOMS® System design meets all applicable requirements. The maximum temperatures calculated using conservative assumptions are within the criteria set forth. The predicted maximum fuel cladding temperature is well below the allowable fuel temperature limits given in Table 4.1-3. The comparison of the results with the allowable ranges is tabulated in Table 4.1-3. Thermal monitoring of the AHSM concrete temperatures is performed in accordance with the requirements of Chapter 12.

**Table 4.4-1**  
**Advanced NUHOMS® System Bulk Air Temperatures**

| AHSM Inlet Air<br>Temperature (°F) | $\Delta T_{\text{air}}^{(2)}$ |       |       |
|------------------------------------|-------------------------------|-------|-------|
|                                    | 24 kW                         | 16 kW | 14 kW |
| -40                                | 72.7                          | 54.7  | 67.0  |
| 0                                  | 79.6                          | 59.8  |       |
| 70                                 | 91.7                          | 68.8  |       |
| 104 <sup>(1)</sup>                 | 96.4                          | 72.4  |       |
| 117 <sup>(1)</sup>                 | 98.0                          | 73.6  |       |

(1) These values represent maximum inlet air temperatures  
A conservative 24 hour average as determined in Section  
4.1 was used in the analysis.

(2)  $\Delta T_{\text{air}} = \text{AHSM outlet Temp.} - \text{AHSM inlet Temp.}$



**Table 4.4-2**  
**Heat Generations Used in the Thermal Model of the 24PT1-DSC in the AHSM**

| Heat Load<br>per Canister (kW) | Heat Generation<br>(Btu/min/in <sup>3</sup> ) |
|--------------------------------|---|
| 24                             | 0.00308                                       |
| 16                             | 0.00205                                       |
| 14                             | 0.00180                                       |

**Table 4.4-3**  
**AHSM Thermal Analysis Results Summary**

| Operating Condition (°F)     | T <sub>amb</sub> (°F) | T <sub>con,max</sub> (°F) | T <sub>hs,max</sub> (°F) | T <sub>sup,max</sub> (°F) <sup>(1)</sup> |
|------------------------------|-----------------------|---------------------------|--------------------------|--|
| Normal                       | 0                     | 103                       | 136                      | 268                                      |
|                              | 70                    | 187                       | 225                      | 328                                      |
|                              | 104                   | 219                       | 258                      | 351                                      |
| Off-Normal                   | -40                   | 56                        | 87                       | 233                                      |
|                              | 117                   | 231                       | 270                      | 360                                      |
| 40 hr Blocked Vent Transient | -40                   | 243                       | 426                      | 526                                      |
|                              | 117                   | 392 <sup>(2)</sup>        | 542                      | 615                                      |

- (1) The 24PT1-DSC bottom maximum temperature conservatively represents the maximum support structure temperature
- (2) 392°F is above the 350°F limit given in Reference [4.5] - Testing will be performed to document that concrete compressive strength will be greater than that assumed in structural analyses

**Nomenclature used in table**

|                      |   |
|----------------------|---|
| T <sub>amb</sub>     | Ambient temperature                             |
| T <sub>con,max</sub> | Maximum concrete temperature                    |
| T <sub>hs,max</sub>  | Maximum heat shield temperature                 |
| T <sub>sup,max</sub> | Maximum 24PT1-DSC support structure temperature |

**Table 4.4-4**  
**24PT1-DSC Shell Results, 16 and 14 kW at Hottest Cross Section**

| Operating Condition   | Temperature at the<br>Top of the DSC<br>[°F] |
|---|--|
| <b>NORMAL</b>   |  |
| 24PT1-DSC in AHSM, 0°F amb (16 kW)  | 230  |
| 24PT1-DSC in AHSM, 70°F amb (16 kW)   | 297  |
| 24PT1-DSC in AHSM, 104°F amb (16 kW)  | 322  |
| 0°F amb, Horizontal in Cask (16 kW)   | 310  |
| 104°F amb, Horizontal in Cask (16 kW)   | 367  |
| <b>OFF-NORMAL</b>   |  |
| 24PT1-DSC in AHSM, -40°F amb (16 kW)  | 192  |
| 24PT1-DSC in AHSM, 117°F amb (16 kW)  | 332  |
|   |  |
| -40°F amb, Horizontal in Cask (16 kW)   | 294  |
| 117°F amb, Horizontal in Cask, sunshade (16 kW)                               | 364  |
| <b>ACCIDENT</b>   |  |
| 24PT1-DSC in AHSM, -40°F amb, blk vt (16 kW)                                  | 428  |
| 24PT1-DSC in AHSM, 117°F amb, blk vt (14 kW)                                  | 479  |
| 117°F amb, Horizontal in Cask, loss of sunshade<br>and neutron shield (16 kW) | 447  |

**Table 4.4-5**  
**24PT1-DSC Maximum Shell Temperatures at 24 kW**

| Configuration Ref                       | T <sub>amb</sub><br>(°F) | T <sub>shell</sub><br>(°F) | T <sub>toc</sub><br>(°F) | T <sub>tic</sub><br>(°F) | T <sub>tsp</sub><br>(°F) | T <sub>bic</sub><br>(°F) | T <sub>obc</sub><br>(°F) | T <sub>bsp</sub><br>(°F) |
|---|--------------------------|----------------------------|--------------------------|--------------------------|--------------------------|--------------------------|--------------------------|--------------------------|
| 24PT1-DSC in AHSM                       | 104                      | 399                        | 294                      | 296                      | 316                      | 315                      | 299                      | 313                      |
| 24PT1-DSC in AHSM                       | -40                      | 271                        | 166                      | 168                      | 190                      | 191                      | 174                      | 189                      |
| 24PT1-DSC in AHSM                       | 117                      | 408                        | 304                      | 306                      | 325                      | 324                      | 309                      | 323                      |
| 24PT1-DSC in AHSM 40 hr blk vt          | 117                      | 646                        | 423                      | 424                      | 444                      | 450                      | 434                      | 448                      |
| 24PT1-DSC in AHSM 40 hr blk vt          | -40                      | 565                        | 313                      | 314                      | 335                      | 348                      | 332                      | 346                      |
| 24PT1-DSC horizontal in cask            | -40                      | 380                        | 258                      | 258                      | 267                      | 335                      | 326                      | 333                      |
| 24PT1-DSC horizontal in cask with shade | 125 <sup>(1)</sup>       | 443                        | 350                      | 350                      | 358                      | 408                      | 400                      | 406                      |
| 24PT1-DSC horizontal in cask            | 0                        | 393                        | 276                      | 276                      | 284                      | 350                      | 341                      | 348                      |
| 24PT1-DSC horizontal in cask            | 100 <sup>(1)</sup>       | 439                        | 337                      | 337                      | 345                      | 402                      | 393                      | 400                      |

- (1) The 24PT1-DSC shell temperature results are taken from previous analysis for C of C 72-1004. The ambient conditions are based on the previous analysis (100°F steady state) and are not based on a daily average temperature as was derived in Section 4.1.2 (97°F steady state, equivalent temperature). Therefore, these temperatures bound the daily averages defined in Section 4.1.2.

**Nomenclature used in table**

- T<sub>amb</sub> Ambient temperature  
T<sub>shell</sub> 24PT1-DSC shell temperature  
T<sub>toc</sub> 24PT1-DSC top outer cover plate temperature  
T<sub>tic</sub> 24PT1-DSC top inner cover plate temperature  
T<sub>tsp</sub> 24PT1-DSC top shield plug temperature  
T<sub>bic</sub> 24PT1-DSC bottom inner cover plate temperature  
T<sub>obc</sub> 24PT1-DSC outer bottom cover plate temperature  
T<sub>bsp</sub> 24PT1-DSC bottom shield plug temperature

**Table 4.4-6**  
**24PT1-DSC Basket Temperature Results**

| Configuration <sup>(1)</sup>                                     | T <sub>amb</sub><br>(°F) | T <sub>sp</sub><br>(°F) | T <sub>sr</sub><br>(°F) | T <sub>gs</sub><br>(°F) | T <sub>Boral™</sub><br>(°F) |
|--|--------------------------|-------------------------|-------------------------|-------------------------|-----------------------------|
| 24PT1-DSC in AHSM  | 0                        | 565                     | 417                     | 566                     | 566                         |
| 24PT1-DSC in AHSM  | 104                      | 617                     | 479                     | 618                     | 618                         |
| 24PT1-DSC in AHSM  | -40                      | 544                     | 392                     | 545                     | 545                         |
| 24PT1-DSC in AHSM  | 117                      | 623                     | 486                     | 624                     | 624                         |
| 24PT1-DSC in AHSM blk vt   | -40                      | 683                     | 558                     | 684                     | 684                         |
| 24PT1-DSC in AHSM blk vt   | 117                      | 695                     | 588                     | 696                     | 696                         |
| 24PT1-DSC horizontal in cask                                     | 0                        | 622                     | 480                     | 623                     | 623                         |
| 24PT1-DSC horizontal in cask                                     | 104                      | 658                     | 522                     | 658                     | 658                         |
| 24PT1-DSC horizontal in cask                                     | -40                      | 612                     | 469                     | 613                     | 613                         |
| 24PT1-DSC horizontal in cask with shade                          | 117                      | 656                     | 520                     | 657                     | 657                         |
| 24PT1-DSC horizontal in cask loss of sunshade and neutron shield | 117                      | 682                     | 567                     | 682                     | 682                         |
| Vacuum Drying, steady state                                      | 120                      | 741                     | 502                     | 751                     | 751                         |

(1) See Table 4 1-6 for a listing of the limiting heat loads analyzed for each component.

**Nomenclature used in table**

|                     |                                  |
|---------------------|----------------------------------|
| T <sub>amb</sub>    | Ambient temperature              |
| T <sub>sp</sub>     | Maximum spacer disc temperature  |
| T <sub>sr</sub>     | Maximum support rod temperature  |
| T <sub>gs</sub>     | Maximum guidesleeve temperature  |
| T <sub>Boral™</sub> | Maximum poison plate temperature |

**Table 4.4-7**  
**Maximum Fuel Cladding Temperature Results, 16 kW**

| Case  | Calculated Maximum Cladding Temperature (°F) <sup>(1)</sup> | MOX/SC Fuel Temperature Limit (°F) |
|---|---|------------------------------------|
| 24PT1-DSC in AHSM, 0°F amb <sup>(2)</sup>                                   | 566   | 1058/806                           |
| 24PT1-DSC in AHSM, 70°F amb   | 604   | 618/690                            |
| 24PT1-DSC in AHSM, 104°F amb <sup>(2)</sup>                                 | 618   | 1058/806                           |
| 24PT1-DSC in AHSM, -40°F amb  | 545   | 1058/806                           |
| 24PT1-DSC in AHSM, 117°F amb  | 624   | 1058/806                           |
| 24PT1-DSC in AHSM, -40°F amb, blk vt  | 684   | 1058/806                           |
| 24PT1-DSC in AHSM, 117°F amb, blk vt  | 749   | 1058/806                           |
| 24PT1-DSC horizontal in cask, -40°F amb                                     | 613   | 1058/806                           |
| 24PT1-DSC horizontal in cask, 0°F amb <sup>(2)</sup>                        | 623   | 1058/806                           |
| 24PT1-DSC horizontal in cask, 104°F amb <sup>(2)</sup>                      | 658   | 1058/806                           |
| 24PT1-DSC horizontal in cask, 117°F amb with sunshade                       | 657   | 1058/806                           |
| 24PT1-DSC horizontal in cask, 117°F amb loss of sunshade and neutron shield | 711   | 1058/806                           |
| Vacuum drying, Steady state (14kW)  | 751   | 1058/806                           |

- (1) The calculated cladding temperature is based on a conservative heat load of 16kW even though the maximum heat load allowed is 14kW.
- (2) The short term temperature limit is applied to the minimum and maximum normal ambient temperature since this temperature is not maintained, during normal conditions, for a sufficient period of time to apply a long term temperature condition criteria.

**Table 4.4-8**  
**Summary of Cases Considered for Thermal Stress Analysis**

| Component                | Operation     | Heat Load (kW) | Ambient Temperature (°F) | Condition                         |
|--------------------------|---------------|----------------|--------------------------|-----------------------------------|
| AHSM concrete            | Storage       | 24             | -40                      | Off-Normal                        |
| AHSM concrete            | Storage       | 24             | 0                        | Normal                            |
| AHSM concrete            | Storage       | 24             | 70                       | Normal                            |
| AHSM concrete            | Storage       | 24             | 104                      | Normal                            |
| AHSM concrete            | Storage       | 24             | 117                      | Off-Normal                        |
| AHSM concrete            | Storage       | 24             | -40                      | Accident, 40 hr blk vt            |
| AHSM concrete            | Storage       | 24             | 117                      | Accident, 40 hr blk vt            |
| 24PT1-DSC Shell Assembly | Transfer      | 24             | -40                      | Off-Normal                        |
| 24PT1-DSC Shell Assembly | Transfer      | 24             | 100 <sup>(1)</sup>       | Normal, Off-Normal <sup>(2)</sup> |
| 24PT1-DSC Shell Assembly | Storage       | 24             | -40                      | Off-Normal                        |
| 24PT1-DSC Shell Assembly | Storage       | 24             | 104                      | Normal                            |
| 24PT1-DSC Shell Assembly | Storage       | 24             | 117                      | Off-Normal                        |
| 24PT1-DSC Spacer Disc    | Storage       | 16             | -40                      | Off-Normal                        |
| 24PT1-DSC Spacer Disc    | Storage       | 16             | 117                      | Off-Normal                        |
| 24PT1-DSC Spacer Disc    | Transfer      | 16             | -40                      | Off-Normal                        |
| 24PT1-DSC Spacer Disc    | Transfer      | 16             | 104                      | Normal                            |
| 24PT1-DSC Spacer Disc    | Transfer      | 16             | 117                      | Off-Normal                        |
| 24PT1-DSC Spacer Disc    | Vacuum Drying | 14             | 120                      | Normal                            |

(1) These results are taken from the previous analysis to support 72-1004. This ambient condition is from the previous analysis and is not based on a daily average temperature as was derived in Section 4.1. Therefore, this temperature still bounds the daily average defined in Section 4.1 for a maximum of 104°F.

(2) The normal case is used to bound the off-normal case, which requires use of a sunshade.

**Table 4.4-9**  
**Fuel Assembly Characteristics for Pressure Analysis**

| Parameter           | WE 14x14<br>SS304 Clad | WE 14x14<br>MOX | WE 14x14<br>SS304 Clad<br>w/ IFBA Rods |
|---------------------|------------------------|-----------------|--|
| Number of fuel rods | 180                    | 180             | 180                                    |
|                     |                        |                 |  |



**Table 4.4-10**  
**Control Component Characteristics for Pressure Analysis**



**Table 4.4-11**  
**24PT1-DSC Cavity Pressure Analysis Summary**

| Condition  | $T_{\text{He,ave}}$ (°F) | $n_{\text{He}}$ | $n_{\text{fill}}$ | $n_{\text{fiss}}$ | $n_{\text{ns}}$ | P (psig) | Criteria (psig) <sup>(1)</sup> |
|------------|--------------------------|-----------------|-------------------|-------------------|-----------------|----------|--------------------------------|
| Normal     | 483                      | 226             | 0.8               | 1.7               | 0.0245          | 9.8      | 10                             |
| Off-Normal | 483                      | 226             | 8.0               | 17.0              | 0.245           | 12.2     | 20                             |
| Accident   | 595                      | 226             | 80.0              | 170.0             | 2.45            | 42.7     | 60                             |

- (1) These criteria are recommended for structural analyses. The off-normal and accident criteria have additional margin to account for the effect of the fission gases in the 24PT1-DSC cavity on the thermal results

**Nomenclature used in table**

|                     |   |
|---------------------|---|
| $T_{\text{He,ave}}$ | Average helium temperature  |
| $n_{\text{He}}$     | Number of moles of helium backfill                                |
| $n_{\text{fill}}$   | Number of moles of fuel rod fill gas released to 24PT1-DSC cavity |
| $n_{\text{fiss}}$   | Number of moles of fission gas released to 24PT1-DSC cavity       |
| $n_{\text{ns}}$     | Number of moles of neutron source released to 24PT1-DSC cavity    |
| P                   | 24PT1-DSC cavity pressure   |

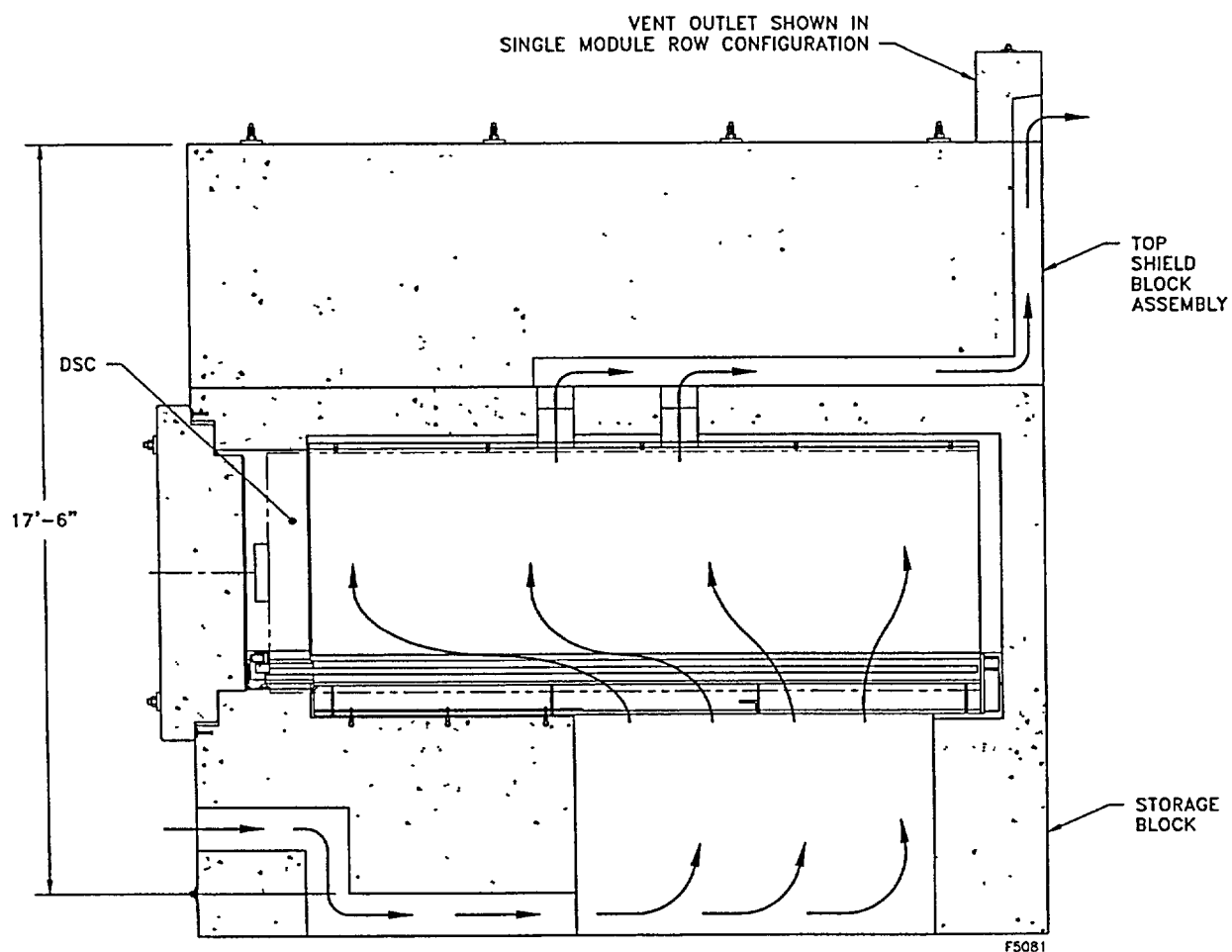


**Figure 4.4-1**  
**Illustration of Air Flow Paths through AHSM**

**Figure 4.4-2**  
**AHSM HEATING7 Model; Cross Section Along x=0.0 –**

**Figure 4.4-3**  
**Details 1, 2 and 3 From AHSM HEATING7 Model –**

**Figure 4.4-4**  
**Sections A-A and B-B From AHSM HEATING7 Model –**

**Figure 4.4-5**  
**AHSM HEATING7 Model; 24PT1-DSC and Heat Shield –**

**Figure 4.4-6**  
**Cross Section of 24PT1-DSC Basket Model –**



**Figure 4.4-7**  
**24PT1-DSC Basket Model; Fuel Regions 1 and 2 with Surrounding Regions**

**Figure 4.4-8**  
**Simplified Axial View of 24PT1-DSC Basket Model –**

## 4.5 Thermal Evaluation for Off-Normal Conditions

### 4.5.1 Overview of Off-Normal Analysis

For off-normal conditions of storage, the Advanced NUHOMS® System components are evaluated for a range of extreme ambient temperatures listed in Table 4.1-1. Should these extreme conditions ever occur, they would be expected to last for a very short time. Nevertheless, these ambient temperatures are conservatively assumed to occur for a sufficient duration to cause a steady-state temperature distribution in the Advanced NUHOMS® System components. For off-normal and accident summer ambient conditions, 123 BTU/hr.-ft<sup>2</sup>, is conservatively applied to the AHSM roof surface. The enveloping solar heat flux of 123 Btu/hr.-ft<sup>2</sup> Reference [4.20] for the extreme off-normal case is based on a flat horizontal surface averaged over a 24 hour day [4.5]. Solar heat loads are conservatively neglected for the AHSM thermal analysis for off-normal winter ambient conditions. The solar heat loads are listed in Table 4.1-1.

The same models are used for the 24PT1-DSC inside the AHSM, the 24PT1-DSC inside the transfer cask, and the 24PT1-DSC basket as described in Sections 4.4.2, 4.4.3 and 4.4.4, respectively. For the transfer cask, a sunshade is required to be placed over the cask for temperatures above 100°F. This requirement is listed in Reference [4.17].

### 4.5.2 Thermal Analysis Results

The maximum AHSM temperatures for this condition are listed Table 4.4-3. The maximum 24PT1-DSC shell assembly temperatures for off-normal conditions are given in Table 4.4-5 for 24 kW, and Table 4.4-4 for 16 and 14 kW. The maximum 24PT1-DSC basket assembly temperatures for the 14 and 16 kW cases are given in Table 4.4-6. The maximum fuel cladding temperature results for off-normal conditions is given in Table 4.4-7. The AHSM, 24PT1-DSC, and fuel cladding maximum temperatures are compared against their limits in Table 4.1-4 or off-normal conditions.

The cases providing data for thermal stress analyses are given in Table 4.4-8.

### 4.5.3 Maximum Pressure

The methodology for calculating the maximum pressure in the 24PT1-DSC cavity during off-normal conditions is described in Section 4.4.8. The criterion for the off-normal pressure is established by accounting for the possible presence of fission gases in the 24PT1-DSC cavity which will reduce the effective cover gas conductivity, and thus increase temperatures and pressures.

Based on the basket temperature results in Table 4.4-6 and the fuel cladding temperature results of Table 4.4-7, the maximum pressure in the 24PT1-DSC cavity for off-normal conditions will occur while it is in the transfer cask during the maximum normal summer ambient conditions. These temperatures bound the maximum off-normal ambient temperature case because of the required sunshade over the cask. The resulting maximum average helium temperature for the off-normal case is given in Table 4.4-11.

For off-normal conditions, 10% failure of the fuel rods and control components is assumed. For the ruptured rods, 100% release of the fuel rod fill gas and 30% release of the fission gas is assumed, based on guidance in Reference [4.5]. The maximum off-normal pressure is calculated using the ideal gas law and is presented in Table 4.4-11.

#### 4.5.4 Evaluation of System Performance for Off-Normal Conditions of Storage and Transfer

The thermal analysis for off-normal storage and transfer concludes that the Advanced NUHOMS® System design meets all applicable requirements. The maximum temperatures calculated using conservative assumptions are within the criteria set forth. The predicted maximum fuel cladding temperature is well below the allowable fuel temperature limits given in Table 4.1-4. The comparison of the results with the allowable ranges is tabulated in Table 4.1-4.

#### 4.6 Thermal Evaluation for Accident Conditions

##### 4.6.1 Accident Ambient Conditions

As with the off-normal condition of storage, the accident conditions in the Advanced NUHOMS® System components are evaluated for an extreme range of design basis ambient temperatures given in Table 4.1-1. In addition, for postulated accident conditions the AHSM ventilation inlet and outlet openings are assumed to be completely blocked for a 40 hour period concurrent with the extreme hot and cold ambient conditions given in Table 4.1-1.

##### 4.6.2 Blockage of AHSM Inlet and Outlet Vents

This accident conservatively postulates the complete blockage of the AHSM ventilation air inlet and outlet opening for a maximum of 40 hours.

###### 4.6.2.1 Cause of Accident

Since the NUHOMS® AHSMs are located outdoors, there is a remote probability that the ventilation air inlet and outlet openings could become blocked by debris from such unlikely events as floods and tornados. The NUHOMS® design features such as the perimeter security fence and the mesh screen covering of the air inlet and outlet openings reduce the probability of occurrence of such an accident. Nevertheless, for this conservative generic analysis, such an accident is postulated to occur and is analyzed.

###### 4.6.2.2 Accident Analysis

The thermal effects of this accident result from the increased temperatures of the 24PT1-DSC and the AHSM due to blockage of the ventilation air inlet and outlet openings. The thermal model of the concrete is identical to the model described in Section 4.4.2.2 and shown in Figure 4.4-2, Figure 4.4-3, and Figure 4.4-4. To determine the maximum 24PT1-DSC shell temperature during the blocked vent accident, the configuration of the 24PT1-DSC and heat shield shown in Figure 4.4-5 is used. To determine the maximum temperature of the concrete, the dimensions of the heat shield and 24PT1-DSC shown in Figure 4.4-5 were enlarged slightly in order to more accurately model the radiation heat transfer input to the concrete. The total heat load inside the canister was preserved. The model which is used to calculate 24PT1-DSC basket component and fuel cladding temperatures is identical to the model described in Section 4.4.4. The accident duration is assumed to be 40 hours, at which time the air inlet and outlet opening obstructions would be cleared by site personnel and natural circulation air flow restored to the AHSM.

Heat-up of the spent fuel, 24PT1-DSC and AHSM are limited by the heatup of the AHSM. The spent fuel assemblies and the 24PT1-DSC quickly rise in temperature to the level required to radiate and conduct the decay heat to the AHSM internal surfaces. In turn, the AHSM surface heatup is limited by the heatup of the entire AHSM. Because the heatup rate of the AHSM is much lower than that of the 24PT1-DSC, or the spent fuel, the 24PT1-DSC can be assumed to be at steady state at any instant in time and transferring 14 kW of heat to the AHSM. Therefore, the calculated surface temperatures of the 24PT1-DSC shell from the AHSM thermal model are used to

determine the maximum 24PT1-DSC basket component and fuel cladding temperatures with a steady state evaluation of the 24PT1-DSC basket.

The initial conditions for the transient analysis correspond to the steady state temperatures calculated at the off-normal analysis extreme ambient temperatures. The heat source included in the analysis is 24 kW for the qualification of the concrete and 14 kW for the qualification of the 24PT1-DSC. The solution is carried out to 40 hours. At that time, corrective action is required to restore natural circulation air flow to the AHSM. The maximum concrete temperature during the 40 hour blocked vent condition is given in Table 4.4-3. The maximum 24PT1-DSC shell assembly and basket component temperatures for the blocked vent accident are given in Table 4.4-5 and Table 4.4-6, respectively. The maximum fuel cladding temperature for the 40 hour blocked vent accident are given in Table 4.4-7.

These temperatures are below the associated safety limits for the AHSM or 24PT1-DSC. The short time exposure of the 24PT1-DSC and the spent fuel assemblies to the elevated temperatures will not cause any damage. The maximum 24PT1-DSC internal pressure during this event is calculated in Section 4.6.6.

In order to calculate the maximum thermal stresses in the concrete, additional runs were made with the side surfaces of the AHSM exposed to the prevailing ambient conditions to maximize gradients in the concrete, as discussed in Section 4.4.2.2. The thermal-induced stresses for the blocked vent case are presented for the AHSM in Chapter 3. Temperature profiles for both extreme ambient conditions were derived for the AHSM concrete for determining thermal stresses. These cases are listed in Table 4.4-8.

#### 4.6.3 Transfer Cask Loss of Neutron Shield and Sunshade

The transfer cask and 24PT1-DSC are analyzed for a postulated accident in which the transfer cask loses the water annular neutron shielding and the required sunshade during transfer at the extreme off-normal summer ambient condition given in Table 4.1-1. Even though such a scenario would likely result in immediate corrective action, the duration of the accident is conservatively assumed to result in steady state temperature distributions in the transfer cask and 24PT1-DSC. This analysis was performed previously to support the addition of the OS197 transfer cask to the NUHOMS® design described in Reference [4.17]. Therefore, the cask has already been analyzed for such an event. As described in Section 4.4.3, an identical model was used with a conservative heat load of 16 kW to determine the 24PT1-DSC shell temperatures so that an analysis of the 24PT1-DSC basket could be performed. The resulting maximum shell temperature is listed Table 4.4-4 for a conservative heat load of 16 kW. The 24PT1-DSC basket model used to determine the maximum fuel cladding and 24PT1-DSC basket component maximum temperatures is identical to that described in Section 4.4.4. This model is analyzed with 14 kW heat load for the shell temperature boundary condition derived for 16 kW heat load. The resulting maximum 24PT1-DSC basket component temperatures are listed in Table 4.4-6. The results in Table 4.4-6 show that this accident is bounded by the blocked vent analysis so that end point criteria for the 24PT1-DSC, such as cavity pressure, fuel cladding integrity, compliance of the 24PT1-DSC structural materials with ASME B&PV Code temperature limit criteria of the blocked vent scenario can be used.

#### 4.6.4 Fire Accident Evaluation

The Advanced NUHOMS® System will be stored on a concrete basemat away from combustible material. Therefore, a credible fire would be very small and of short duration such as that due to a fire or explosion from a vehicle or portable crane. A hypothetical fire accident is evaluated for the Advanced NUHOMS® System based on a fuel fire, the source of fuel being a ruptured fuel tank of the canister transporter tow vehicle or any other source of combustible fuel. The bounding capacity of combustible fuel is assumed to be 300 gallons and the bounding hypothetical fire is an engulfing fire. In addition, the postulated fire can only occur during transfer operations when personnel will be present to rapidly effect extinguishment of the fire.

From IAEA requirements [4.23] for a transport (10CFR 71) condition, the "pool" of fuel is assumed to extend 1 meter beyond the ends of the cask. For this analysis, a pool diameter of 201.5 inches, which is approximately 6 inches shorter than the nominal length of the cask is conservatively assumed to engulf the entire cask. The thickness of this fuel pool would be 2.17 inch. A fuel consumption rate of 0.15 in/min. was selected from a Sandia Report [4.24] concerning gasoline/tractor kerosene experimental burning rates. Therefore, the 300 gallons of fuel will sustain a fire for about 14 minutes and hence a 15 minute fire is conservatively evaluated. The fire parameters, other than time duration, from 10CFR 71.73 [4.20] are used. The recommended fire temperature is 1475°F. Forced convection from the fire to the cask is described by using a constant heat transfer coefficient of  $5.21\text{E-}4$  Btu/min-in<sup>2</sup>-°F, which is conservative based on measurements made at fire tests [4.24]. The recommendations of 10CFR 71.73 are also used to determine the radiation heat transfer from the fire to the cask.

This conservative fire evaluation is only performed to demonstrate the confinement integrity and fuel retrievability of the Advanced NUHOMS® System.

The model of the 24PT1-DSC inside the OS197 transfer cask which is described in Section 4.4.3 is used to determine the response of the DSC to the fire described above. The external boundary conditions of the OS197 transfer cask are set to the fire temperature and forced convection boundary conditions during the fire. Following the fire, the cask is subjected to the prevailing maximum off-normal ambient conditions. The initial temperature distribution is conservatively calculated at steady state conditions at the maximum off-normal ambient temperature with no sunshade. The transient analysis was performed in two steps; the fifteen-minute fire followed by a post fire heatup of the OS197 transfer cask and 24PT1-DSC. During the post fire heatup period, complete loss of the water in the annular neutron shield of the OS197 cask is assumed. Chapter 11 provides an evaluation of the affect on doses as a result of the potential loss of the neutron shield. The points monitored in the OS197 cask and 24PT1-DSC shell assembly are; (1) cask annular water neutron shield region, (2) cask structural steel, (3) the cask lead, (4) the 24PT1-DSC shell assembly, and (5) the cask lid.

The results of the analysis show that the cask neutron shields will be compromised as a result of the fire, but this will not impact the retrievability of the fuel, since the 24PT1-DSC shell assembly components are well within allowable temperatures. The maximum calculated DSC shell temperature for this conservative fire condition is 467 °F. Comparing this to the results for the 24PT1-DSC in Table 4.4-4 shows that this extremely conservative fire accident is bounded

by the blocked vent accident. Therefore, the end point criteria of the fire for the 24PT1-DSC shell assembly, basket assembly, and fuel cladding are bounded by the blocked vent condition, including accident pressure, fuel cladding and 24PT1-DSC structural component temperatures.

A design basis fire (300 gallons of fuel lasting approximately 15 minutes) at the AHSM inlet would have little impact on a loaded 24PT1-DSC inside the AHSM based on the following considerations:

- The conservative quantity of combustibles is small, resulting in a maximum 15 minute fire duration (the actual fire duration would be expected to be less than 15 minutes since plant personnel are likely to be present when ignition sources are in the vicinity of the combustibles). The likely ignition sources would be associated with operation of manned equipment.
- Given the types of activities performed at the ISFSI, and the limited use of ignition sources, ignition of diesel fuel and hydraulic fluid is highly unlikely.
- The assumption of a pool fire with a pool of 200" diameter and 2" thickness in the Section 4.6.4 evaluation is very conservative and has a very low probability of occurrence.
- The AHSM inlet vent is 2 feet above the ISFSI pad precluding flow of combustible liquid into the AHSM.
- No direct radiation from flames outside the AHSM to the 24PT1-DSC is possible as a result of the labyrinth configuration of the intake vent.
- The flow of hot smoke into the AHSM is negligible due to the significant flow losses and tortuous path for flow through the AHSM as compared to a direct unrestrained path for upward flow generated by the fire outside the AHSM. The buoyancy effect in the vicinity of the fire will likely cause a reverse flow of air from the AHSM to the fire. This scenario would be bounded by the blocked vent analysis.
- The AHSM concrete structure insulates the 24PT1-DSC from flame temperatures and will ensure that the AHSM fire is bounded by the OS197 cask fire analysis due to the large thermal mass and isolation from flames and products of combustion by the concrete structure.

Based on the above discussion, a fire at the inlet of the AHSM with a 24PT1-DSC located within the AHSM is bounded by the analysis provided for a fire accident with the 24PT1-DSC in the transfer cask.

A fire occurring during transfer operations (during 24PT1-DSC transfer between the cask and AHSM) will be bounded by the cask/AHSM scenarios discussed above.

See Chapter 11 for further discussion of this scenario and associated corrective actions.

Based on the thermal analyses results and the criteria which has been evaluated for the fire accident conditions, the Advanced NUHOMS® System can withstand the hypothetical fire accident event without compromising its confinement integrity and fuel retrievability.



#### 4.6.5 Flood Accident

The Advanced NUHOMS® System was evaluated for the impact of a worst case flood accident which completely covers the AHSM. The thermal consequences of such an accident are beneficial. 24PT1-DSC shell temperatures are shown in Table 4.4-4 for the design basis decay heat. The maximum temperature of the 24PT1-DSC canister is higher than the saturation temperature of water. Under these conditions the water which contacts the 24PT1-DSC surface would eventually boil, providing an extremely effective heat removal mechanism for the 24PT1-DSC. Calculations were performed, using a boiling correlation to show that given the expected heat flux of the design basis heat load on the 24PT1-DSC surface, the temperature of the canister cannot differ more than 5°F from the water temperature, which is limited by the boiling process. Therefore, thermal effects of the flood accident are bounded by the other thermal accidents which are considered.

#### 4.6.6 Maximum Pressure

The methodology for calculating maximum pressure in the 24PT1-DSC cavity during accident conditions is identical to the method described in Section 4.4.8.

Based on observation of the basket temperature results in Table 4.4-6 and the fuel cladding temperature results of Table 4.4-7, the maximum pressure in the 24PT1-DSC cavity for accident conditions will occur during the 40 hour blocked vent condition. The resulting maximum average helium temperature for the accident case is given in Table 4.4-11.

For accident conditions, 100% failure of the fuel rods and control components is assumed. For the ruptured rods, 100% release of the fill gas from fuel rod and control component rods and 30% release of the fission gas is assumed, which is based on guidance in Reference [4.5]. Based on this guidance the maximum accident pressure is calculated by using the ideal gas law and is presented in Table 4.4-11. The criteria for the accident pressure is established by adding additional margin to the calculated values to account for the presence of fission gases in the 24PT1-DSC cavity which might reduce the effective cover gas conductivity, and thus increase temperatures and pressures.

#### 4.6.7 Evaluation of System Performance for Accident Conditions of Storage and Transfer

The thermal analysis for storage and transfer accidents concludes that the Advanced NUHOMS® System design meets all applicable requirements. The maximum temperatures calculated for components necessary to ensure structural integrity, confinement and retrievability of the fuel using conservative assumptions are within the criteria set forth. The predicted maximum fuel cladding temperature is well below the allowable fuel temperature limits given in Table 4.1-5. The comparison of the results with the allowable ranges is tabulated in Table 4.1-5.

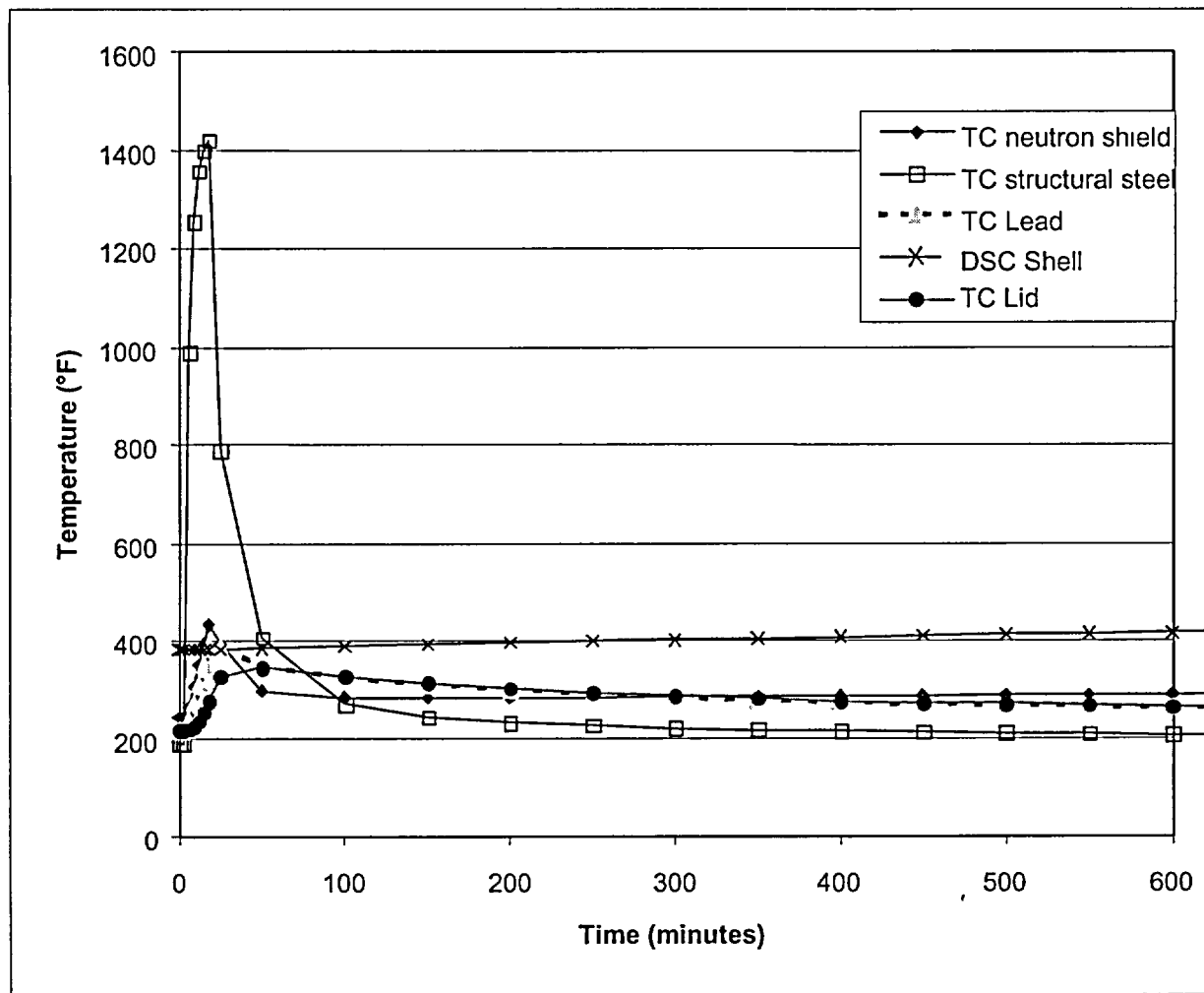


**Figure 4.6-1**  
**OS197 Cask and 24PT1-DSC Response to Fire Accident**

#### 4.7 Thermal Evaluation for Loading/Unloading Conditions

All fuel transfer operations occur when the 24PT1-DSC is in the spent fuel pool. The fuel is always submerged in free-flowing pool water permitting heat dissipation. After fuel loading is complete, the 24PT1-DSC is removed from the pool, drained, dried, and backfilled with helium.

The two loading conditions evaluated for the Advanced NUHOMS® System are the heatup of the 24PT1-DSC before its cavity can be backfilled with helium and the vacuum drying transient. Transient thermal analyses are performed to predict the heatup time history for the 24PT1-DSC components during these events.

The unloading operation considered is the reflood of the 24PT1-DSC with water.

##### 4.7.1 Vacuum Drying Thermal Analysis

Analyses were performed for the vacuum drying condition in order to ensure that the fuel cladding and 24PT1-DSC structural component temperatures remain below the maximum allowable limits shown in Table 4.7-1. For every component except the spacer disc, steady state temperature distributions gave satisfactory results. To show compliance with the ASME B&PV Code [4.7] temperature limits for the spacer disc material, transient analyses were performed to determine the time to reach 700°F, the temperature limit for SA-537, Class 2 plate. These time limits for the vacuum drying case are shown in Table 4.7-2.

For the steady state analysis, the model is similar to the model described in Section 4.4.3 and shown in Figure 4.4-6, Figure 4.4-7, and Figure 4.4-8. The exception is that the helium regions are replaced with air. Assuming that the cavity is filled with air during the vacuum drying operation provides conservative results since during the majority of the vacuum drying operation, the 24PT1-DSC cavity void volume is filled with a mixture of air, water and water vapor, and no credit is taken for evaporation of water, which is a strong cooling mechanism that takes place during this operation. Air thermal conductivity does not change significantly at lower pressures, therefore, the use of a thermal conductivity for a pressure higher than 3 Torr is acceptable. In accordance with Chapter 8, water is required to be in the annulus between the 24PT1-DSC and the transfer cask during the vacuum drying process. Therefore, the 24PT1-DSC shell boundary is set to a temperature of 230°F as a conservative estimate of the shell wall temperature during this operation. A heat load of 14 kW is considered in computing the maximum fuel cladding temperature. The 14 kW heat load is also used to *calculate* the maximum 24PT1-DSC component temperatures. The resulting maximum temperatures are tabulated in Table 4.4-6 and Table 4.4-7 for the basket structural components and fuel cladding respectively.

For the transient analysis, the model from Section 4.4.4 is used with the constant temperature boundary condition described above and the change to the helium regions described above. The density and specific heat of the basket materials and fuel assembly from Section 4.2 are also used in the HEATING7 model. The time transient is measured from the beginning of the blowdown procedure to the beginning of the final helium backfill procedure. Therefore, the initial temperature of the basket is conservatively set to the saturation temperature of water as an initial condition. The transient vacuum drying case is performed for heat loads of 13 and 14 kW.

The results of the transient analysis are presented in Table 4.7-2 and Figure 4.7-1. The resulting time limitations are incorporated into Chapter 12.

#### 4.7.2 Pressure During Unloading of Cask

To unload the fuel from the 24PT1-DSC, reflooding of the 24PT1-DSC cavity is required. This occurs by first reducing the pressure in the 24PT1-DSC to atmospheric conditions followed by introducing water into the 24PT1-DSC through the drain port and venting through the vent port. Since fuel temperatures are expected to be significantly higher than the saturation temperature of water, flooding of the hot 24PT1-DSC will result in steam being generated which, if not vented, will result in a higher cavity pressure.

The flow rate of water into the 24PT1-DSC during reflood is controlled during this operation such that the pressure within the 24PT1-DSC stays below the design pressure of 20 psig for this condition.

#### 4.7.3 Cask Heatup Analysis

Heatup of the water within the 24PT1-DSC cavity prior to blowdown and backfilling with helium occurs as operations are being performed to decon the cask and drain and dry the 24PT1-DSC. Prevention of boiling in the Advanced NUHOMS® System is not required to ensure public health and safety for the following reasons:

1. The criticality analysis already considers a wide range of moderator densities which include that of steam (Chapter 6). Criticality limits were shown to be met even at conditions of low moderator density (boiling water).
2. The cavity is always vented during the water heatup transient.
3. Although steam may be produced through boiling of the water in the 24PT1-DSC, its presence in the weld joint area during inner cover plate installation operations will be essentially blocked at the interface between the shield plug and the support ring. What little steam that may be present is displaced by the argon shielding gas used in the GTAW process. This shielding gas is heavier than air (and steam) and is delivered at a sufficiently high rate (usually 30 – 50 ft<sup>3</sup>/hr) to assure that the steam will be effectively excluded from the weld joint. Finally, if moisture somehow did enter the weld area, the resulting weld bead porosity would be readily detectable by the visual inspection of each pass performed by the welding operator and the dye penetrant (PT) examination performed on the surface of the root pass.

Therefore, the only potential concern associated with steam generation is shielding. An unexpectedly high loss of water within the 24PT1-DSC cavity during these loading operations could result in increased occupational exposure. The following analysis is presented to identify to the license holders the time for the water in the 24PT1-DSC cavity to boil so that corrective action can be planned and implemented as necessary to address ALARA concerns.

The Advanced NUHOMS® System finite difference model discussed in Section 4.4.3 is modified for this transient analysis. The 24PT1-DSC inside the transfer cask model is modified to omit the top and bottom 24PT1-DSC cover plates and the top and bottom cask cover plates. Hence, the model conservatively does not credit any heat transfer in the axial direction. Homogenized effective thermal properties of the 24PT1-DSC cavity are calculated based on the weight, volume and material of the components. Radiation heat transfer within the 24PT1-DSC cavity is neglected. All temperatures in the 24PT1-DSC are initially assumed to be at the maximum spent fuel pool temperature. The exterior of the cask is assumed to radiate and convect heat to the prevailing ambient conditions of the fuel building. The analyses are performed for two separate maximum building and fuel pool conditions, which are given in Table 4.7-3. The results are tabulated in Table 4.7-3 and shown in Figure 4.7-2 for canister decay heat loads ranging from 10 to 14 kW for the 2 cases.

#### 4.7.4 Pressure During Loading of Cask

The maximum pressure during cask blowdown is 20 psig (hydrostatic pressure of DSC water is balanced by hydrostatic pressure of DSC cask annulus). This is discussed in Chapter 3.

**Table 4.7-1**  
**Steady State Vacuum Drying Results**

| Component Heat Load | Maximum Temperature (°F) | Limit Ref (°F) |
|---------------------|--------------------------|----------------|
| Fuel [14 kW]        | 751                      | 806 Sect 3.5   |
| Support Rod [14 kW] | 502                      | 650 [4.7]      |
| Guidesleeve [14 kW] | 751                      | 800 [4.7]      |
| Boral™ [14 kW]      | 751                      | 1000 [4.7]     |
| Spacer Disc [14 kW] | 740 <sup>(1)</sup>       | 700 [4.7]      |

(1) See Table 4.7-2 for administrative time limits on vacuum drying to ensure spacer disc temperature does not exceed ASME allowable limit

**Table 4.7-2**  
**Transient Vacuum Drying Results for the Spacer Disc**

| Heat Load (kW) | Time Limit (hr) <sup>(1)</sup> |
|----------------|--------------------------------|
| <12            | No limit                       |
| 12 < q ≤ 13    | 71                             |
| 13 < q ≤ 14    | 54                             |

- (1) Time limit is defined as time for the spacer disc to reach the ASME Code limit of 700°F [4 7]. The time limit is applicable to the time from the start of blowdown of water to the time of final helium backfill, see Figure 4.7-1.

**Table 4.7-3**  
**Summary of Water Heatup Calculation**

|                                  | Case 1         | Case 2         |
|----------------------------------|----------------|----------------|
| Spent Fuel Pool Temperature (°F) | 140            | 100            |
| Building Temperature (°F)        | 120            | 100            |
| Time to reach boiling (hr)       | 14 kW. 22.5 hr | 14 kW: 37.0 hr |
|                                  | 13 kW. 24.5 hr | 13 kW: 41.0 hr |
|                                  | 12 kW: 27.0 hr | 12 kW: 45.5 hr |
|                                  | 11 kW: 30.0 hr | 11 kW: 51.0 hr |
|                                  | 10 kW: 34.0 hr | 10 kW: 58.5 hr |



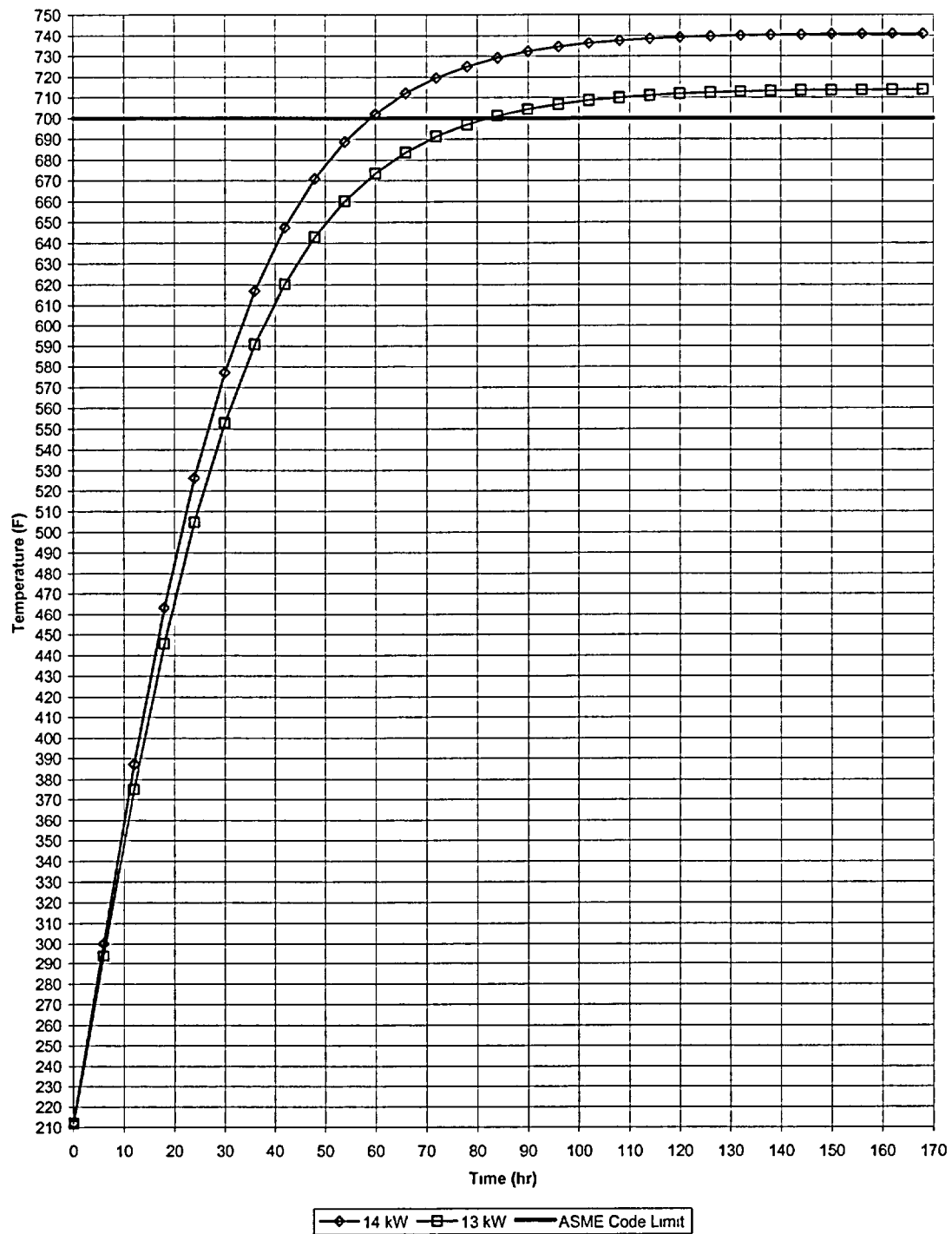


**Figure 4.7-1**  
**Vacuum Drying Transient Response of Spacer Disc**

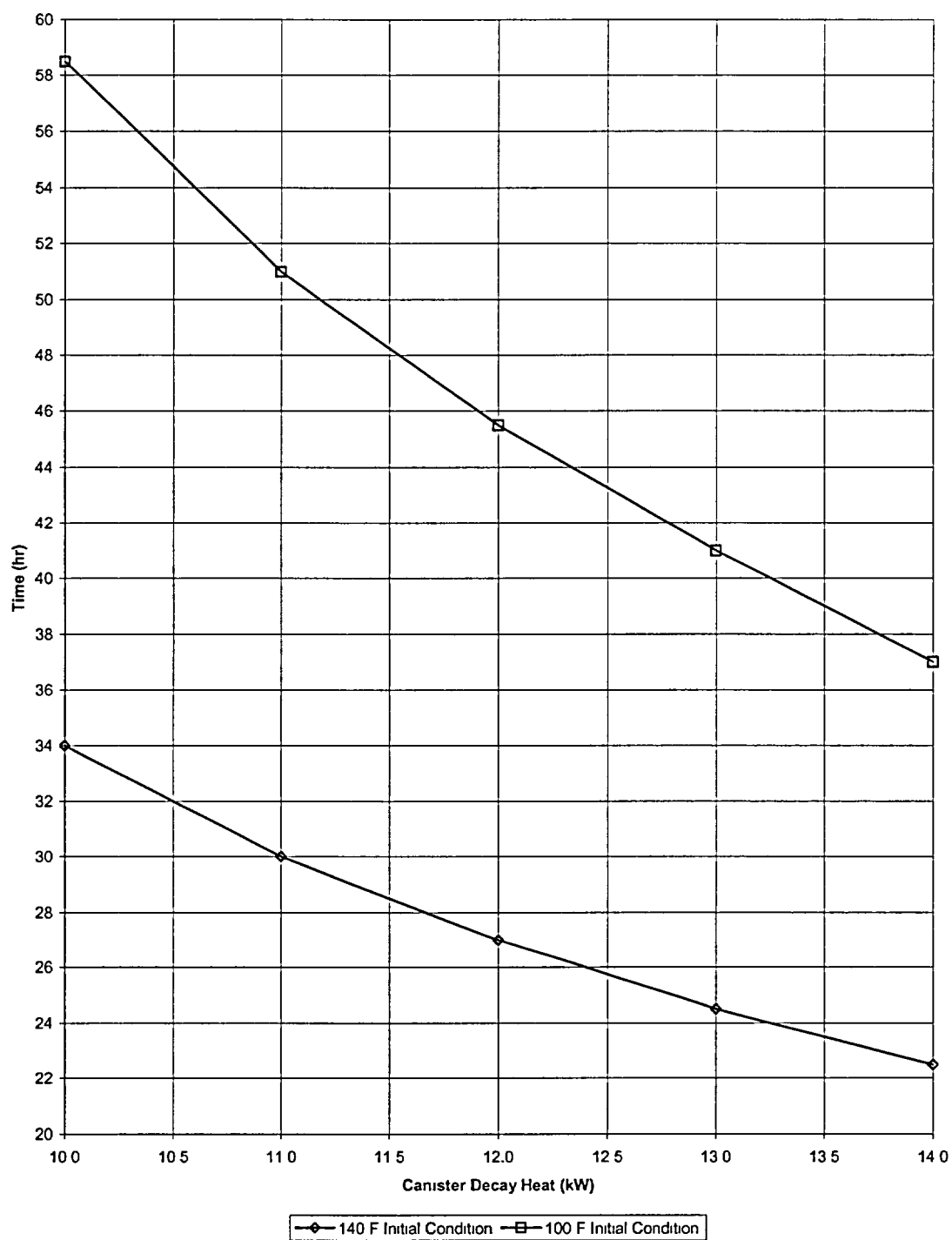


**Figure 4.7-2**  
**Results of the Water Heatup Calculations**

#### 4.8 Supplemental Information

##### 4.8.1 References

- [4.1] Levy, et. al., "Recommended Temperature Limits for Dry Storage of Spent Light Water Reactor Zircalloy - Clad Fuel Rods in Inert Gas," Pacific Northwest Laboratory, PNL-6189, 1987.
- [4.2] M. Cunningham, E. Gilbert and A. Johnson, Jr., M. A. McKinnon, "Evaluation of Expected Behavior of LWR Stainless Steel-Clad Fuel in Long-Term Dry Storage", April 1996, Electric Power Research Institute, EPRI Document TR-106440.
- [4.3] ASHRAE Handbook 1981 Fundamentals, 4th Printing, 1983.
- [4.4] "Topical Report on Actinide-Only Burnup Credit for PWR Spent Nuclear Fuel Packages," Office of Civilian Radioactive Waste Management, DOE/RW-0472, Revision 2, September 1998.
- [4.5] NRC NUREG-1536, Standard Review Plan for Dry Cask Storage Systems, January 1997.
- [4.6] Bolz, R. E., G. L. Tuve, CRC Handbook of Tables for Applied Engineering Science, 2nd Edition, 1973.
- [4.7] American Society of Mechanical Engineers, Boiler & Pressure Vessel Code, Section III, 1992 Edition with Addenda through 1994 with Code Case N-595-1.
- [4.8] "Standard Specification for BORAL™ Composite Sheet," Specification Number BPS-9000-04, AAR Advanced Structures, Livonia, Michigan. PROPRIETARY.
- [4.9] E.A. Brandes (editor), Smithells Metals Reference Book, 6th Ed., Butterworths, London, UK, 1983.
- [4.10] Roshenow, W. M., J. P. Hartnett, and Y. I. Cho, Handbook of Heat Transfer, 3rd Edition, 1998.
- [4.11] Fintel, M., Handbook of Concrete Engineering, Van Nostrand, 1974.
- [4.12] Incropera, F. P., D. P. DeWitt, Fundamentals of Heat and Mass Transfer, 3rd Edition, Wiley, 1990.
- [4.13] Bucholz, J. A., Scoping Design Analysis for Optimized Shipping Casks Containing 1-, 2-, 3-, 5-, 7-, or 10-Year old PWR Spent Fuel, Oak Ridge National Laboratory, January 1983, ORNL/CSD/TM-149.
- [4.14] Siegel, R. and J. R. Howell, Thermal Radiation Heat Transfer, 2nd Edition, Hemisphere, 1981.

- [4.15] Westinghouse Electric Corporation, Spent Fuel Dry Storage Testing at E-MAD, (March 1978 - March 1982), PNL-4533, September 1983.
- [4.16] MATPRO – Version 11: A Handbook of Materials Properties for Use in the Analysis of Light Water Reactor Fuel Rod Behavior, EG&G Idaho, Idaho Falls, February 1979, NUREG-CR/0497.
- [4.17] TN West, Final Safety Analysis Report for the Standardized NUHOMS® Horizontal Modular Storage System for Irradiated Nuclear Fuel, Revision 6, *November 2001*, NRC Docket No. 72-1004.
- [4.18] Blevins, R.D., Applied Fluid Dynamics Handbook, Van Nostrand Reinhold Company.
- [4.19] Scale, Book V. NUREG/CR-0200 Volumes 1,2, 3, ORNL/NUREG/CSD-2.
- [4.20] CFR Title 10, Part 71, Packaging and Transportation of Radioactive Material.
- [4.21] Electric Power Research Institute, “The TN-24P PWR Spent Fuel Storage Cask: Testing and Analysis”, EPRI NP-5128, April 1987.
- [4.22] Ozisik, N. M., "Basic Heat Transfer," McGraw Hill Book Company, 1977.
- [4.23] IAEA Safety Standards, “Regulations for the Safe Transport of Radioactive Materials,” 1985 Edition.
- [4.24] SAND85-0196, TTC-0659, Gregory et. al., “Thermal Measurement in a Series of Large Pool Fires,” Sandia National Laboratories, 1987.
- [4.25] White, F. M., Fluid Mechanics, 2nd Edition, McGraw-Hill, 1986.
- [4.26] Hottel, H.C. and Sarofim, A.F., “Radiative Transfer,” Chapter 4, p. 164, McGraw-Hill, New York, 1967.
- [4.27] *Nishimura, M., H. Shibasaki, S. Fujii, and I. Maekawa, Natural Convection Heat Transfer in the Horizontal Dry Storage System for the LWR Spent Fuel Assemblies, Journal of Nuclear Science and Technology, Vol. 33, No. 11, pp. 821-828, November 1996.*
- [4.28] *“NUHOMS® Modular Spent-Fuel Storage System: Performance Testing”, Report PNL-7327/UC-812/EPRI NP-6941, Pacific Northwest Laboratory & Carolina Power and Light Company, September 1990.*
- [4.29] *Calculation, “Alternative Thermal Analysis of the 24PT1 and 24PT4 Canister for SCE,” Calculation Number SCE-23.0404, Revision 1.*

#### 4.8.2 Computer Code

The HEATING7 computer program is used for the heat transfer analysis of the AHSM and 24PT1-DSC. The HEATING7 program is known as "The HEATING Program," where HEATING is an acronym for "Heat Engineering and Transfer In Nine Geometries." HEATING7 is designed to be a functional module within the SCALE system of computer programs [4.19] for performing standardized analysis for licensing evaluations of nuclear systems. Thus its features are designed to perform thermal analyses on problems arising in licensing evaluations, and its input format is designed to be compatible with that of other functional modules within the SCALE system. HEATING7 may also be used as a stand-alone heat conduction code.

HEATING7 solves steady state and/or transient heat conduction problems in one-, two-, or three-dimensional Cartesian or cylindrical coordinates or in one-dimensional spherical coordinates. The thermal conductivity, density, and specific heat may be both spatially and temperature-dependent. Selected materials may undergo a change of phase for transient calculations involving one of the explicit procedures specified. The heat generation rates may be dependent on time, temperature and position. Boundary temperatures may be dependent on time and position. Boundary conditions which may be applied along surfaces of an analytical model include specified temperatures or any combination of prescribed heat flux, forced convection, natural convection, and radiation. Models are also available to simulate the thermal fin efficiency of certain finned surfaces. In addition, one may specify radiative heat transfer across gaps or regions which are embedded in the model. The boundary condition parameters may be time- and/or temperature-dependent. The mesh spacing may be variable along each axis.

The HEATING7 thermal calculations performed for the AHSM and 24PT1-DSC employed the optional SOR solution technique of the program. This technique generally required from 200 to 300 iterations per calculation to obtain results with a convergence of better than 0.1% on the temperatures at each node in the analytical model. The -40°F ambient condition analyses required the use of the conjugate gradient technique, with the same level of accuracy and taking less than 20 iterations.

#### 4.8.3 Validation of the Thermal Analysis Methodology Using HEATING7 Model for 24PT1-DSC Basket

*This section provides a validation of the thermal analysis methodology using the HEATING7 model of the 24PT1-DSC basket as described in Section 4.4.4. This methodology is similar to the one used for the NUHOMS®-24P DSC basket described in Section 8.1.3 of Reference [4.17]. As discussed in Sections 4.2.k and 4.2.l, the effective fuel conductivity values are taken directly from Appendix B of Reference [4.17], and are used in the thermal model of the 24PT1-DSC to calculate maximum fuel cladding temperature.*

*A validation of the thermal analysis methodology, typical of the NUHOMS® basket designs which use spacer discs, has been performed against test data for NUHOMS®-7P DSC reported in Reference [4.28]. This validation methodology is documented in Appendix B of Reference [4.17]. A comparison of the calculated temperatures by this validation methodology versus measured NUHOMS®-7P test data are reproduced from Reference [4.17] in Table 4.8-1 below:*

**Table 4.8-1**  
***Comparison of DSC Component Temperatures for NUHOMS®-7P, Test Measurements vs  
Calculated from Appendix B of Reference [4.17]***

| <b>DSC Component</b>  | <b>Test<br/>Measurement<br/>(°F)</b> | <b>Calculated<br/>(°F)</b> |
|-----------------------|--------------------------------------|----------------------------|
| Maximum Fuel Cladding | 357                                  | 356 <sup>(1)</sup>         |
| Maximum Guidesleeve   | 341                                  | 361                        |

(1) Corresponds to the location of the test thermocouple. The maximum calculated temperature for the assembly is 361 °F

*These results show that the methodology, typical of NUHOMS® thermal design calculations, including the fuel effective conductivity values used, gives conservative results in predicting fuel cladding and guide sleeve temperatures.*

*In the specific case of the test data for the NUHOMS®-7P obtained from the PNL/EPRI testing [4.28], the peak system temperatures noted under helium backfill conditions was <365 °F. These temperature levels are less than the typical peak design temperatures for initial storage conditions of approximately 650 °F. Despite this fact, the use of NUHOMS®-7P test data is appropriate for validating the thermal model intended for use at the higher temperature level based on the justification provided in Section B.3.4 of Reference [4.17] and the following:*

- For a thermal model that captures the basic thermophysical processes (i.e., conduction, convection, and radiation) present, the primary areas of uncertainty will be the modeling of the geometry and the thermal properties used for each component. Once the correct geometry and thermal properties are captured, the effect of higher temperature levels on the fundamental heat transfer processes involved is well understood and documented. Thus, simply changing the temperature level for a simulation will not necessarily increase the uncertainty level for the thermal model.*
- Changes to the thermal conductivity of the metallic components with temperature are well understood and documented for temperature levels well in excess of 700 °F. As such, the effect is easily captured through the use of temperature dependant properties.*
- Radiation heat transfer is a function of view factor, surface area, and emissivity. View factors and surface area do not change with increased temperature level. As such, a thermal model that incorporates radiation exchange and which has been validated at a lower temperature will typically be conservative (i.e., yield higher temperatures) for application at the higher temperature level.*

*Therefore, a thermal model that has been properly constructed and validated using the lower temperature data from the NUHOMS®-7P test can be fully expected to yield accurate results at higher temperature levels similar to the 24PT1-DSC design.*

#### 4.8.4 Alternative Confirmatory Thermal Analysis of the 24PT1-DSC

An alternative confirmatory analysis [4.29] of the heat transfer within the 24PT1-DSC, including the effects of convection heat transfer, was conducted using the Thermal Desktop™ and SINDA/FLUINT™ software codes. These programs are designed to function together to provide the functions needed to build, exercise, and post-process a thermal model. The Thermal Desktop™ computer program is used to provide graphical input and output display function, as well as computing the radiation exchange conductors for the defined geometry and optical properties. Thermal Desktop™ is designed to run as an AutoCAD™ application. As such, all of the CAD tools available for generating geometry within AutoCAD™ can be used for generating a thermal model. In addition, the use of the AutoCAD™ layers tool presents a convenient means of segregating the thermal model into its various elements.

The SINDA/FLUINT™ computer program is a general purpose code suitable for either finite difference or finite-element models. The code can be used to compute the steady-state and transient behavior of the modeled system. SINDA/FLUINT™ has been validated for simulating the thermal response of spent fuel packages and has been used in the safety analysis of a recently approved license application.

The confirmatory calculation is based on an alternative methodology to that used for the HEATING7 model and is intended to provide a confirmation of the peak fuel cladding and critical basket temperatures determined using the HEATING7 model.

Section 4.2 obtains effective fuel conductivity values from Reference [4.17]. In contrast, the confirmatory analysis [4.29] uses a detailed model of the fuel assembly geometry to determine the thermal conductivity in the radial and axial directions for the WE 14x14 PWR fuel assemblies. The model accounts for conduction and radiation heat transfer between the individual pins of the fuel assembly, and across the gap between the edge of the fuel assembly and the guide sleeve wall. The results of this detailed modeling are used to compute an 'effective thermal conductivity' for the fuel assembly wherein the assembly is treated as a homogenized solid that extends to fill the interior of the guide sleeve. The effective thermal conductivity values are computed assuming no convection within the fuel assembly.

The effective thermal conductivity values for PWR fuel assemblies obtained from Reference [4.17] are 3 to 6 times higher than those obtained from detailed fuel assembly modeling, since they include the effects of convection outside of the fuel region. In contrast, the modeling methodology used in this confirmatory analysis provides a separate evaluation for the convection outside of the fuel regions.

To account for the natural convection heat transfer interaction within the basket assembly, the internal flow environment is divided into a series of related flow regions and the results from each region superimposed on the global solution to arrive at a unified result. Convection heat transfer coefficients are determined for each flow region based on its particular physical and behavioral characteristics. The analytical algorithms used to determine these coefficients are computed as a function of the local environment (i.e., geometry, temperatures, and pressures) and are incorporated into the SINDA/FLUINT™ thermal model iterative solution.

*The thermal model of the 24PT1-DSC developed for use in the confirmatory analysis is based on the same basket geometry, gap assumptions and material properties as the HEATING7 model.*

*Table 4.8-2 presents a comparison of the 24PT1-DSC component temperatures obtained using the HEATING7 model vs. those obtained using the confirmatory analysis methodology. In each case, the shell temperature distribution around the circumference of the 24PT1-DSC was input to the analysis as a boundary condition. As seen from the table, the results from the HEATING7 model are within 2% of the absolute maximum fuel cladding temperature (°R) as predicted by the alternative methodology and conservatively bound the confirmatory analysis predicted peak temperatures for the guidesleeve and spacer disc.*

*These results demonstrate that the HEATING7 model predicts accurate fuel cladding temperatures and conservatively bounding basket component temperature levels for the 24PT1-DSC.*

*The confirmatory testing methodology has also been validated against the NUHOMS® system test data [4.27] and [4.28]. A comparison of these tests against the SINDA/FLUINT™ confirmatory analysis model is provided in Table 4.8-3, Figure 4.8-1 and Figure 4.8-2. These comparisons show a very good agreement between the confirmatory analysis method and the test results.*

*A comparison of the SINDA/FLUINT™ analysis as well as the test results to the HEATING7 model indicates a more pronounced shift in the maximum temperature toward the top of the 24PT1-DSC. This temperature shift is expected as a result of the convection within the 24PT1-DSC. The convection causes the hot air to shift the peak temperatures toward the top of the horizontally stored 24PT1-DSC.*

*Figure 4.8-3 provides a pictorial representation of the convection flow patterns expected within the 24PT1-DSC based on KHI test data [4.27].*



Table 4.8-2

**Comparison of 24PT1-DSC Component Temperatures, FSAR Analysis vs. Confirmatory Analysis with Internal Convection**

| <b>DSC Component</b>  | <b>FSAR Analysis with HEATING7</b> | <b>Confirmatory Analysis with Internal Convection<sup>(1)</sup></b> |
|-----------------------|------------------------------------|---|
| Maximum Fuel Cladding | 624 °F                             | 623 °F  |
| Maximum Guidesleeve   | 624 °F                             | 594 °F  |
| Maximum Spacer Disc   | 623 °F                             | 576 °F  |

Notes:

(1) Calculated DSC internal pressure of 7.5 psig is used

Table 4.8-3

**Comparison of DSC Component Temperatures for NUHOMS®-7P, Test Measurements vs. Confirmatory Analysis**

| <b>DSC Component</b>  | <b>Test Measurement</b> | <b>Confirmatory Analysis Methodology</b> |
|-----------------------|-------------------------|--|
| Maximum Fuel Cladding | 357 °F                  | 365 °F                                   |
| Maximum Guidesleeve   | 341 °F                  | 350 °F                                   |
| Maximum Spacer Disc   | N/A <sup>(1)</sup>      | 330 °F                                   |

Note:

(1) Spacer disc temperature not measured in test

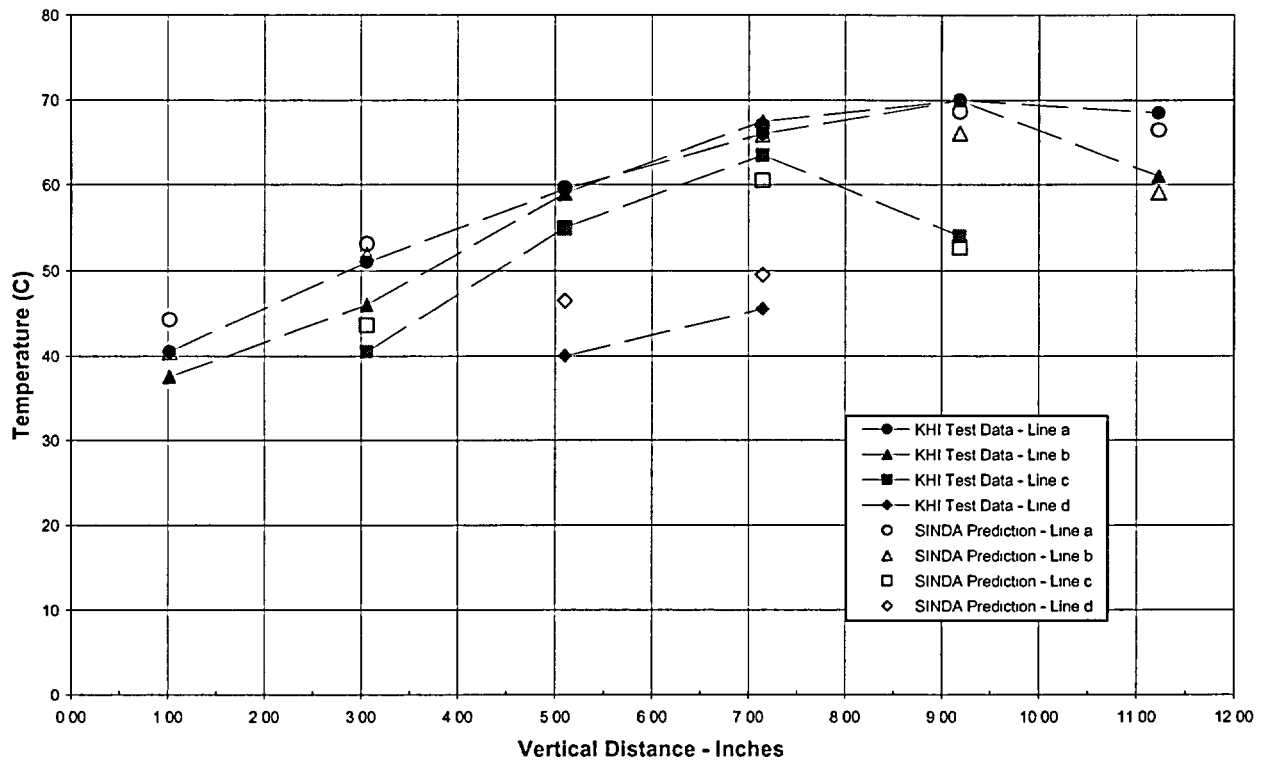


**Figure 4.8-1**  
**Comparison of Predicted SINDA/FLUINT™ Temperatures to KHI Test Results**

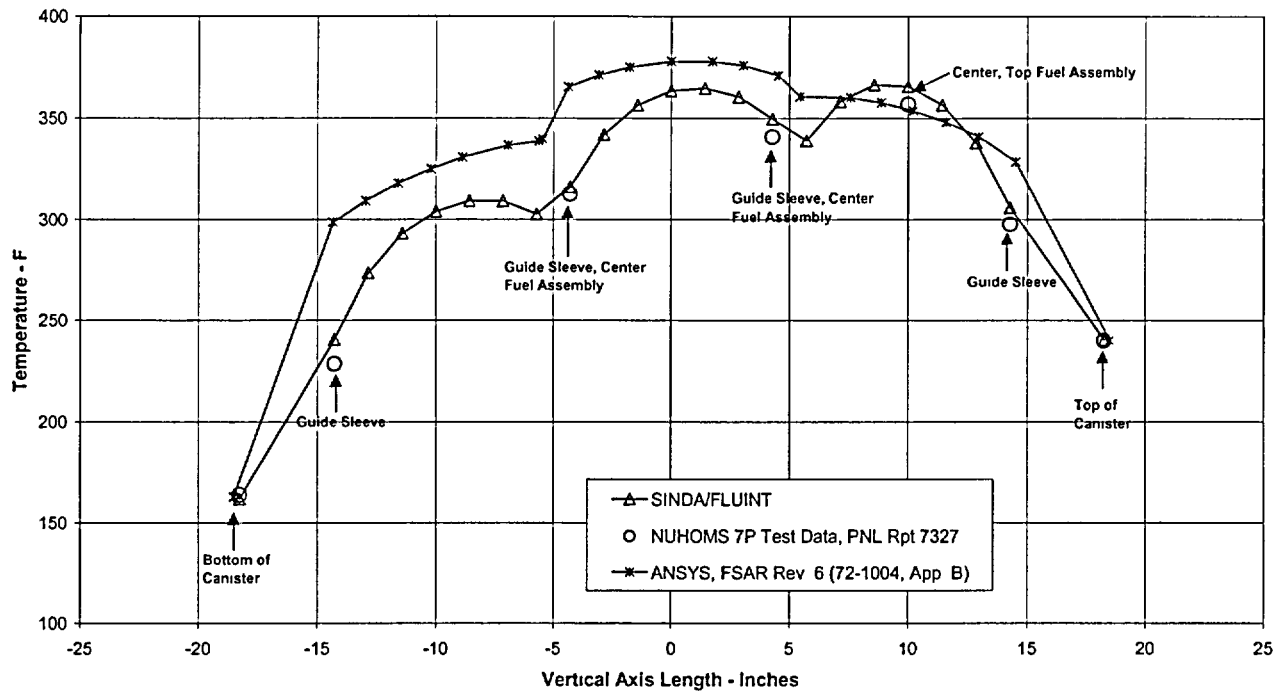


**Figure 4.8-2**  
**Comparison of Predicted vs. Test Results (PNL-7327) for NUHOMS®-7P**

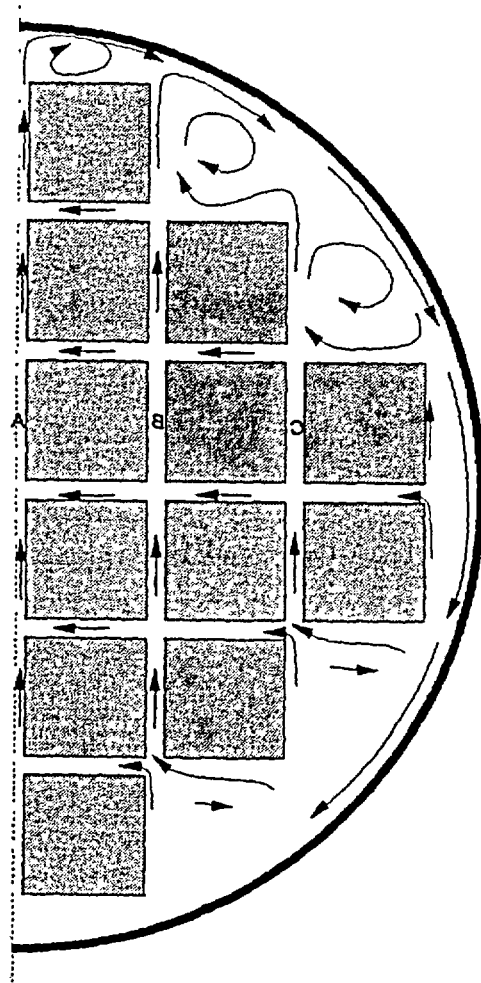


**Figure 4.8-3**  
**General Flow Patterns Expected within Canister**

## 5. SHIELDING EVALUATION

The shielding evaluation presented for the Advanced NUHOMS® System demonstrates adequacy of the shielding design for the payload described in Chapter 2. The geometry of the Advanced NUHOMS® System is described in Section 1.5.2. The heavy concrete walls and roof of the Advanced Horizontal Storage Module (AHSM) provide the bulk of the shielding for the payload in the storage condition. During fuel loading and transfer operations, the combination of thick steel shield plugs at the ends of the 24PT1-DSC and heavy steel/lead/neutron shield material of the OS197 transfer cask (Docket Number 72-1004 [5.8]) provide shielding for personnel loading and transferring the 24PT1-DSC to the AHSM. Figure 5.1-1 through Figure 5.1-4, and Table 5.1-1 provide the general configuration and material thicknesses of the important components of the Advanced NUHOMS® System.

For this shielding evaluation source terms are calculated for two fuel assembly designs:

- Westinghouse 14x14 (WE 14x14) stainless steel clad (SC) PWR assemblies, (with or without IFBA fuel rods)
- WE 14x14 Zircaloy clad Mixed Oxide (MOX) PWR assemblies

Also included in the source term calculation is the Non-Fuel Assembly Hardware (NFAH) including:

- Rod Cluster Control Assembly (RCCA),
- Thimble Plug Assembly (TPA) and
- Neutron Source Assembly (NSA).

A single bounding burnup/enrichment and cooling time is addressed for MOX fuel. Several burnup/enrichment combinations with 10 year cooling are addressed for the SC fuel to provide more flexibility in qualifying fuel for storage. These combinations form the basis for the Advanced NUHOMS® System fuel specifications in Chapter 12. Bounding operating histories are assumed for the NFAH with a minimum cooling time of 10 years. The methodology, assumptions, and criteria used in this evaluation are summarized in the following subsections.

*Section 5.5.2 provides a three dimensional (3-D) shielding analysis for the Advanced NUHOMS® System using MCNPX [5.10]. The results demonstrate that the dose rates predicted by the 3-D analysis are bounded by those predicted by a two dimensional analysis using DORT. In addition, a validation of the 3-D analysis against test data is also provided.*

## 5.1 Discussion and Results

The maximum, minimum and average dose rates due to 24 design basis PWR fuel assemblies stored with 24 design basis NFAH (Thimble Plugs) in the Advanced NUHOMS® System are summarized in Table 5.1-2 through Table 5.1-5. Table 5.1-2 provides the dose rates on the surface of the AHSM while Table 5.1-3 through Table 5.1-5 provide the dose rates on and around the Transfer Cask (top, bottom and sides) during fuel loading, and transfer operations.

As stated above, the Advanced NUHOMS® System is capable of storing stainless steel clad fuel, MOX fuel, and NFAH such as the RCCAs, the TPAs, and the NSAs. Based on the source term calculations presented in Section 5.2, the design basis fuel source term is a stainless steel clad fuel assembly with 45 GWd/MTU burnup, a minimum initial enrichment of 3.8 weight % U-235 and a cooling time of 10 years. The design basis NFAH source term is a TPA assembly irradiated for eleven cycles and a cooling time of 10 years.

A discussion of the method used to determine the design basis fuel and NFAH source terms is included in Section 5.2. The model specification and shielding material densities are given in Section 5.3. The method used to determine the dose rates due to 24 design basis fuel assemblies with 24 design basis NFAH in the Advanced NUHOMS® System is provided in Section 5.4.

Normal and off-normal conditions are modeled with the Advanced NUHOMS® System intact, including the filled neutron shield in the transfer cask. The shielding calculations are performed using the DORT 2-dimensional discrete ordinate deterministic transport code [5.2] with the CASK-81 cross-section library [5.3]. Average and peak dose rates on the front, side, top and back of the AHSM and the OS197 Transfer Cask System are calculated. Occupational doses during loading, transfer to the ISFSI, and maintenance and surveillance operations are provided in Chapter 10. Locations where streaming could occur are discussed in Chapter 10.

For accident conditions (e.g., cask drop, fire), the transfer cask neutron shield (water) including the steel skin (shown in Figure 5.1-4) are assumed to be removed. The results of this analysis are addressed in Chapter 11. Site dose and occupational dose analyses are addressed in Chapter 10 (including requirements for site specific 72.104 and 72.106 analyses).

**Table 5.1-1**  
**Advanced NUHOMS® System Shielding Materials**

**AHSM**

| Components            | Thickness/Material Modeled    |
|-----------------------|-------------------------------|
| Side Walls            | 1' concrete                   |
| Side Shield Wall      | 3' concrete                   |
| Roof                  | 5' concrete                   |
| Rear Wall             | Minimum thickness 1' concrete |
| Rear Shield Wall      | 3' concrete                   |
| Front Door/Front Wall | 2' thick concrete             |

**24PT1-DSC**

| Components                       | Thickness/Material Modeled  |
|----------------------------------|---|
| Bottom Shield Plugs/Cover Plates | 8.75" Steel   |
| Top Shield Plugs/Cover Plates    | 10.25" Steel  |
| Cylindrical shell                | 0.625" Steel  |
| Basket (main components)         | 26 Steel Spacer Discs, 1.25" thick each, and<br>24 Steel Guide Tubes with Boral™ Sheets |

**OS197 Transfer Cask**

| Components         | Thickness/Material Modeled |
|--------------------|----------------------------|
| Top Cover Plate    | 2" NS3 and 3.25" Steel     |
| Bottom Cover Plate | 2.25" NS3 and 2.75" Steel  |
| Radial walls       |                            |
| Inner Shell        | 0.5" Steel                 |
| Lead Gamma Shield  | 3.56" Lead                 |
| Structural Shell   | 1.5" Steel                 |
| Neutron Shield     | 3" Water                   |
| Skin               | 0.19" Steel                |

**Table 5.1-2**  
**Summary AHSM Dose Rates**

| Surface             | Dose Rate Component | Maximum Dose Rate, mrem/hr | Minimum Dose Rate, mrem/hr | Average Surface Dose Rate <sup>(2)</sup> , mrem/hr |
|---------------------|---------------------|----------------------------|----------------------------|--|
| Rear <sup>(1)</sup> | Gamma               | 0.11                       | 1.06E-04                   | 4.06E-03   |
|                     | Neutron             | 0.01                       | 3.04E-06                   | 3.70E-04   |
| Front               | Gamma               | 45.27                      | 1.59E-02                   | 1.89   |
|                     | Neutron             | 0.54                       | 6.99E-04                   | 0.04   |
| Roof                | Gamma               | 3.57                       | 3.57E-04                   | 0.03   |
|                     | Neutron             | 0.05                       | 2.37E-05                   | 8.56E-04   |
| Side <sup>(1)</sup> | Gamma               | 1.35                       | 5.13E-06                   | 0.26   |
|                     | Neutron             | 0.03                       | 4.61E-08                   | 0.01   |

(1) Rear and side does rates are on the outer surfaces of the shield walls

(2) These dose rates are bounding for 1 meter occupational exposures during transfer operations.



**Table 5.1-3**  
**Transfer Cask (Loading/Unloading/Transfer Operations) Side Dose Rate Summary**

| Stage of<br>TC/24PT1-DSC<br>Processing | Dose Rate<br>mrem/hr | On Outside<br>Surface |         | One Foot from<br>Surface |         | Three Feet from<br>Surface |         |
|--|----------------------|-----------------------|---------|--------------------------|---------|----------------------------|---------|
|  |                      | Gamma                 | Neutron | Gamma                    | Neutron | Gamma                      | Neutron |
| Wet Welding                            | Maximum              | 144.88                | 2.85    | 105.21                   | 1.90    | 66.09                      | 1.13    |
|  | Minimum              | 0.04                  | 0.00    | 0.55                     | 0.01    | 1.35                       | 0.03    |
|  | Average<br>Surface   | 63.06                 | 1.19    | 44.13                    | 0.82    | 28.68                      | 0.52    |
|  | At Center<br>Line    | 142.35                | 2.83    | 99.30                    | 1.90    | 64.42                      | 1.13    |
| Dry Welding                            | Maximum              | 390.32                | 99.07   | 282.84                   | 66.22   | 174.45                     | 38.87   |
|  | Minimum              | 1.47                  | 2.51    | 2.96                     | 2.41    | 5.25                       | 2.57    |
|  | Average<br>Surface   | 173.98                | 46.74   | 123.73                   | 31.12   | 80.75                      | 19.39   |
|  | At Center<br>Line    | 382.61                | 97.51   | 263.04                   | 65.72   | 169.63                     | 38.57   |
| Transfer                               | Maximum              | 427.15                | 207.63  | 307.27                   | 97.99   | 188.42                     | 57.54   |
|  | Minimum              | 1.65                  | 3.22    | 2.32                     | 2.98    | 5.79                       | 4.05    |
|  | Average<br>Surface   | 187.44                | 72.65   | 134.29                   | 48.08   | 87.58                      | 29.88   |
|  | At Center<br>Line    | 419.24                | 144.53  | 286.54                   | 97.32   | 183.18                     | 57.14   |

**Table 5.1-4**  
**Transfer Cask (Loading/Unloading/Transfer Operations) Top End Dose Rate Summary**

| Stage of<br>TC/24PT1-DSC<br>Processing | Dose Rate<br>mrem/hr | On Outside<br>Surface |         | One Foot from<br>Surface |         | Three Feet from<br>Surface |         |
|--|----------------------|-----------------------|---------|--------------------------|---------|----------------------------|---------|
|  |                      | Gamma                 | Neutron | Gamma                    | Neutron | Gamma                      | Neutron |
| Wet Welding                            | Maximum              | 238.36                | 0.13    | 158.49                   | 0.08    | 85.09                      | 0.05    |
|  | Minimum              | 2.09                  | 0.00    | 3.95                     | 0.00    | 4.05                       | 0.00    |
|  | Average<br>Surface   | 28.58                 | 0.06    | 26.10                    | 0.04    | 22.04                      | 0.02    |
|  | At Center<br>Line    | 194.50                | 0.01    | 158.02                   | 0.00    | 84.26                      | 0.00    |
| Dry Welding                            | Maximum              | 697.26                | 17.53   | 301.15                   | 7.61    | 99.37                      | 3.99    |
|  | Minimum              | 7.37                  | 4.51    | 5.89                     | 3.53    | 4.29                       | 1.81    |
|  | Average<br>Surface   | 26.15                 | 7.84    | 18.62                    | 5.36    | 13.16                      | 2.83    |
|  | At Center<br>Line    | 44.79                 | 9.31    | 33.59                    | 6.46    | 16.91                      | 2.71    |
| Transfer-<br>Storage                   | Maximum              | 26.09                 | 22.91   | 15.99                    | 14.35   | 5.98                       | 6.99    |
|  | Minimum              | 1.35                  | 2.62    | 1.89                     | 3.81    | 1.35                       | 2.52    |
|  | Average<br>Surface   | 14.32                 | 13.35   | 7.35                     | 8.12    | 3.23                       | 3.91    |
|  | At Center<br>Line    | 7.15                  | 20.00   | 5.26                     | 14.33   | 2.56                       | 6.36    |

Table 5.1-5

**Transfer Cask (Loading/Unloading/Transfer Operations) Bottom End Dose Rate Summary**

| Stage of<br>TC/24PT1-DSC<br>Processing | Dose Rate<br>mrem/hr | On Outside<br>Surface |         | One Foot from<br>Surface |         | Three Feet from<br>Surface |         |
|--|----------------------|-----------------------|---------|--------------------------|---------|----------------------------|---------|
|  |                      | Gamma                 | Neutron | Gamma                    | Neutron | Gamma                      | Neutron |
| Transfer                               | Maximum              | 293.41                | 426.56  | 122.65                   | 148.32  | 44.32                      | 46.21   |
|  | Minimum              | 0.66                  | 11.07   | 2.44                     | 9.02    | 2.51                       | 4.98    |
|  | Average<br>Surface   | 18.93                 | 26.84   | 11.64                    | 19.91   | 6.85                       | 12.05   |
|  | At Center<br>Line    | 293.41                | 426.56  | 122.65                   | 148.32  | 39.57                      | 46.21   |

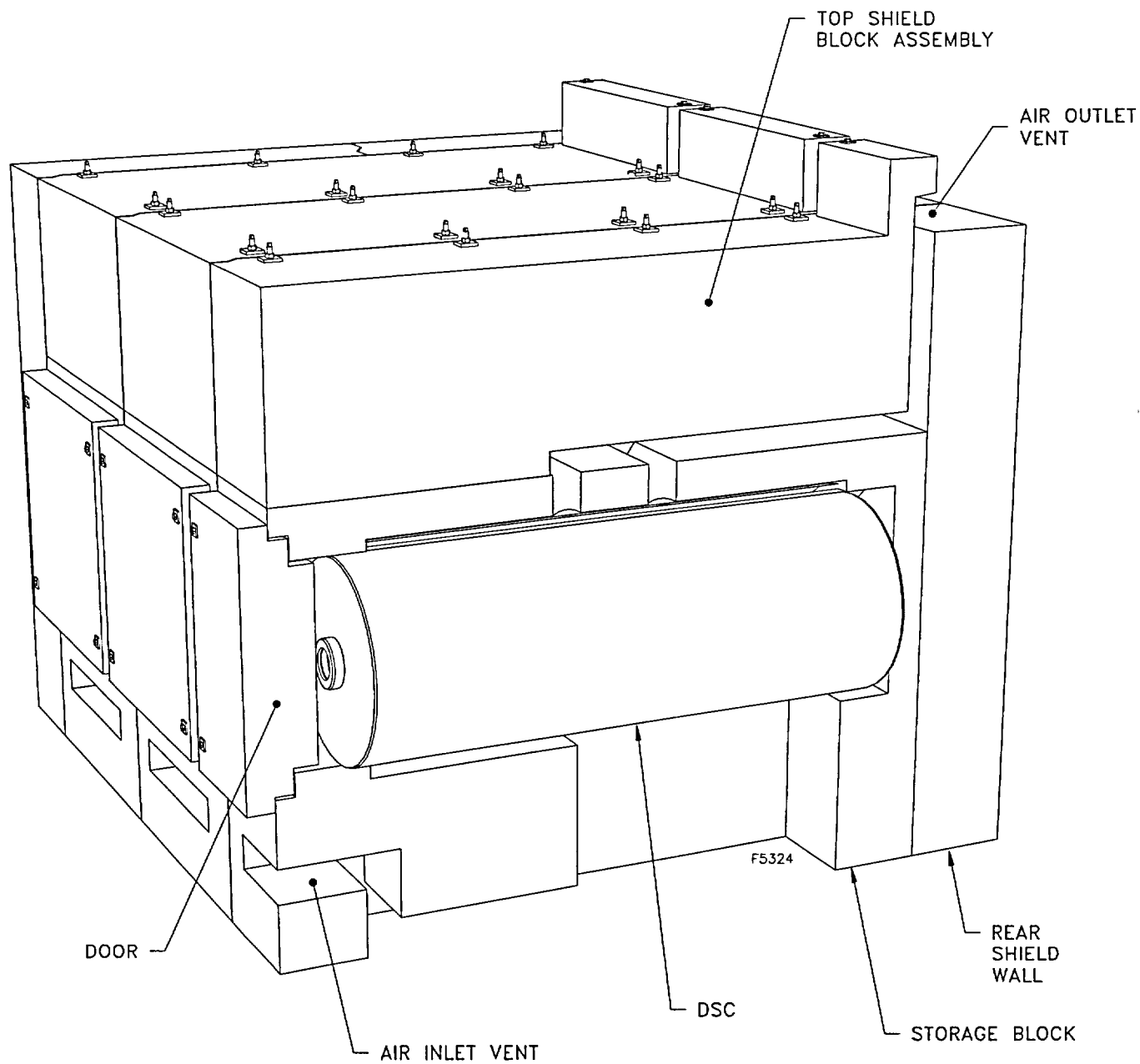


**Figure 5.1-1**  
**Advanced NUHOMS® System Shielding Configuration**

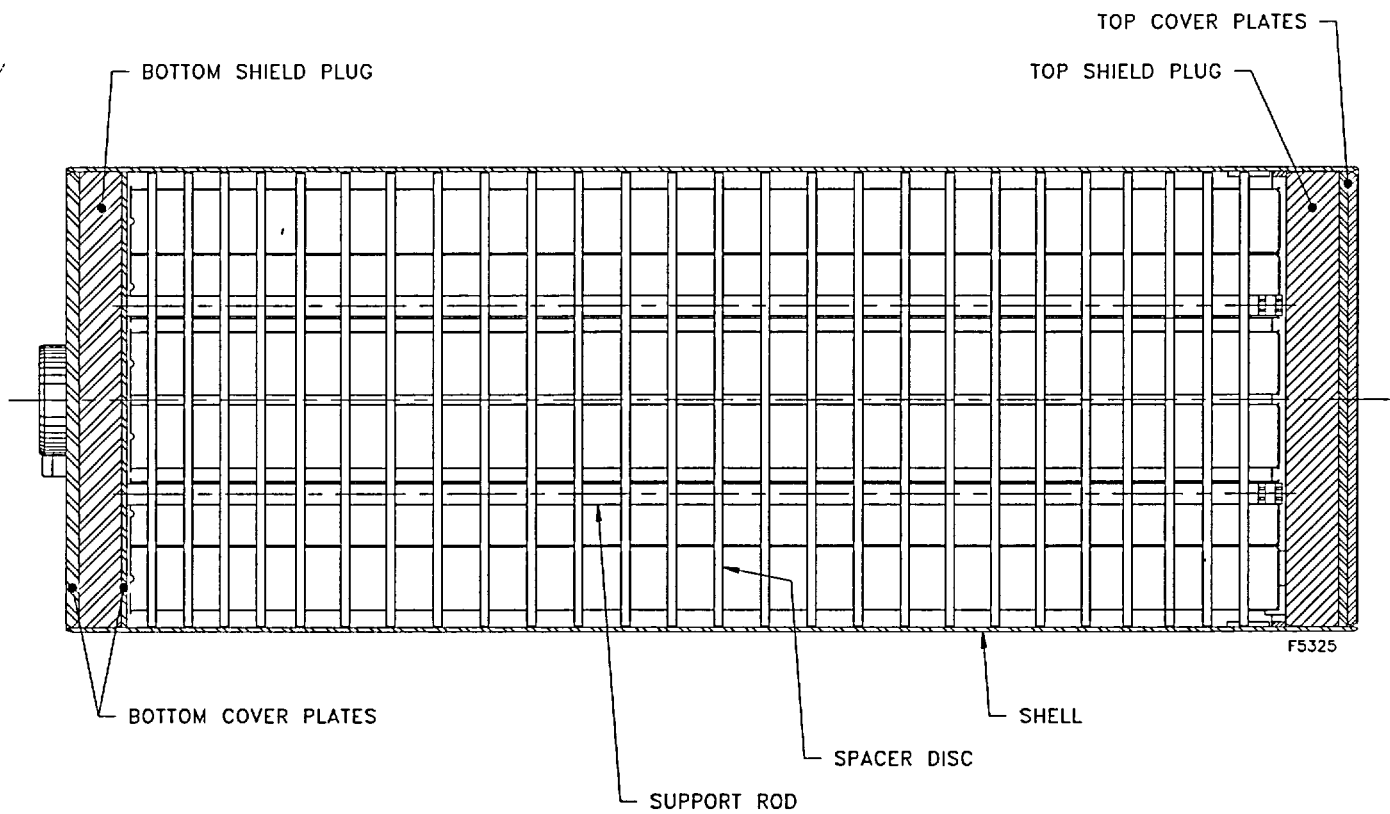


**Figure 5.1-2**  
**Dry Shielded Canister Shielding Configuration**

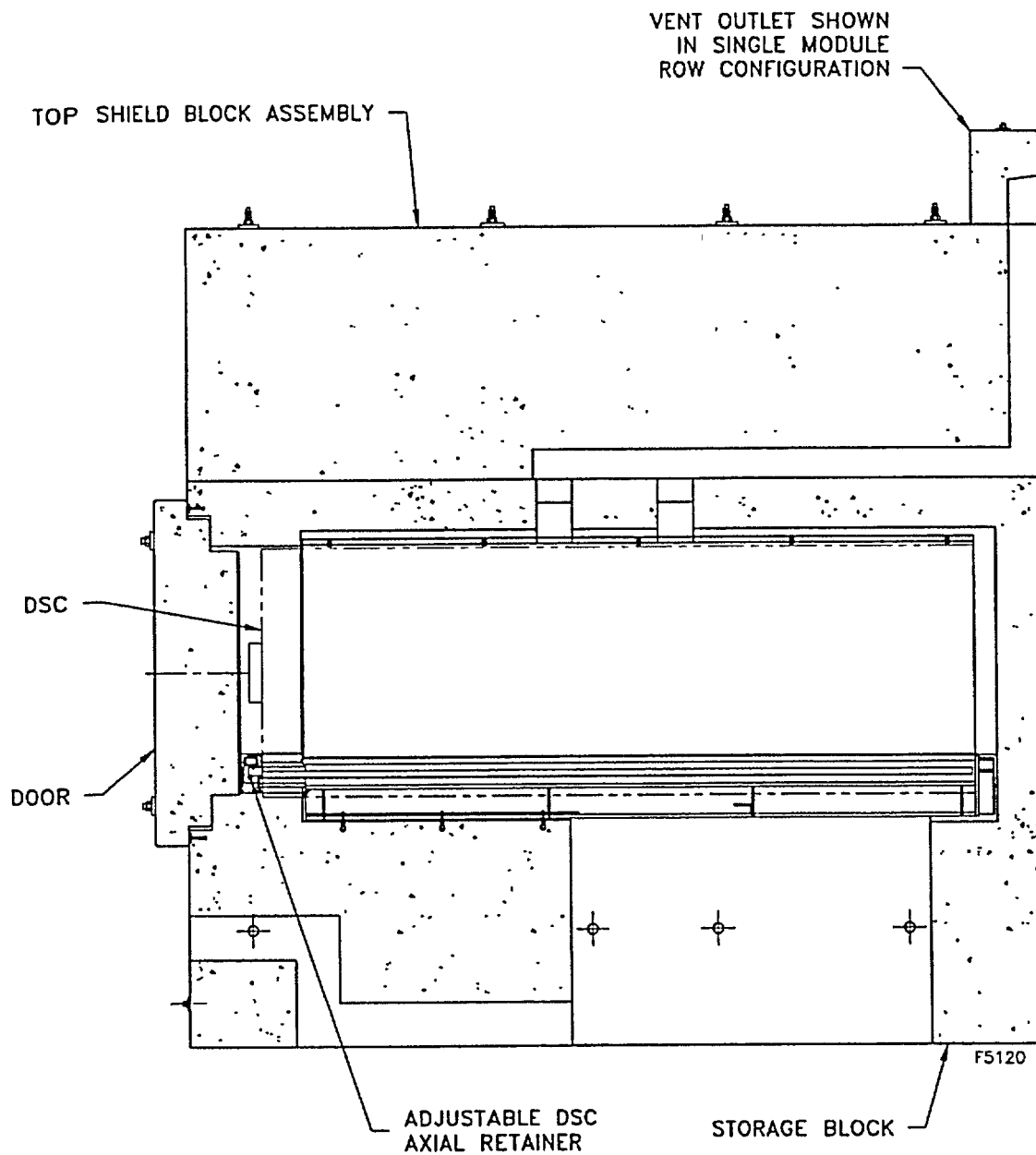


**Figure 5.1-3**  
**Right Elevation Cross Section View of AHSM**

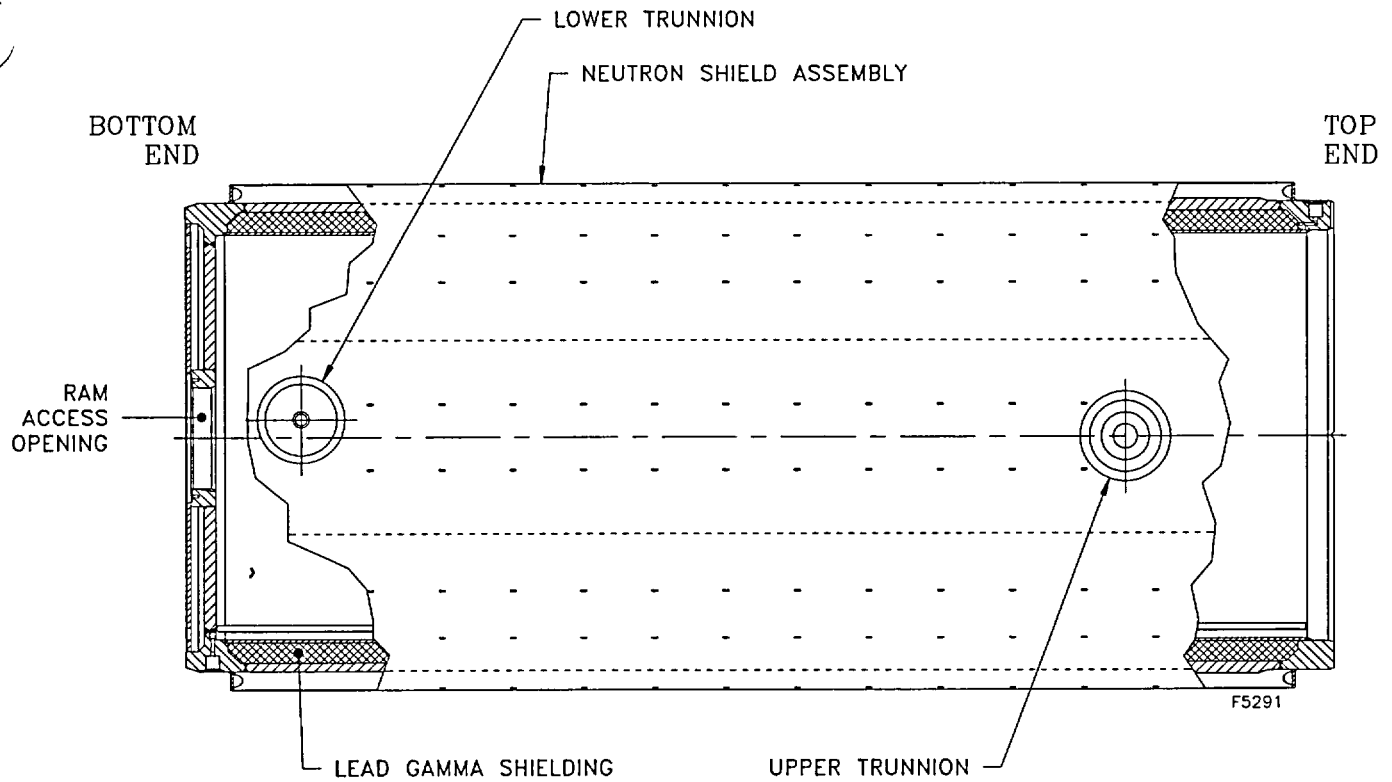


**Figure 5.1-4**  
**Shielding Configuration of the OS197 Transfer Cask**

## 5.2 Source Specification

Source terms are calculated with the SAS2H (ORIGEN-S) module of SCALE 4.4 [5.1]. The following sub-sections provide a discussion of the fuel assembly and Non-Fuel Assembly Hardware (NFAH) material weights and composition, gamma and neutron source terms and energy spectrum. The SAS2H results are used to develop source terms suitable for use in the shielding calculations.

There are five principal sources of radiation associated with the Advanced NUHOMS<sup>®</sup> System that are of concern for radiation protection. These are:

1. Primary gamma radiation from the spent fuel
2. Primary gamma radiation from activation products in the structural materials found in the spent fuel assembly and the NFAH
3. Primary neutron radiation from the spent fuel
4. Neutrons produced from sub-critical multiplication in the fuel
5. Capture gammas from (n, $\gamma$ ) reactions in the Advanced NUHOMS<sup>®</sup> System materials

The first three sources of radiation are evaluated using SAS2H. The capture gamma radiation and sub-critical multiplication are handled as part of the shielding analysis which is performed with DORT [5.2] and the CASK-81 [5.3] cross-section library.

The neutron flux during reactor operation is peaked in the active fuel (in-core) region of the fuel assembly and drops off rapidly outside the in-core region. Much of the fuel assembly hardware is outside of the in-core region of the fuel assembly. To account for this reduction in neutron flux, each fuel assembly type is divided into four exposure zones. A neutron flux (fluence) correction is applied to each region to account for this reduction in neutron flux outside the in-core region. The correction factors are given in Table 5.2-1. The four exposure zones, or regions are [5.4]:

Bottom—location of fuel assembly bottom nozzle and fuel rod end plugs  
In-core—location of active fuel  
Plenum—location of fuel rod plenum spring and top plug  
Top—location of top nozzle

A fifth region, the above top nozzle region, encompasses any material located above the top nozzle region. RCCAs are the only non-fuel hardware (NFAH) components considered in this calculation that extend into this region during irradiation.

### WE 14x14 SC Assemblies

The fuel assembly materials and masses for each irradiation zone of the assembly are listed in Table 5.2-2 for the WE 14x14 SC assembly. These materials are irradiated in the appropriate



fuel assembly region in the SAS2H models for the following three burnup, minimum weight percentage (weight %) initial enrichment and post irradiation cooling time cases:

- 35 GWd/MTU, 3.16 weight % U-235, 10-year cooled
- 40 GWd/MTU, 3.40 weight % U-235, 10-year cooled
- 45 GWd/MTU, 3.80 weight % U-235, 10-year cooled

The minimum enrichments associated with maximum burnups provide conservative source terms.

#### WE 14x14 MOX Assemblies

The fuel assembly materials and masses for each irradiation zone of the assembly are listed in Table 5.2-3 for the WE 14x14 MOX assembly. These materials are irradiated in the appropriate fuel assembly region in the SAS2H models for the following burnup and cooling time case:

- 25 GWd/MTU, 0.71 weight % U-235, 20-year cooled
- Minimum Fissile Pu weight percent\* of 2.78 (64 rods), corresponding to fuel rods with a maximum enrichment of 2.84 weight %
- Minimum Fissile Pu weight percent\* of 3.05 (92 rods), corresponding to fuel rods with a maximum enrichment of 3.1 weight %
- Minimum Fissile Pu weight percent\* of 3.25 (24 rods), corresponding to fuel rods with a maximum enrichment of 3.31 weight %

\* Fissile Pu weight percent =  
$$(\text{weight of Pu}^{239} + \text{weight of Pu}^{241}) / (\text{total weight of Pu} + \text{Total weight of U})$$

#### TPA

The TPA materials and masses for each irradiation zone are listed in Table 5.2-4. These materials are irradiated in the appropriate zone for eleven cycles of operation. The TPA is irradiated to an equivalent assembly life burnup of 165 GWd/MTU over 11 cycles. The model assumes that the TPA is irradiated in four separate WE 14x14 SC assemblies each with an initial enrichment of 3.80 weight % U-235 (minimum enrichment for design basis fuel assembly). Each fuel assembly, containing the TPA, except the fourth, is burned for three cycles with a burnup of 15 GWd/MTU per cycle. This is equivalent to an assembly life burnup of 45 GWd/MTU over the three cycles. The fourth assembly is only burned for two cycles of 15 GWd/MTU each.

#### RCCA

The RCCA materials and masses for each irradiation zone are listed in Table 5.2-5. These materials are irradiated in the appropriate zone for eleven cycles of operation. The RCCA is irradiated to an equivalent assembly life burnup of 165 GWd/MTU over 11 cycles. The model assumes that the RCCA is irradiated in four separate WE 14x14 SC Assemblies each with an initial enrichment of 3.80 weight % U-235 (minimum enrichment for design basis fuel assembly). Each fuel assembly containing the RCCA, except the fourth, is burned for three cycles with a burnup of 15 GWd/MTU per cycle. This is equivalent to an assembly life burnup of

45 GWd/MTU over the three cycles. The fourth is only burned for two cycles of 15 GWd/MTU each.

### NSA

The NSA materials and masses for each irradiation zone are listed in Table 5.2-6. These materials are irradiated in the appropriate zone for four cycles of operation. The model assumes that the NSA is irradiated in a single WE 14x14 SC assembly with an initial enrichment of 3.80 weight % U-235 (minimum enrichment for design basis fuel assembly). The fuel assembly is burned for four cycles with a burnup of 15 GWd/MTU per cycle. The NSA is irradiated to an equivalent assembly life burnup of 60 GWd/MTU over the four cycles.

### Elemental Compositions of Structural Materials

To account for the source terms due to the elemental composition of the fuel assembly and NFAH structural materials the following methodology is used:

- 1) The material composition for each irradiation region is determined for each assembly and NFAH type.
- 2) The elemental compositions for each of the structural materials present in each region is determined by multiplying the total weight of each material in a specific irradiation zone by the elemental compositions given in Table 5.2-18. The fuel assembly and NFAH elemental composition, including impurities, for each material are taken from Reference [5.9].
- 3) The results of each material are summed to determine the total elemental composition for each irradiation zone.
- 4) The elemental composition is multiplied by the appropriate flux factor given Table 5.2-1.
- 5) Finally, the elemental composition is entered in the light element card of the SAS2H input.

The SAS2H calculation applies the total flux to the light elements; therefore, the total composition must be adjusted by the appropriate flux factor in the input. A SAS2H input is created for each irradiation zone of each fuel assembly and NFAH type.

#### 5.2.1 Gamma Sources

Source terms for each fuel assembly type and associated burnup/initial enrichment/cooling times and NFAH components are calculated with SAS2H module. The SAS2H calculated contributions from actinides, fission products, and activation products, as applicable, are included for each irradiation region. The results from the SAS2H calculations are modified with ORIGEN-S to output the sources in the CASK-81 [5.3] group structure. Table 5.2-7 provides the CASK-81 neutron and gamma energy group structure. The 10-year post irradiation cooling time results for the WE 14x14 SC fuel with burnup/initial enrichment (weight % U-235) combinations

of 45 GWd/MTU/ 3.80 weight % U-235; 40 GWd/MTU/3.40 weight % U-235; and 35 GWd/MTU/3.16 weight % U-235 are shown in Table 5.2-8, Table 5.2-9, and Table 5.2-10, respectively. The 20-year post irradiation cooling time results for the 25 GWd/MTU burnup of the WE 14x14 MOX fuel assembly are shown in Table 5.2-11. The 10-year post irradiation cooling time results for the TPA, RCCA and NSA are shown in Table 5.2-12, Table 5.2-13, and Table 5.2-14, respectively.

Based on the results presented in Table 5.2-8 through Table 5.2-11 it is determined that the design basis fuel assembly source term is for the WE 14x14 SC assembly with 45 GWd/MTU Burnup, 3.80 weight % U-235 initial enrichment and 10-year cooling time. Based on the results presented in Table 5.2-12 through Table 5.2-14 (maximum gamma source term) the design basis NFAH is the TPA because it contains the maximum volumetric gamma source ( $\gamma/\text{cm}^3\text{-s}$ ). Although the TPA does not represent the highest total gamma source ( $\gamma/\text{s}$ ), the highest volumetric source generates the most conservative source term. The spectrum is dominated by Co-60 for all NFAH. These design basis sources are used in the DORT calculations to determine the bounding dose rates on and around the Advanced NUHOMS® System, including the Transfer Cask.

In the DORT models the bottom nozzle region is modeled as a cylinder 3.9 inches tall with a diameter of 56.7 inches. The volume of this cylinder is, therefore,  $1.61 \times 10^5 \text{ cm}^3$ . The in-core region is modeled as a cylinder 120 inches tall. The volume of this cylinder is, therefore,  $4.96 \times 10^6 \text{ cm}^3$ . The plenum region is modeled as a cylinder 6.0 inches tall with a volume of  $2.48 \times 10^5 \text{ cm}^3$ . Finally, the top region is modeled as a cylinder 8.6 inches tall for a volume of  $3.56 \times 10^5 \text{ cm}^3$ . The resulting volumetric gamma sources in the CASK-81 group structure for use in DORT models are shown in Table 5.2-15.

### 5.2.2 Neutron Source

The total neutron source for the Advanced NUHOMS® System is calculated with SAS2H. The total neutron sources for each assembly type and burnup/initial enrichment combination is summarized in Table 5.2-16. Again, the design basis source term is for the WE 14x14 SC fuel with 45 GWd/MTU burnup, 3.80 weight % U-235 initial enrichment and 10-year cooling time. The neutron source term consists primarily of spontaneous fission neutrons (largely from Cm-244) with ( $\alpha$ ,O-18) sources of lesser importance, both causing secondary fission neutrons. The overall spectrum is well represented by the Cm-244 fission spectrum. The neutron source term for DORT models is generated by taking the total neutron source for the design basis fuel assembly multiplying by 24 assemblies and dividing by the active fuel region (in-core) volume ( $4.96 \times 10^6 \text{ cm}^3$ ) and multiplying by the fraction (Cm-244 spectrum) of neutrons in each group. The resulting volumetric neutron sources in the CASK-81 group structure for use in DORT models are shown in Table 5.2-17.

### 5.2.3 Evaluation of Effect of Uncertainty in Minimum Initial Enrichment

The analysis results presented in Section 5.1 do not include uncertainties (manufacturing tolerance) in minimum initial enrichment for U-235 and fissile Pu. To address these uncertainties, a comparison of the source terms associated with the limiting fuel configurations specified in the Fuel Qualification Table (Table 12.2-4) was done to the shielding analysis design

basis source terms specified in Table 5.2-8. This comparison is provided in Table 5.2-19. Similarly, a .04 weight % reduction in the MOX fuel enrichment specified in Section 5.2 (2.74 , 3.01 and 3.21 weight % respectively) may be used in the table specifying the MOX fuel qualification (Table 12.2-1). The limits specified in the Fuel Qualification Table are associated with minimum enrichments (including an uncertainty of  $-.04$  weight %), burnup and cooling time limits imposed to limit fuel assembly heat load to .581 kW to support the 24PT1-DSC maximum heat load of 14 kW.

**Table 5.2-1**  
**Flux Factor By Fuel Assembly Region**

| <b>Fuel Assembly<br/>Region</b> | <b>Flux Factor</b> |
|---------------------------------|--------------------|
| Bottom                          | 0.20               |
| In-Core                         | 1.00               |
| Plenum                          | 0.20               |
| Top                             | 0.10               |
| Above Top                       | 0.01               |

**Table 5.2-2**  
**WE 14x14 SC Assembly Materials and Masses**

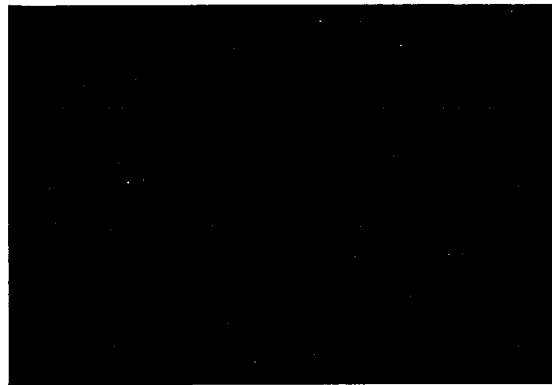


**Table 5.2-3**  
**WE 14x14 MOX Assembly Materials and Masses**




**Table 5.2-4**  
**Thimble Plug Assemblies Materials and Masses**

A large black rectangular box redacting the content of the table.



**Table 5.2-5**  
**RCCA Materials and Masses**



**Table 5.2-6**  
**Neutron Source Assembly Materials and Masses**

A large black rectangular box redacting the content of Table 5.2-6. The table is intended to list Neutron Source Assembly Materials and Masses.

**Table 5.2-7**  
**CASK-81 Neutron and Gamma Group Structure**

| Neutron Group Number | Max Energy (MeV) |  | Gamma Group Number | Max Energy (MeV) |
|----------------------|------------------|--|--------------------|------------------|
| 1                    | 15.0             |  | 23                 | 10.0             |
| 2                    | 12.2             |  | 24                 | 8.0              |
| 3                    | 10.0             |  | 25                 | 6.5              |
| 4                    | 8.18             |  | 26                 | 5.0              |
| 5                    | 6.36             |  | 27                 | 4.0              |
| 6                    | 4.96             |  | 28                 | 3.0              |
| 7                    | 4.06             |  | 29                 | 2.5              |
| 8                    | 3.01             |  | 30                 | 2.0              |
| 9                    | 2.46             |  | 31                 | 1.66             |
| 10                   | 2.35             |  | 32                 | 1.33             |
| 11                   | 1.83             |  | 33                 | 1.0              |
| 12                   | 1.11             |  | 34                 | 0.8              |
| 13                   | 0.550            |  | 35                 | 0.6              |
| 14                   | 0.111            |  | 36                 | 0.4              |
| 15                   | 3.35E-03         |  | 37                 | 0.3              |
| 16                   | 5.83E-04         |  | 38                 | 0.2              |
| 17                   | 1.01E-04         |  | 39                 | 0.1              |
| 18                   | 2.90E-05         |  | 40 <sup>(2)</sup>  | 0.05             |
| 19                   | 1.07E-05         |  |                    |                  |
| 20                   | 3.06E-06         |  |                    |                  |
| 21                   | 1.12E-06         |  |                    |                  |
| 22 <sup>(1)</sup>    | 4.14E-07         |  |                    |                  |

(1) Group 22 lower energy boundary is 1.00E-08 MeV

(2) Group 40 lower energy boundary is 0.01 MeV

**Table 5.2-8**  
**SAS2H Gamma Sources for 45 GWd/MTU, 10-Year Cooled**  
**WE 14x14 SC Fuel Per Fuel Assembly**

| Group | Top<br>Region<br>$\gamma/s$ | Plenum<br>Region<br>$\gamma/s$ | Fuel<br>Region<br>$\gamma/s$ | Bottom<br>Region<br>$\gamma/s$ |
|-------|-----------------------------|--------------------------------|------------------------------|--------------------------------|
| 23    | 0.000E+00                   | 0.000E+00                      | 1.633E+05                    | 0.000E+00                      |
| 24    | 0.000E+00                   | 0.000E+00                      | 7.691E+05                    | 0.000E+00                      |
| 25    | 0.000E+00                   | 0.000E+00                      | 3.921E+06                    | 0.000E+00                      |
| 26    | 0.000E+00                   | 0.000E+00                      | 9.770E+06                    | 0.000E+00                      |
| 27    | 2.055E-11                   | 6.963E-11                      | 3.685E+08                    | 5.800E-15                      |
| 28    | 2.559E+04                   | 3.402E+04                      | 2.919E+09                    | 3.690E+04                      |
| 29    | 1.650E+07                   | 2.194E+07                      | 4.762E+10                    | 2.379E+07                      |
| 30    | 1.593E-03                   | 5.117E-03                      | 1.027E+11                    | 1.224E-05                      |
| 31    | 6.953E+11                   | 9.245E+11                      | 5.888E+13                    | 1.003E+12                      |
| 32    | 2.462E+12                   | 3.274E+12                      | 2.316E+14                    | 3.550E+12                      |
| 33    | 1.492E+09                   | 1.815E+09                      | 7.635E+13                    | 2.123E+09                      |
| 34    | 2.342E+08                   | 7.477E+08                      | 1.416E+15                    | 4.195E+06                      |
| 35    | 8.377E+06                   | 1.114E+07                      | 1.413E+14                    | 1.208E+07                      |
| 36    | 1.326E+08                   | 1.763E+08                      | 2.876E+13                    | 1.911E+08                      |
| 37    | 1.011E+08                   | 1.347E+08                      | 4.496E+13                    | 1.457E+08                      |
| 38    | 2.035E+09                   | 2.708E+09                      | 1.544E+14                    | 2.934E+09                      |
| 39    | 8.436E+09                   | 1.122E+10                      | 2.093E+14                    | 1.216E+10                      |
| 40    | 6.700E+10                   | 9.002E+10                      | 1.060E+15                    | 9.581E+10                      |

**Table 5.2-9**  
**SAS2H Gamma Sources for 40 GWd/MTU, 10-Year Cooled**  
**WE 14x14 SC Fuel Per Fuel Assembly**

| Group | Top<br>Region<br>$\gamma/s$ | Plenum<br>Region<br>$\gamma/s$ | Fuel<br>Region<br>$\gamma/s$ | Bottom<br>Region<br>$\gamma/s$ |
|-------|-----------------------------|--------------------------------|------------------------------|--------------------------------|
| 23    | 0.000E+00                   | 0.000E+00                      | 1.236E+05                    | 0.000E+00                      |
| 24    | 0.000E+00                   | 0.000E+00                      | 5.820E+05                    | 0.000E+00                      |
| 25    | 0.000E+00                   | 0.000E+00                      | 2.967E+06                    | 0.000E+00                      |
| 26    | 0.000E+00                   | 0.000E+00                      | 7.393E+06                    | 0.000E+00                      |
| 27    | 1.224E-11                   | 4.169E-11                      | 3.249E+08                    | 4.040E-15                      |
| 28    | 2.373E+04                   | 3.156E+04                      | 2.577E+09                    | 3.423E+04                      |
| 29    | 1.530E+07                   | 2.035E+07                      | 4.239E+10                    | 2.207E+07                      |
| 30    | 1.296E-03                   | 4.161E-03                      | 9.092E+10                    | 1.161E-05                      |
| 31    | 6.449E+11                   | 8.576E+11                      | 5.410E+13                    | 9.301E+11                      |
| 32    | 2.284E+12                   | 3.037E+12                      | 2.111E+14                    | 3.294E+12                      |
| 33    | 1.347E+09                   | 1.648E+09                      | 6.393E+13                    | 1.909E+09                      |
| 34    | 2.151E+08                   | 6.870E+08                      | 1.250E+15                    | 3.891E+06                      |
| 35    | 7.769E+06                   | 1.033E+07                      | 1.191E+14                    | 1.121E+07                      |
| 36    | 1.229E+08                   | 1.635E+08                      | 2.542E+13                    | 1.773E+08                      |
| 37    | 9.380E+07                   | 1.250E+08                      | 3.953E+13                    | 1.351E+08                      |
| 38    | 1.888E+09                   | 2.512E+09                      | 1.355E+14                    | 2.721E+09                      |
| 39    | 7.824E+09                   | 1.041E+10                      | 1.854E+14                    | 1.128E+10                      |
| 40    | 6.214E+10                   | 8.348E+10                      | 9.362E+14                    | 8.890E+10                      |

**Table 5.2-10**  
**SAS2H Gamma Sources for 35 GWd/MTU, 10-Year Cooled**  
**WE 14x14 SC Fuel Per Fuel Assembly**

| Group | Top<br>Region<br>$\gamma/s$ | Plenum<br>Region<br>$\gamma/s$ | Fuel<br>Region<br>$\gamma/s$ | Bottom<br>Region<br>$\gamma/s$ |
|-------|-----------------------------|--------------------------------|------------------------------|--------------------------------|
| 23    | 0.000E+00                   | 0.000E+00                      | 8.169E+04                    | 0.000E+00                      |
| 24    | 0.000E+00                   | 0.000E+00                      | 3.848E+05                    | 0.000E+00                      |
| 25    | 0.000E+00                   | 0.000E+00                      | 1.962E+06                    | 0.000E+00                      |
| 26    | 0.000E+00                   | 0.000E+00                      | 4.889E+06                    | 0.000E+00                      |
| 27    | 6.378E-12                   | 2.188E-11                      | 2.736E+08                    | 2.480E-15                      |
| 28    | 2.130E+04                   | 2.834E+04                      | 2.184E+09                    | 3.073E+04                      |
| 29    | 1.374E+07                   | 1.828E+07                      | 3.687E+10                    | 1.982E+07                      |
| 30    | 1.002E-03                   | 3.214E-03                      | 7.945E+10                    | 1.087E-05                      |
| 31    | 5.789E+11                   | 7.701E+11                      | 4.815E+13                    | 8.352E+11                      |
| 32    | 2.050E+12                   | 2.727E+12                      | 1.865E+14                    | 2.957E+12                      |
| 33    | 1.184E+09                   | 1.457E+09                      | 5.158E+13                    | 1.673E+09                      |
| 34    | 1.922E+08                   | 6.136E+08                      | 1.086E+15                    | 3.494E+06                      |
| 35    | 6.974E+06                   | 9.278E+06                      | 9.708E+13                    | 1.006E+07                      |
| 36    | 1.104E+08                   | 1.468E+08                      | 2.243E+13                    | 1.592E+08                      |
| 37    | 8.421E+07                   | 1.122E+08                      | 3.457E+13                    | 1.213E+08                      |
| 38    | 1.695E+09                   | 2.256E+09                      | 1.180E+14                    | 2.444E+09                      |
| 39    | 7.024E+09                   | 9.347E+09                      | 1.635E+14                    | 1.013E+10                      |
| 40    | 5.578E+10                   | 7.495E+10                      | 8.211E+14                    | 7.984E+10                      |

**Table 5.2-11**  
**SAS2H Gamma Sources for 25 GWd/MTU, 20-Year Cooled**  
**WE 14x14 MOX Fuel Per Fuel Assembly**

| Group | Bottom<br>Nozzle<br>Region $\gamma/s$ | Top<br>Region<br>$\gamma/s$ | Plenum<br>Region<br>$\gamma/s$ | Fuel<br>Region<br>$\gamma/s$ |
|-------|---------------------------------------|-----------------------------|--------------------------------|------------------------------|
| 23    | 0.000E+00                             | 0.000E+00                   | 0.000E+00                      | 2.679E+04                    |
| 24    | 0.000E+00                             | 0.000E+00                   | 0.000E+00                      | 1.263E+05                    |
| 25    | 0.000E+00                             | 1.800E-13                   | 0.000E+00                      | 6.444E+05                    |
| 26    | 0.000E+00                             | 2.825E+03                   | 0.000E+00                      | 1.608E+06                    |
| 27    | 0.000E+00                             | 1.822E+06                   | 6.597E-13                      | 5.042E+06                    |
| 28    | 1.571E-16                             | 3.198E-04                   | 2.193E+03                      | 2.773E+07                    |
| 29    | 4.077E+03                             | 7.677E+10                   | 1.414E+06                      | 8.798E+08                    |
| 30    | 2.629E+06                             | 2.719E+11                   | 3.613E+00                      | 1.647E+10                    |
| 31    | 8.860E-08                             | 1.176E+08                   | 5.959E+10                      | 2.445E+12                    |
| 32    | 1.108E+11                             | 1.096E+08                   | 2.110E+11                      | 1.495E+13                    |
| 33    | 3.924E+11                             | 9.249E+05                   | 3.484E+08                      | 5.509E+12                    |
| 34    | 1.777E+07                             | 1.464E+07                   | 5.048E+08                      | 5.043E+14                    |
| 35    | 4.636E+05                             | 1.121E+07                   | 2.963E+08                      | 6.739E+12                    |
| 36    | 1.335E+06                             | 2.251E+08                   | 2.466E+07                      | 6.457E+12                    |
| 37    | 2.112E+07                             | 9.327E+08                   | 1.221E+07                      | 1.026E+13                    |
| 38    | 1.610E+07                             | 7.654E+09                   | 2.320E+08                      | 3.512E+13                    |
| 39    | 3.242E+08                             | 0.000E+00                   | 7.303E+08                      | 7.935E+13                    |
| 40    | 1.344E+09                             | 0.000E+00                   | 6.984E+09                      | 2.910E+14                    |

**Table 5.2-12**  
**Gamma Source Term for Thimble Assembly, Eleven Cycles In-core,**  
**10 Year Cooled Per Assembly**

| Group | Top<br>Region<br>$\gamma/s$ | Plenum<br>Region<br>$\gamma/s$ |
|-------|-----------------------------|--------------------------------|
| 23    | 0.000E+00                   | 0.000E+00                      |
| 24    | 0 000E+00                   | 0.000E+00                      |
| 25    | 0.000E+00                   | 0.000E+00                      |
| 26    | 0 000E+00                   | 0.000E+00                      |
| 27    | 2.153E-11                   | 4.235E-15                      |
| 28    | 1.991E+04                   | 1.996E+04                      |
| 29    | 1.284E+07                   | 1.287E+07                      |
| 30    | 4.108E-04                   | 3.519E-06                      |
| 31    | 5.410E+11                   | 5.424E+11                      |
| 32    | 1.916E+12                   | 1.921E+12                      |
| 33    | 4.065E+08                   | 6 068E+08                      |
| 34    | 7.574E+07                   | 2.269E+06                      |
| 35    | 6 517E+06                   | 6.535E+06                      |
| 36    | 1.031E+08                   | 1.034E+08                      |
| 37    | 7.863E+07                   | 7.880E+07                      |
| 38    | 1.583E+09                   | 1.587E+09                      |
| 39    | 6.563E+09                   | 6.580E+09                      |
| 40    | 5.210E+10                   | 5.212E+10                      |



**Table 5.2-13**  
**Gamma Source Term for RCCA, Eleven Cycles In-core,**  
**10 Year Cooled Per Assembly**

| Group | Above Top<br>Region<br>$\gamma/s$ | Top<br>Region<br>$\gamma/s$ | Plenum<br>Region<br>$\gamma/s$ | Fuel<br>Region<br>$\gamma/s$ |
|-------|-----------------------------------|-----------------------------|--------------------------------|------------------------------|
| 23    | 0.000E+00                         | 0.000E+00                   | 0.000E+00                      | 0.000E+00                    |
| 24    | 0.000E+00                         | 0.000E+00                   | 0.000E+00                      | 0.000E+00                    |
| 25    | 0.000E+00                         | 0.000E+00                   | 0.000E+00                      | 0.000E+00                    |
| 26    | 0.000E+00                         | 0.000E+00                   | 0.000E+00                      | 0.000E+00                    |
| 27    | 1.077E-11                         | 4.939E-16                   | 6.937E-16                      | 1.064E-14                    |
| 28    | 6.764E+03                         | 1.050E+02                   | 1.481E+02                      | 5.308E+04                    |
| 29    | 4.362E+06                         | 6.774E+04                   | 9.552E+04                      | 3.423E+07                    |
| 30    | 2.052E-04                         | 3.504E-07                   | 4.968E-07                      | 8.601E-06                    |
| 31    | 1.838E+11                         | 2.854E+09                   | 4.025E+09                      | 1.442E+12                    |
| 32    | 6.509E+11                         | 1.011E+10                   | 1.425E+10                      | 5.108E+12                    |
| 33    | 1.921E+08                         | 6.119E+07                   | 8.622E+07                      | 1.537E+09                    |
| 34    | 3.751E+07                         | 1.194E+04                   | 1.684E+04                      | 6.035E+06                    |
| 35    | 2.214E+06                         | 3.439E+04                   | 4.849E+04                      | 1.738E+07                    |
| 36    | 3.504E+07                         | 5.441E+05                   | 7.672E+05                      | 2.750E+08                    |
| 37    | 2.672E+07                         | 4.147E+05                   | 5.848E+05                      | 2.096E+08                    |
| 38    | 5.379E+08                         | 8.359E+06                   | 1.178E+07                      | 4.221E+09                    |
| 39    | 2.230E+09                         | 3.490E+07                   | 4.912E+07                      | 1.750E+10                    |
| 40    | 1.784E+10                         | 3.734E+08                   | 5.248E+08                      | 1.385E+11                    |

**Table 5.2-14**  
**Gamma Source Term for Neutron Source Assemblies, Four Cycles In-core,**  
**10 Year Cooled Per Assembly**

| Group | Top<br>Region<br>$\gamma/s$ | Plenum<br>Region<br>$\gamma/s$ | Fuel<br>Region<br>$\gamma/s$ |
|-------|-----------------------------|--------------------------------|------------------------------|
| 23    | 0.000E+00                   | 0.000E+00                      | 0.000E+00                    |
| 24    | 0.000E+00                   | 0.000E+00                      | 0.000E+00                    |
| 25    | 0.000E+00                   | 0.000E+00                      | 0.000E+00                    |
| 26    | 0.000E+00                   | 0.000E+00                      | 0.000E+00                    |
| 27    | 2.671E-11                   | 6.135E-15                      | 1.951E-14                    |
| 28    | 2.194E+04                   | 2.165E+04                      | 5.144E+04                    |
| 29    | 1.415E+07                   | 1.396E+07                      | 3.317E+07                    |
| 30    | 5.072E-04                   | 4.635E-06                      | 1.459E-05                    |
| 31    | 5.961E+11                   | 5.883E+11                      | 1.398E+12                    |
| 32    | 2.111E+12                   | 2.083E+12                      | 4.950E+12                    |
| 33    | 7.160E+08                   | 8.885E+08                      | 2.751E+09                    |
| 34    | 5.671E+07                   | 2.461E+06                      | 5.848E+06                    |
| 35    | 7.181E+06                   | 7.087E+06                      | 1.684E+07                    |
| 36    | 1.136E+08                   | 1.121E+08                      | 2.665E+08                    |
| 37    | 8.663E+07                   | 8.547E+07                      | 2.031E+08                    |
| 38    | 1.744E+09                   | 1.721E+09                      | 4.090E+09                    |
| 39    | 7.231E+09                   | 7.135E+09                      | 1.696E+10                    |
| 40    | 5.711E+10                   | 5.610E+10                      | 1.337E+11                    |

**Table 5.2-15**  
**Design Basis Volumetric Gamma Source Terms**

| Group | WE 14x14 SC Fuel                            |  |   |  | Thimble Plug                                |  |
|-------|---|--|---|--|---|--|
|       | Top Region<br>$\gamma/\text{cm}^3\text{-s}$ | Plenum Region<br>$\gamma/\text{cm}^3\text{-s}$ | In-Core Region<br>$\gamma/\text{cm}^3\text{-s}$ | Bottom Region<br>$\gamma/\text{cm}^3\text{-s}$ | Top Region<br>$\gamma/\text{cm}^3\text{-s}$ | Plenum Region<br>$\gamma/\text{cm}^3\text{-s}$ |
| 23    | 0.000E+00                                   | 0.000E+00                                      | 7.897E-01                                       | 0.000E+00                                      | 0.000E+00                                   | 0.000E+00                                      |
| 24    | 0.000E+00                                   | 0.000E+00                                      | 3.720E+00                                       | 0.000E+00                                      | 0.000E+00                                   | 0.000E+00                                      |
| 25    | 0.000E+00                                   | 0.000E+00                                      | 1.896E+01                                       | 0.000E+00                                      | 0.000E+00                                   | 0.000E+00                                      |
| 26    | 0.000E+00                                   | 0.000E+00                                      | 4.725E+01                                       | 0.000E+00                                      | 0.000E+00                                   | 0.000E+00                                      |
| 27    | 1.386E-15                                   | 6.735E-15                                      | 1.782E+03                                       | 8.636E-19                                      | 1.453E-15                                   | 4.096E-19                                      |
| 28    | 1.726E+00                                   | 3.291E+00                                      | 1.412E+04                                       | 5.494E+00                                      | 1.343E+00                                   | 1.931E+00                                      |
| 29    | 1.113E+03                                   | 2.122E+03                                      | 2.303E+05                                       | 3.543E+03                                      | 8.661E+02                                   | 1.245E+03                                      |
| 30    | 1.075E-07                                   | 4.949E-07                                      | 4.968E+05                                       | 1.822E-09                                      | 2.771E-08                                   | 3.404E-10                                      |
| 31    | 4.691E+07                                   | 8.942E+07                                      | 2.847E+08                                       | 1.493E+08                                      | 3.650E+07                                   | 5.246E+07                                      |
| 32    | 1.661E+08                                   | 3.166E+08                                      | 1.120E+09                                       | 5.286E+08                                      | 1.292E+08                                   | 1.858E+08                                      |
| 33    | 1.007E+05                                   | 1.756E+05                                      | 3.692E+08                                       | 3.160E+05                                      | 2.742E+04                                   | 5.869E+04                                      |
| 34    | 1.580E+04                                   | 7.232E+04                                      | 6.847E+09                                       | 6.246E+02                                      | 5.110E+03                                   | 2.195E+02                                      |
| 35    | 5.651E+02                                   | 1.077E+03                                      | 6.832E+08                                       | 1.799E+03                                      | 4.397E+02                                   | 6.320E+02                                      |
| 36    | 8.943E+03                                   | 1.705E+04                                      | 1.391E+08                                       | 2.846E+04                                      | 6.957E+03                                   | 1.000E+04                                      |
| 37    | 6.823E+03                                   | 1.303E+04                                      | 2.174E+08                                       | 2.169E+04                                      | 5.305E+03                                   | 7.622E+03                                      |
| 38    | 1.373E+05                                   | 2.619E+05                                      | 7.466E+08                                       | 4.368E+05                                      | 1.068E+05                                   | 1.535E+05                                      |
| 39    | 5.691E+05                                   | 1.085E+06                                      | 1.012E+09                                       | 1.811E+06                                      | 4.427E+05                                   | 6.364E+05                                      |
| 40    | 4.520E+06                                   | 8.707E+06                                      | 5.126E+09                                       | 1.427E+07                                      | 3.515E+06                                   | 5.041E+06                                      |

**Table 5.2-16**  
**Calculated Total Neutron Sources per Fuel Assembly**

| WE 14x14 SC Fuel    |                     |                     | WE 14x14 MOX        |
|---------------------|---------------------|---------------------|---------------------|
| 45 GWd/MTU n/s      | 40 GWd/MTU n/s      | 35 GWd/MTU n/s      | 25 GWd/MTU n/s      |
| $2.844 \times 10^8$ | $2.154 \times 10^8$ | $1.427 \times 10^8$ | $4.895 \times 10^7$ |

**Table 5.2-17**  
**Design Basis Volumetric Neutron Source Term**

| Group | Normalized<br>Cm-244<br>Fission Source | In-Core<br>Region<br>n/(cm <sup>3</sup> -s) |
|-------|--|---|
| 1     | 2.018E-04                              | 2.78E-01                                    |
| 2     | 1.146E-03                              | 1.58E+00                                    |
| 3     | 4.471E-03                              | 6.15E+00                                    |
| 4     | 1.768E-02                              | 2.43E+01                                    |
| 5     | 4.167E-02                              | 5.73E+01                                    |
| 6     | 5.641E-02                              | 7.76E+01                                    |
| 7     | 1.197E-01                              | 1.65E+02                                    |
| 8     | 9.616E-02                              | 1.32E+02                                    |
| 9     | 2.256E-02                              | 3.10E+01                                    |
| 10    | 1.227E-01                              | 1.69E+02                                    |
| 11    | 2.110E-01                              | 2.90E+02                                    |
| 12    | 1.794E-01                              | 2.47E+02                                    |
| 13    | 1.138E-01                              | 1.57E+02                                    |
| 14    | 1.301E-02                              | 1.79E+01                                    |
| 15    | 6.555E-05                              | 9.02E-02                                    |
| 16    | 4.765E-06                              | 6.55E-03                                    |
| 17    | 3.134E-07                              | 4.31E-04                                    |
| 18    | 4.527E-08                              | 6.23E-05                                    |
| 19    | 9.759E-09                              | 1.34E-05                                    |
| 20    | 1.521E-09                              | 2.09E-06                                    |
| 21    | 3.353E-10                              | 4.61E-07                                    |
| 22    | 9.683E-11                              | 1.33E-07                                    |

**Table 5.2-18**  
**Elemental Composition of LWR Structural Materials**

| Element | Atomic Number | Material Composition, grams per kg of material |             |               |                     |
|---------|---------------|--|-------------|---------------|---------------------|
|         |               | Zircaloy-4                                     | Inconel-718 | Inconel X-750 | Stainless Steel 304 |
| H       | 1             | 1.30E-02                                       | -           | -             | -                   |
| Li      | 3             | -  | -           | -             | -                   |
| B       | 5             | 3.30E-04                                       | -           | -             | -                   |
| C       | 6             | 1.20E-01                                       | 4.00E-01    | 3.99E-01      | 8.00E-01            |
| N       | 7             | 8.00E-02                                       | 1.30E+00    | 1.30E+00      | 1.30E+00            |
| O       | 8             | 9.50E-01                                       | -           | -             | -                   |
| F       | 9             | -  | -           | -             | -                   |
| Na      | 11            | -  | -           | -             | -                   |
| Mg      | 12            | -  | -           | -             | -                   |
| Al      | 13            | 2.40E-02                                       | 5.99E+00    | 7.98E+00      | -                   |
| Si      | 14            | -  | 2.00E+00    | 2.99E+00      | 1.00E+01            |
| P       | 15            | -  | -           | -             | 4.50E-01            |
| S       | 16            | 3.50E-02                                       | 7.00E-02    | 7.00E-02      | 3.00E-01            |
| Cl      | 17            | -  | -           | -             | -                   |
| Ca      | 20            | -  | -           | -             | -                   |
| Ti      | 22            | 2.00E-02                                       | 7.99E+00    | 2.49E+01      | -                   |
| V       | 23            | 2.00E-02                                       | -           | -             | -                   |
| Cr      | 24            | 1.25E+00                                       | 1.90E+02    | 1.50E+02      | 1.90E+02            |
| Mn      | 25            | 2.00E-02                                       | 2.00E+00    | 6.98E+00      | 2.00E+01            |
| Fe      | 26            | 2.25E+00                                       | 1.80E+02    | 6.78E+01      | 6.88E+02            |
| Co      | 27            | 1.00E-02                                       | 4.69E+00    | 6.49E+00      | 8.00E-01            |
| Ni      | 28            | 2.00E-02                                       | 5.20E+02    | 7.22E+02      | 8.92E+01            |
| Cu      | 29            | 2.00E-02                                       | 9.99E-01    | 4.99E-01      | -                   |
| Zn      | 30            | -  | -           | -             | -                   |
| Zr      | 40            | 9.79E+02                                       | -           | -             | -                   |
| Nb      | 41            | -  | 5.55E+01    | 8.98E+00      | -                   |
| Mo      | 42            | -  | 3.00E+01    | -             | -                   |
| Ag      | 47            | -  | -           | -             | -                   |
| Cd      | 48            | 2.50E-04                                       | -           | -             | -                   |
| In      | 49            | -  | -           | -             | -                   |
| Sn      | 50            | 1.60E+01                                       | -           | -             | -                   |
| Gd      | 64            | -  | -           | -             | -                   |
| Hf      | 72            | 7.80E-02                                       | -           | -             | -                   |
| W       | 74            | 2.00E-02                                       | -           | -             | -                   |
| Pb      | 82            | -  | -           | -             | -                   |
| U       | 92            | 2.00E-04                                       | -           | -             | -                   |

**Table 5.2-19**  
**Comparison of Design Basis Shielding Analysis Source Term**  
**to Fuel Qualification Table Source Terms**

|                                 | Shielding Analysis Design Basis       | Fuel Qualification Table Limiting Fuel Characteristics |                                       |                                       |                                       |                                       |
|---------------------------------|---------------------------------------|--|---------------------------------------|---------------------------------------|---------------------------------------|---------------------------------------|
| Enrichment, wt. %               | 3.80                                  | 3.12   | 3.36                                  | 3.76                                  | 3.76                                  | 3.96                                  |
| Burn-Up, MWd/MTU                | 45,000                                | 35,000   | 40,000                                | 36,800                                | 45,000                                | 43,300                                |
| Cool time, years                | 10.0                                  | 10.0   | 10.9                                  | 10.0                                  | 15.2                                  | 11.5                                  |
| Decay Heat, Watts/Fuel Assembly | 694                                   | 514  | 581                                   | 535                                   | 581                                   | 581                                   |
| Energy, MeV                     | $\gamma/(\text{sec} \cdot \text{FA})$ | $\gamma/(\text{sec} \cdot \text{FA})$                  | $\gamma/(\text{sec} \cdot \text{FA})$ | $\gamma/(\text{sec} \cdot \text{FA})$ | $\gamma/(\text{sec} \cdot \text{FA})$ | $\gamma/(\text{sec} \cdot \text{FA})$ |
| 0.1                             | 1.06E+15                              | 8.19E+14   | 9.02E+14                              | 8.85E+14                              | 8.97E+14                              | 9.34E+14                              |
| 0.1                             | 2.09E+14                              | 1.63E+14   | 1.79E+14                              | 1.77E+14                              | 1.82E+14                              | 1.87E+14                              |
| 0.2                             | 1.54E+14                              | 1.18E+14   | 1.29E+14                              | 1.28E+14                              | 1.26E+14                              | 1.34E+14                              |
| 0.3                             | 4.49E+13                              | 3.45E+13   | 3.79E+13                              | 3.76E+13                              | 3.76E+13                              | 3.95E+13                              |
| 0.4                             | 2.88E+13                              | 2.23E+13   | 2.44E+13                              | 2.45E+13                              | 2.44E+13                              | 2.57E+13                              |
| 0.6                             | 1.41E+14                              | 9.73E+13   | 9.27E+13                              | 1.02E+14                              | 4.20E+13                              | 7.07E+13                              |
| 0.8                             | 1.42E+15                              | 1.09E+15   | 1.20E+15                              | 1.14E+15                              | 1.17E+15                              | 1.21E+15                              |
| 1.0                             | 7.63E+13                              | 5.17E+13   | 5.14E+13                              | 5.41E+13                              | 2.67E+13                              | 4.09E+13                              |
| 1.3                             | 2.41E+14                              | 1.95E+14   | 1.97E+14                              | 1.91E+14                              | 1.30E+14                              | 1.57E+14                              |
| 1.7                             | 6.15E+13                              | 5.06E+13   | 5.01E+13                              | 4.92E+13                              | 3.12E+13                              | 3.88E+13                              |
| 2                               | 1.03E+11                              | 7.94E+10   | 7.67E+10                              | 8.44E+10                              | 6.42E+10                              | 7.19E+10                              |
| 2.5                             | 4.77E+10                              | 3.70E+10   | 2.30E+10                              | 3.80E+10                              | 4.80E+09                              | 1.12E+10                              |
| 3                               | 2.92E+09                              | 2.20E+09   | 1.49E+09                              | 2.15E+09                              | 3.30E+08                              | 7.62E+08                              |
| 4                               | 3.68E+08                              | 2.76E+08   | 1.87E+08                              | 2.66E+08                              | 3.57E+07                              | 8.72E+07                              |
| 5                               | 9.76E+06                              | 4.99E+06   | 7.29E+06                              | 4.36E+06                              | 8.23E+06                              | 6.40E+06                              |
| 6.5                             | 3.92E+06                              | 2.00E+06   | 2.92E+06                              | 1.75E+06                              | 3.30E+06                              | 2.57E+06                              |
| 8                               | 7.68E+05                              | 3.93E+05   | 5.73E+05                              | 3.43E+05                              | 6.48E+05                              | 5.04E+05                              |
| 10                              | 1.63E+05                              | 8.34E+04   | 1.22E+05                              | 7.29E+04                              | 1.38E+05                              | 1.07E+05                              |
| Total Gamma                     | 3.43E+15                              | 2.64E+15   | 2.86E+15                              | 2.79E+15                              | 2.67E+15                              | 2.83E+15                              |
| Total Neutrons                  | 2.84E+08                              | 1.46E+08   | 2.12E+08                              | 1.28E+08                              | 2.40E+08                              | 1.87E+08                              |

### 5.3 Model Specification

The neutron and gamma dose rates on the surface of the AHSM, and on the surface, and at 1 and 3 feet from the surface of the OS197 Transfer Cask are evaluated with the deterministic two-dimensional (2-D) transport code DORT. The CASK-81 cross-section library (22 for neutrons, and 18 for gamma ray energy groups) is used in the DORT evaluation. In addition, the flux-to-dose conversion factors specified by the ANSI/ANS 6.1.1-1977 [5.5], Table 5.3-4, are used.

#### 5.3.1 Description of the Radial and Axial Shielding Configurations

Figure 5.1-1 is a sketch of an AHSM cut away at the mid-vertical plane. Figure 5.1-3 is also a cut through the vertical mid-plane, the 24PT1-DSC is shown in phantom lines, and the front door is at the left hand side. The rear wall of the AHSM module has a minimum thickness of 1 foot. A 3-foot shield wall is placed along the rear and sides of the AHSM array, as shown in Figure 5.1-1.

DORT computer models are built to evaluate the dose rate along the front wall surface, the rear shield wall surface, the vent openings, the roof surface, and on the side shield walls.

Figure 5.1-4 shows the shielding configuration of the OS197 transfer cask.

##### 5.3.1.1 Storage Configuration

The geometry of nearly all components of the AHSM is Cartesian, except for the 24PT1-DSC, which is cylindrical. However, DORT is a 2-D code. Therefore, three conservative 2-D models are used to estimate the AHSM surface dose rates. Two models are cylindrical (R-Z) geometry, and a third is an X-Z model of the midsection of the AHSM.

The DORT (R-Z) geometry refers to a cylindrical symmetry that has Z along the axis of the 24PT1-DSC, and an X-Z geometry where Z is the vertical axis and X is the radial axis centered at the centerline of the 24PT1-DSC.

Since the AHSM possesses limited azimuthal cylindrical symmetries, all approximations result in an overestimate of the dose rates on the AHSM surfaces. The two R-Z models are used to evaluate the dose rate on the rear and front of the AHSM. The X-Z model has axial symmetry and is used to evaluate the dose on the side walls of the AHSM. Figure 5.4-1 and Figure 5.4-2 are the DORT generated material ID, mesh ID and dimensions of the top and bottom R-Z models, respectively. Figure 5.4-3 is the corresponding X-Z model.

To model the AHSM using R-Z symmetry, an imaginary horizontal plane is drawn through the 24PT1-DSC centerline up through the roof, and down through the floor of the AHSM (the AHSM walls and roof are their minimum thickness at this location). The R-Z model referred to as the "roof model" (Figure 5.4-2) represents the features of the top half of the AHSM as a model with symmetry around the 24PT1-DSC axis. This conservative model represents the ray *traveling* through the lowest density shell and through the thinnest shell possible in the real 3-D model of the AHSM. Also, whenever an air flow vent is modeled in this cylindrical model, it has a greater cross-section at any radial or axial position than the actual vents. Hence, the radiation attenuation is always under-estimated, and the radiation streaming is always over



estimated. This results in a conservative flux estimate at the surface, and this radiation will be more energetic than the actual radiation. Hence, the dose rate is over estimated. Similarly, an azimuthal cylindrical model is built to estimate the dose rates on the lower half (floor models) of the AHSM. Radiation doses are evaluated on the surface with similar conservatism as in the "roof model."

Finally, in the X-Z-model, in addition to conservatism similar to those mentioned for the R-Z models above, and due to the axial symmetry (along Y), the source is over-estimated as being of infinite length with no axial leakage.

#### 5.3.1.2 Loading/Unloading Configurations

The dose rates on the surface, and at 1 and 3 feet from the surface of the 24PT1-DSC/ Transfer Cask are evaluated with DORT. Three different key configurations representing the 4 stages in the loading/unloading of the spent fuel are analyzed. The four different stages modeled are, (1) Cask decontamination, (2) Wet Welding, (3) Dry Welding and (4) Transfer.

#### Definition of Transfer Cask and 24PT1-DSC Loading Stages

- 1) Cask decontamination. The 24PT1-DSC and the Transfer Cask are assumed to be completely filled with water, including the region between 24PT1-DSC and cask, which is referred to as the "Cask/24PT1-DSC annulus." The 24PT1-DSC top shield plug is assumed to be in place and the temporary shielding has not yet been installed.
- 2) Wet welding. The water level in the 24PT1-DSC cavity is assumed to be lowered four inches below the bottom of the top shield plug. Temporary shielding consisting of three inches of NS3 and one inch of steel is assumed to cover the 24PT1-DSC top shield plug. The Cask/24PT1-DSC annulus is assumed to remain completely filled with water.
- 3) Dry welding. The 24PT1-DSC cavity is assumed to be completely dry, the 24PT1-DSC inner and outer top cover plates have been installed, and temporary shielding consisting of three inches of NS3 and one inch of steel covers the outer top cover plate of the 24PT1-DSC. The Cask/24PT1-DSC annulus is assumed to remain completely filled with water.
- 4) Transfer. The 24PT1-DSC and 24PT1-DSC/Cask annulus are dry.

Figure 5.4-4 through Figure 5.4-7 provide the DORT generated material ID, mesh ID and dimensions used with the above configurations. Dose analysis results for the above conditions are provided in Table 5.1-3 through Table 5.1-5.

#### 5.3.1.3 Transfer Configuration

For the transfer configuration the Transfer Cask/24PT1-DSC annulus is completely dry. The 24PT1-DSC inner and outer top cover plates are installed. The top end of the Transfer Cask is in place which consists of a 3" thick carbon steel cover plate and a 2" thick solid neutron shield, and a 1/4" thick stainless steel plate cover is over the NS3 shield.

Nearly all the applicable geometries of the Transfer Cask and the 24PT1-DSC have cylindrical symmetry. R-Z DORT models are employed for shielding analyses of the Transfer Cask. The Z-axis in the DORT models coincides with the axis of rotation of the Transfer Cask and the 24PT1-DSC. The non-symmetric regions such as the 24 Neutron Shield Panel (NSP) support angles, the 4 trunnions, relief valves, clevises, eyebolts, etc are modeled such that the dose rate on the surfaces of the cask is overestimated. Figure 5.4-4 provides the DORT generated material ID, mesh ID and dimensions used in this model.

With the exception of the 24 neutron shield support angles and the trunnions the balance of the items listed as non-symmetric regions are local features that increase the amount of shielding in a small area without replacing any of the shielding material which is included in the model. The additional shielding material that these features provide is not smeared into the bulk shielding nor is any credit taken for them for the occupational exposure calculation. The 24 neutron shield support angles provide support for the skin, which contains the water for the neutron shield. The steel that forms these angles is not smeared with the water in the neutron shield; rather it is modeled as water. This is conservative for gamma radiation because water is less than one seventh the density of steel. The density of the neutron shield water used in the cask DORT models is 0.96 g/cm<sup>3</sup>. The resultant reduction in the hydrogen density as compared to full density water results in the water attenuating the neutron dose rate at about the same rate as that for full density steel. Therefore, replacing the steel with the lower density water results in little to no effect on the neutron dose rate outside the cask. The trunnions penetrate the neutron shield, which locally changes the shielding configuration of the neutron shield. The trunnions are thick steel structures filled with NS-3 neutron shielding material. These structures provide much more gamma and neutron shielding than the water that they replace, because they protrude well past the neutron shield and are made of materials which provide more gamma shielding and comparable neutron shielding as compared to the 0.96 g/cm<sup>3</sup> water that they replace. In addition, with the exception of the neutron shield support angles, none of these features is located near the axial center of the cask where surface dose rate is the largest.

### 5.3.2 Shield Regional Densities

Table 5.3-1 and Table 5.3-2 provide the shield regional densities for the AHSM models. Table 5.3-2 provides the concrete densities for those regions which contain rebar. The amount of rebar used for the shielding analysis is conservatively underestimated to maximize dose rates. The unit of measurement of steel areas is [in<sup>2</sup>/in]. The volume fraction  $V_r$  of steel in reinforced areas can be calculated by,

$$V_r = \frac{A_h + A_v}{d}$$

where,  $d$  (= 4") is the zone thickness, and  $A_h$  and  $A_v$  are the cross-sectional areas of vertical and horizontal rebars, respectively.

The actual fuel layout in the 24PT1-DSC is a cartesian array of fuel assemblies inside guidesleeves surrounded by sheets of poison material. These regions are smeared into a homogenous cylinder of equal volume and material loading. This smeared geometry represents a major part of the shield (fuel, steel, Boral™ sheets, etc.) and the neutron and gamma source volumetric distribution itself. As for the source, when the source is smeared into a cylinder, the

source is moved closer to the surface of the source region. This results in less self-shielding of the source in the model as compared to the actual geometry, which results in an overestimate of the surface dose rates.

For dose rate evaluations made on surfaces that are parallel to the spacer discs (perpendicular to the DSC longitudinal axis), credit is taken for the presence of the carbon steel spacer discs and the fuel grid spacers and hold down springs by smearing them in the fuel material regions. For dose rate evaluations made on surfaces that are perpendicular to the spacer discs (parallel to the DSC longitudinal axis), a considerable fraction of the radiation will travel between the spacer discs, without being attenuated by the spacer discs. Therefore, the spacer discs and fuel grid spacers and hold down springs are not included in these number densities. For the AHSM evaluation, no credit for the shielding properties of the spacer discs, fuel grid spacers and hold-down springs. Table 5.3-3 provides the shield regional densities for models of the various stages of the loading/unloading and transfer conditions.

When the transfer cask/24PT1-DSC annulus and 24PT1-DSC are filled with water, the wet axial densities are used for the homogenized regions.

**Table 5.3-1**  
**Materials Composition and Atom Number Densities**

| Material Name             | Composition   | Densities of components<br>Atoms/barn-cm   |
|---------------------------|---|--|
| Stainless Steel           | Cr<br>Fe<br>Ni  | 1.743e-2<br>6.128e-2<br>7.511e-3   |
| Carbon Steel              | Fe  | 8.465e-2   |
| Concrete                  | See Table 5.3-2   | See Table 5.3-2  |
| Air                       | N<br>O  | 3.587e-5<br>9.534e-6   |
| Front Concrete            | See Table 5.3-2   | See Table 5.3-2  |
| Roof Concrete             | See Table 5.3-2   | See Table 5.3-2  |
| Inside Concrete           | See Table 5.3-2   | See Table 5.3-2  |
| Rear Concrete             | See Table 5.3-2   | See Table 5.3-2  |
| Inner Rear Concrete       | See Table 5.3-2   | See Table 5.3-2  |
| Outer Rear Concrete       | See Table 5.3-2   | See Table 5.3-2  |
| Bottom Nozzle             | B <sup>10</sup><br>C<br>Al<br>Cr<br>Fe<br>Ni                      | 2.007e-4<br>9.927e-4<br>6.902e-4<br>3.371e-3<br>1.185e-2<br>1.454e-3                                     |
| In-Core                   | B <sup>10</sup><br>C<br>O<br>Al<br>Cr<br>Fe<br>Ni<br>U235<br>U238 | 2.009e-4<br>9.934e-4<br>7.936e-3<br>6.906e-4<br>1.488e-3<br>5.231e-3<br>6.417e-4<br>1.520e-4<br>3.799e-3 |
| Plenum                    | B <sup>10</sup><br>C<br>Al<br>Cr<br>Fe<br>Ni                      | 2.009e-4<br>9.933e-4<br>6.906e-4<br>1.565e-3<br>5.502e-3<br>6.750e-4                                     |
| Top Nozzle                | B <sup>10</sup><br>C<br>Al<br>Cr<br>Fe<br>Ni                      | 2.009e-4<br>9.933e-4<br>6.906e-4<br>2.156e-3<br>7.580e-3<br>9.298e-3                                     |
| Rear Shield Wall Concrete | See Table 5.3-2   | See Table 5.3-2  |
| BISCO NS3                 | H<br>B <sup>10</sup><br>C<br>O<br>Al<br>Si<br>Ca<br>Fe            | 4.498e-2<br>3.054e-4<br>9.595e-3<br>3.704e-2<br>6.887e-3<br>1.243e-3<br>1.454e-3<br>1.042e-4             |
| Lead                      | Pb  | 3.296e-2   |

**Table 5.3-2**  
**Density Calculations for Concrete**

| Element | Concrete<br>(at/b·cm)  | Front<br>Concrete<br>(at/b·cm)<br>Vr=0.008 | Inner<br>Concrete<br>(at/b·cm)<br>Vr=0.014 | Roof<br>Concrete<br>(at/b·cm)<br>Vr=0.033 | Rear Shield<br>Wall Concrete<br>(at/b·cm)<br>Vr=0.046 | Rear<br>Concrete<br>(at/b·cm)<br>Vr=0.067 |
|---------|------------------------|--|--|---|---|---|
| H       | $7.767 \times 10^{-3}$ | 7.705E-03                                  | 7.658E-03                                  | 7.511E-03                                 | 7.410E-03   | 7.247E-03                                 |
| O       | $4.317 \times 10^{-2}$ | 4.282E-02                                  | 4.257E-02                                  | 4.175E-02                                 | 4.118E-02   | 4.028E-02                                 |
| Na      | $1.022 \times 10^{-3}$ | 1.014E-03                                  | 1.008E-03                                  | 9.883E-04                                 | 9.750E-04   | 9.535E-04                                 |
| Al      | $2.343 \times 10^{-3}$ | 2.324E-03                                  | 2.310E-03                                  | 2.266E-03                                 | 2.235E-03   | 2.186E-03                                 |
| Si      | $1.559 \times 10^{-2}$ | 1.547E-02                                  | 1.537E-02                                  | 1.508E-02                                 | 1.487E-02   | 1.455E-02                                 |
| K       | $6.776 \times 10^{-4}$ | 6.722E-04                                  | 6.681E-04                                  | 6.552E-04                                 | 6.464E-04   | 6.322E-04                                 |
| Ca      | $2.855 \times 10^{-3}$ | 2.832E-03                                  | 2.815E-03                                  | 2.761E-03                                 | 2.724E-03   | 2.664E-03                                 |
| Fe      | $3.019 \times 10^{-4}$ | 9.764E-04                                  | 1.482E-03                                  | 3.084E-03                                 | 4.180E-03   | 5.951E-03                                 |

**Table 5.3-3**  
**Materials Composition and Atom Densities During Decontamination**  
**and Wet Welding Stage Calculation**

| Material Name | Composition     | Densities of Components<br>Atoms/barn-cm |
|---------------|-----------------|--|
| Water         | H               | 6.393e-2                                 |
|               | O               | 3.203e-2                                 |
| Bottom Nozzle | H               | 4.278e-2                                 |
|               | B <sup>10</sup> | 2.007e-4                                 |
|               | C               | 9.927e-4                                 |
|               | O               | 2.364e-2                                 |
|               | Al              | 6.902e-4                                 |
|               | Cr              | 3.371e-3                                 |
|               | Fe              | 1.185e-2                                 |
|               | Ni              | 1.454e-3                                 |
| In-Core       | H               | 4.000e-2                                 |
|               | B <sup>10</sup> | 2.009e-4                                 |
|               | C               | 9.934e-4                                 |
|               | O               | 2.794e-2                                 |
|               | Al              | 6.929e-4                                 |
|               | Ti              | 1.707e-6                                 |
|               | Cr              | 1.525e-3                                 |
|               | Fe              | 5.264e-3                                 |
|               | Zr              | 7.321e-4                                 |
|               | Ni              | 6.713e-4                                 |
|               | Mo              | 3.192e-6                                 |
|               | U235            | 1.520e-4                                 |
|               | U238            | 3.799e-3                                 |
| Plenum        | H               | 4.173e-2                                 |
|               | B <sup>10</sup> | 2.009e-4                                 |
|               | C               | 9.933e-4                                 |
|               | O               | 2.086e-2                                 |
|               | Al              | 6.906e-4                                 |
|               | Ti              | 6.572e-6                                 |
|               | Cr              | 1.565e-3                                 |
|               | Fe              | 5.502e-3                                 |
|               | Ni              | 6.750e-4                                 |
|               | Zr              | 2.585e-5                                 |
|               | Mo              | 1.229e-5                                 |
| Top Nozzle    | H               | 5.313e-2                                 |
|               | B <sup>10</sup> | 2.009e-4                                 |
|               | C               | 9.933e-4                                 |
|               | O               | 2.657e-2                                 |
|               | Al              | 6.943e-4                                 |
|               | Ti              | 2.806e-6                                 |
|               | Cr              | 2.217e-3                                 |
|               | Fe              | 7.634e-3                                 |
|               | Ni              | 1.078e-3                                 |
|               | Zr              | 1.104e-5                                 |
|               | Mo              | 5.274e-6                                 |

**Table 5.3-4**  
**ANSI Standard-6.1.1-1977 Flux-to-Dose Factors**

| Group Number   | E <sub>upper</sub><br>(MeV) | E <sub>mean</sub><br>(MeV) | Flux-Dose ANSI/ANS-6.1.1-1977<br>(mR/hr)/(γ/cm <sup>2</sup> -sec) |
|----------------|-----------------------------|----------------------------|---|
| Neutron Groups |                             |                            |   |
| 1              | 1.49E+01                    | 1.25E+01                   | 1.597E-01   |
| 2              | 1.22E+01                    | 1.11E+01                   | 1.597E-01   |
| 3              | 1.00E+01                    | 9.09E+00                   | 1.471E-01   |
| 4              | 8.18E+00                    | 7.27E+00                   | 1.477E-01   |
| 5              | 6.36E+00                    | 5.66E+00                   | 1.534E-01   |
| 6              | 4.96E+00                    | 4.51E+00                   | 1.506E-01   |
| 7              | 4.06E+00                    | 3.54E+00                   | 1.389E-01   |
| 8              | 3.01E+00                    | 2.74E+00                   | 1.284E-01   |
| 9              | 2.46E+00                    | 2.41E+00                   | 1.253E-01   |
| 10             | 2.35E+00                    | 2.09E+00                   | 1.263E-01   |
| 11             | 1.83E+00                    | 1.47E+00                   | 1.289E-01   |
| 12             | 1.11E+00                    | 8.30E-01                   | 1.169E-01   |
| 13             | 5.50E-01                    | 3.31E-01                   | 6.521E-02   |
| 14             | 1.11E-01                    | 5.72E-02                   | 9.188E-03   |
| 15             | 3.35E-03                    | 1.97E-03                   | 3.713E-03   |
| 16             | 5.83E-04                    | 3.42E-04                   | 4.009E-03   |
| 17             | 1.01E-04                    | 6.50E-05                   | 4.295E-03   |
| 18             | 2.90E-05                    | 1.96E-05                   | 4.476E-03   |
| 19             | 1.01E-05                    | 6.58E-06                   | 4.567E-03   |
| 20             | 3.06E-06                    | 2.09E-06                   | 4.536E-03   |
| 21             | 1.12E-06                    | 7.67E-07                   | 4.370E-03   |
| 22             | 4.14E-07                    | 2.12E-07                   | 3.714E-03   |
| Gamma Groups   |                             |                            |   |
| 23             | 10                          | 9                          | 8.772E-03   |
| 24             | 8                           | 7.25                       | 7.479E-03   |
| 25             | 6.5                         | 5.75                       | 6.375E-03   |
| 26             | 5                           | 4.5                        | 5.414E-03   |
| 27             | 4                           | 3.5                        | 4.622E-03   |
| 28             | 3                           | 2.75                       | 3.960E-03   |
| 29             | 2.5                         | 2.25                       | 3.469E-03   |
| 30             | 2                           | 1.83                       | 3.019E-03   |
| 31             | 1.66                        | 1.495                      | 2.628E-03   |
| 32             | 1.33                        | 1.165                      | 2.205E-03   |
| 33             | 1                           | 0.9                        | 1.833E-03   |
| 34             | 0.8                         | 0.7                        | 1.523E-03   |
| 35             | 0.6                         | 0.5                        | 1.173E-03   |
| 36             | 0.4                         | 0.35                       | 8.759E-04   |
| 37             | 0.3                         | 0.25                       | 6.306E-04   |
| 38             | 0.2                         | 0.15                       | 3.834E-04   |
| 39             | 0.1                         | 0.08                       | 2.669E-04   |
| 40             | 0.05                        | 0.03                       | 9.348E-04   |

## 5.4 Shielding Evaluation

### 5.4.1 Computer Programs

DORT [5.2] determines the fluence of particles throughout one-dimensional or two-dimensional geometric systems by solving the Boltzmann transport equation using either the method of discrete ordinates or a diffusion theory approximation. Particles can be generated by either particle interaction with the transport medium or extraneous sources incident upon the system. Anisotropic cross-sections can be expressed in a Legendre expansion of arbitrary order. DORT is an industry standard code distributed by ORNL/RSIC.

The DORT code implements the discrete ordinates method as its primary mode of operation. Balance equations are solved for the flow of particles moving in a set of discrete directions in each cell of a space mesh and in each group of a multigroup energy structure.

DORT was chosen for this application because of its ability to solve two dimensional, cylindrical, deep penetration, radiation transport problems applicable to the Advanced NUHOMS<sup>®</sup> System.

#### 5.4.1.1 Spatial Source Distribution

The source components are:

- A neutron source due to the active fuel regions of the 24 fuel assemblies,
- A gamma source due to the active fuel regions of the 24 fuel assemblies,
- A gamma source due to the plenum regions of the 24 fuel assemblies,
- A gamma source due to the top nozzle regions of the 24 fuel assemblies,
- A gamma source due to the bottom nozzle region of the 24 fuel assemblies,
- A gamma source due to the 24 TPAs in the top nozzle and plenum regions of the 24 fuel assemblies

The U-235 fission spectrum is input into the 1\* array of the DORT input file to account for subcritical multiplication, increasing the neutron source in the active fuel region. Axial peaking is accounted for in the active fuel region by inputting a relative flux factor at each node in the 97\* array. The flux factor data is taken from Reference [5.7] for (CE 14x14) PWR fuel. This burn-up profile is conservative for evaluations of a WE 14x14 fuel assembly of similar heavy metal loading, neutron spectrum, and total length. In Reference [5.7], this burnup profile was used for evaluations where the fuel depletion (burn-up) is conservatively overestimated at the center of the fuel region and underestimated at the top and the bottom. This conservatism is also applicable for shielding, where it is intended to conservatively overestimate the source at the middle of the fuel (or transfer cask) where the shielding is lowest. Thus, for the shielding evaluations, this burnup profile is conservative. For the R-Z cask models, this axial profile will underestimate the source at the top and bottom. These two regions are immediately behind the 24PT1-DSC top and bottom thick shield plugs. To preserve the average assembly burn-up, the burn-up in the rest of the assembly is overestimated. This results in an overestimate of the source along most of the fuel region length where the cask shielding is the minimum. Thus, for all shielding considerations, it is conservative to choose a burn-up profile peaked in the central region of the fuel, and it is also conservative to choose this axially peaked shape. Therefore, the



appropriate peak flux factor is 1.07 for neutrons and gamma-rays, assumed to vary linearly with fuel burnup. Differences between PWR fuel designs, including the locations of the grid spacers and associated hardware, is accounted for by applying the maximum peaking factor of 1.07 across the entire middle section of the active fuel region for the X-Y models. The flux factor data used in this analysis is shown in Table 5.4-1.

#### 5.4.1.2 Cross-Section Data

The cross-section data used in this analysis is taken from the CASK-81 22 neutron, 18 gamma-ray energy group, coupled cross-section library [5.3]. CASK-81 is an industry standard cross-section library compiled for the purpose of performing calculations of spent fuel shipping casks and is distributed by ORNL/RSIC. The cross-section data allows coupled neutron/gamma-ray dose rate evaluation to be made that account for secondary gamma radiation ( $n,\gamma$ ).

Microscopic  $P_3$  cross-sections were taken from the CASK-81 library and mixed using the GIP-PC computer program distributed with DORT-PC [5.2] to provide macroscopic cross-sections for the materials in the cask model. The material compositions used in the GIP input file are listed in Table 5.3-1 through Table 5.3-3.

An additional element and material, “fluxdosium,” is included in the cross-section data and mixing table in the GIP input file. Fluxdosium is used to provide flux-to-dose rate conversion factors as described in Section 5.4.2 for use in activity calculations. The presence of fluxdosium in the cross-section data does not impact the actual flux calculations.

#### 5.4.2 Flux-to-Dose-Rate Conversion

The flux distribution calculated by the DORT-PC code is converted to dose rates using the flux-to-dose rate conversion factors provided in ANSI/ANS-6.1.1-1977 [5.5]. The gamma-ray and neutron flux-to-dose rate conversion factors for the CASK-81 energy groups are shown in Table 5.3-4.

The dose rate at each node in the DORT models is calculated using the activity calculation feature of DORT. The “cross-section” data for one material in the input file contains only flux-to-dose rate conversion factors. This material, “fluxdosium”, is then specified for activity calculations which determine the gamma and neutron dose rate at each node.

##### 5.4.2.1 Model Geometry

Figure 5.4-1 through Figure 5.4-3 are the DORT models for the AHSM. Figure 5.4-4 through Figure 5.4-7 are the DORT models of the Transfer Cask (TC) and 24PT1-DSC. The figures show zone number by materials. Bold face cell numbers on the left side are j-intervals along Z-axis. Distances (cm) on the right side represent important points in geometry or points where materials filling cells of the mesh change.

Figures 5.4-8 through 5.4-12 depict in a simplified format the shielding analysis models.

**Table 5.4-1**  
**Normalized Conservative Burn-Up Shape on WE 14×14 Fuel Assembly [5.7]**

| <b>Zone Number</b> | <b>Zone Center in % of height</b> | <b>Zone Center mapped on the axis of the active fuel zone, cm</b> | <b>Flux Factor</b> |
|--------------------|-----------------------------------|---|--------------------|
| 1                  | 2.5                               | 7.6   | 0.655              |
| 2                  | 7.5                               | 22.9  | 0.911              |
| 3                  | 12.5                              | 38.1  | 1.009              |
| 4                  | 17.5                              | 53.3  | 1.041              |
| 5                  | 22.5                              | 68.6  | 1.069              |
| 6                  | 27.5                              | 83.8  | 1.072              |
| 7                  | 32.5                              | 99.1  | 1.072              |
| 8                  | 37.5                              | 114.3   | 1.071              |
| 9                  | 42.5                              | 129.5   | 1.070              |
| 10                 | 47.5                              | 144.8   | 1.069              |
| 11                 | 52.5                              | 160.0   | 1.069              |
| 12                 | 57.5                              | 175.3   | 1.068              |
| 13                 | 62.5                              | 190.5   | 1.068              |
| 14                 | 67.5                              | 205.7   | 1.069              |
| 15                 | 72.5                              | 221.0   | 1.068              |
| 16                 | 77.5                              | 236.2   | 1.066              |
| 17                 | 82.5                              | 251.5   | 1.041              |
| 18                 | 87.5                              | 266.7   | 0.994              |
| 19                 | 92.5                              | 281.9   | 0.879              |
| 20                 | 97.5                              | 297.2   | 0.639              |

**Figure 5.4-1**  
Sheet 1 of 3

**Figure 5.4-1**  
Sheet 2 of 3

**Figure 5.4-1**  
**DORT R-Z Floor Model**  
**Sheet 3 of 3**

**Figure 5.4-2**  
Sheet 1 of 3

**Figure 5.4-2**  
Sheet 2 of 3

**Figure 5.4-2**  
**DORT R-Z Roof Model**  
**Sheet 3 of 3**



**Figure 5.4-3**  
Sheet 1 of 3

**Figure 5.4-3**  
Sheet 2 of 3

**Figure 5.4-3**  
**DORT X-Z Midplane Model**  
**Sheet 3 of 3**

**Figure 5.4-4**  
Sheet 1 of 4

**Figure 5.4-4**  
Sheet 2 of 4

**Figure 5.4-4**  
Sheet 3 of 4

**Figure 5.4-4**  
**Zone Number by Material in TC Model at Transfer-Storage Stage**  
**Sheet 4 of 4**

**Figure 5.4-5**  
**Zone Number by Material in TC Model at Decontamination Stage<sup>(1)</sup>**



**Figure 5.4-6**  
**Zone Number by Material in TC Model at Wet Welding Stage<sup>(1)</sup>**

**Figure 5.4-7**  
**Zone Number by Material in TC Model at Dry Welding Stage<sup>(1)</sup>**

**Figure 5.4-8**  
**AHSM Roof DORT Shielding Analysis Model**

**Figure 5.4-9**  
**AHSM Floor DORT Shielding Analysis Model**

**Figure 5.4-10**  
**AHSM Side DORT Shielding Analysis Model**

**Figure 5.4-11**  
**AHSM Front/Back DORT Shielding Analysis Model**

**Figure 5.4-12**  
**OS197 DORT Shielding Analysis Model**

5.5 Supplemental Information5.5.1 References

- [5.1] Oak Ridge National Laboratory, RSIC Computer Code Collection, "SCALE: A Modular Code System for Performing Standardized Computer Analysis for Licensing Evaluations for Workstations and Personal Computers," NUREG/CR-0200, Revision 6, ORNL/NUREG/CSD-2/V2/R6.
- [5.2] "DORT-PC-Two Dimensional Discrete Ordinates Transport Code System", CCC-532, Oak Ridge National Laboratory, RSIC Computer Code Collection, October 1991.
- [5.3] "CASK-81 22 Neutron, 18 Gamma-Ray, P<sub>3</sub>, Cross Sections for Shipping Cask Analysis", Oak Ridge National Laboratory Report DLC-23.
- [5.4] "Characteristics of Potential Repository Wastes", DOE/RW-0184-R1, Office of Civilian Radioactive Waste Management, July 1992.
- [5.5] "American National Standard Neutron and Gamma-Ray Flux-to-Dose Rate Factors". ANSI/ANS-6.1.1-1977, American Nuclear Society, La Grange Park, Illinois. March 1977.
- [5.6] "MCNP 4- Monte Carlo Neutron and Photon Transport Code System", CCC-200A/B, Oak Ridge National Laboratory, RSIC Computer Code Collection, File Number QA040.215.00002, October 1991.
- [5.7] M. D. DeHart, "Sensitivity and Parametric Evaluations of Significant Aspects of Burn-up Credit for PWR Spent Fuel Packages", ORNL/TM-12973, May 1996.
- [5.8] *TN West, Final Safety Analysis Report for the Standardized NUHOMS<sup>®</sup> Horizontal Modular Storage System for Irradiated Nuclear Fuel, Revision 6, November 2001, NRC Docket No. 72-1004.*
- [5.9] Ludwig, S.B., and J.P. Renier, "Standard- and Extended-Burnup PWR and BWR Reactor Models for the ORIGEN2 Computer Code," ORNL/TM-11018, Oak Ridge National Laboratory, December 1989.
- [5.10] *MCNPX – Radiation Simulation and Nuclear Data for High Energy, Multi-Particle Applications, Version 2.2.3.*



### 5.5.2 Validation of Shielding Analysis

Section 5.5.2.1 provides a supportive three dimensional (3-D) shielding analysis to confirm the validity of the two-dimensional (2-D) shielding analysis reported in Sections 5.1 through 5.4. The computer code, MCNPX, Version 2.2.3 [5.10], is used to perform this 3-D analysis. The 3-D shielding analysis with MCNPX code has also been validated by comparison to actual measured dose rate data from installed NUHOMS® Systems (Section 5.5.2.2).

#### 5.5.2.1 Comparison of 2-D Shielding Analysis versus 3-D Shielding Analysis

Table 5.5-1 compares maximum and averaged dose rates on the AHSM surfaces calculated with DORT (2-D) and MCNP (3-D).

**Table 5.5-1**  
**Comparison of DORT and MCNP Maximum and Averaged Dose Rate Values**  
**on Surfaces of AHSM**

| AHSM Surfaces                | Dose Rate Components | DORT and MCNP Maximum Dose Rates, mrem/hr |                   |           | DORT and MCNP Averaged Surface Dose Rates, mrem/hr |         |           |
|------------------------------|----------------------|---|-------------------|-----------|--|---------|-----------|
|                              |                      | DORT                                      | MCNP <sup>1</sup> | DORT/MCNP | DORT   | MCNP    | DORT/MCNP |
| Back of the Rear Shield Wall | Gamma                | 1.64e-1                                   | 4.96e-2           | 3.3       | 6.09e-3  | 5.70e-3 | 1.1       |
|                              | Neutron              | 1.00e-2                                   | 4.09e-3           | 2.4       | 3.70e-4  | 5.18e-4 | 0.7       |
|                              | Total                | 1.74e-1                                   | 5.37e-2           | 3.2       | 6.46e-3  | 6.21e-3 | 1.0       |
| Front                        | Gamma                | 45.27                                     | 2.07e+1           | 2.2       | 2.84   | 1.78    | 1.6       |
|                              | Neutron              | 5.40e-1                                   | 3.99e-1           | 1.4       | 4.00e-2  | 6.32e-2 | 0.6       |
|                              | Total                | 45.81                                     | 2.11e+1           | 2.2       | 2.88   | 1.84    | 1.6       |
| Side                         | Gamma                | 2.01                                      | 1.64              | 1.2       | 3.90e-1  | 1.85e-1 | 2.1       |
|                              | Neutron              | 2.71e-2                                   | 6.44e-2           | 0.4       | 6.10e-3  | 7.50e-3 | 0.81      |
|                              | Total                | 2.04                                      | 1.71              | 1.2       | 3.96e-1  | 1.93e-1 | 2.1       |
| Top                          | Gamma                | 3.57                                      | 1.69              | 21.2      | 4.50e-2  | 1.42e-2 | 3.2       |
|                              | Neutron              | 5.00e-2                                   | 8.63              | 5.8       | 8.56e-4  | 8.47e-4 | 1.0       |
|                              | Total                | 3.62                                      | 1.77e-1           | 20.4      | 4.59e-2  | 1.50e-2 | 3.1       |

The reported average dose rates corresponding to MCNP are all calculated with the code, while those for DORT are obtained by processing the results with the methodology described in Sections 5.1 to 5.4.

As can be seen from Table 5.5-1, gamma dose rates are substantially higher than neutron dose rates which makes the total MCNP dose rates bounded by the results calculated with DORT.

<sup>1</sup> Minimum and maximum values are given as calculated, shape functions are not applied.

### 5.5.2.2 *Validation of 3-D Shielding Analysis against Test Data*

*Validation of the 3-D MCNPX shielding analysis has been performed by comparison to actual measured dose rate data taken at an operating ISFSI facility. This facility uses the NUHOMS<sup>®</sup>-24P system (CoC 1004) which is similar to the Advanced NUHOMS<sup>®</sup> system. The MCNPX models were used to calculate dose rates at locations around the HSM that correspond to the various survey locations for which the data is reported. Table 5.5-2 and Table 5.5-3 provide a comparison of calculated versus measured dose rates for two HSMs at this ISFSI.*

**Table 5.5-2**  
**Comparison of Calculated MCNP Dose Rates Verses Measured**  
**Dose Rates – No. 1 HSM**

| Description                          | Maximum Measured<br>Dose Rate, mrem/hr |      | Maximum Calculated<br>with MCNP |                        | Ratio,<br>Calculated/<br>Measured |
|--------------------------------------|--|------|---------------------------------|------------------------|-----------------------------------|
|                                      |  |      | mrem/hr                         | Fractional<br>error, % |                                   |
| In Front of HSM Front<br>Bird Screen | Neutron                                | 0.6  | 1.43                            | 2.4                    | 2.4                               |
|                                      | Gamma                                  | 30   | 281.98                          | 6.8                    | 9.4                               |
|                                      | Total                                  | 30.6 | 283.42                          | 6.8                    | 9.3                               |
| Above HSM Roof Bird<br>Screen        | Neutron                                | 3    | 2.53                            | 1.6                    | 0.8                               |
|                                      | Gamma                                  | 130  | 661.46                          | 2.0                    | 5.1                               |
|                                      | Total                                  | 133  | 663.99                          | 2.0                    | 5.0                               |
| On HSM Door                          | Neutron                                | 3    | 7.36                            | 1.1                    | 2.5                               |
|                                      | Gamma                                  | 7    | 13.17                           | 2.1                    | 1.9                               |
|                                      | Total                                  | 10   | 20.53                           | 1.4                    | 2.1                               |

**Table 5.5-3**  
**Comparison of Calculated MCNP Dose Rates Verses Measured**  
**Dose Rates – No. 2 HSM**

| Description                          | Maximum Measured<br>Dose Rate, mrem/hr |       | Maximum Calculated<br>with MCNP |                        | Ratio,<br>Calculated/<br>Measured |
|--------------------------------------|--|-------|---------------------------------|------------------------|-----------------------------------|
|                                      |  |       | mrem/hr                         | Fractional<br>error, % |                                   |
| In Front of HSM Front<br>Bird Screen | Neutron                                | 0.3   | 1.34                            | 2.4                    | 4.5                               |
|                                      | Gamma                                  | 20    | 266.20                          | 7.0                    | 13.3                              |
|                                      | Total                                  | 20.3  | 267.54                          | 6.9                    | 13.2                              |
| Above HSM Roof Bird<br>Screen        | Neutron                                | 0.7   | 2.39                            | 1.6                    | 3.4                               |
|                                      | Gamma                                  | 180   | 635.22                          | 2.1                    | 3.5                               |
|                                      | Total                                  | 180.7 | 637.61                          | 2.1                    | 3.5                               |
| On HSM Door                          | Neutron                                | 1.5   | 6.95                            | 1.1                    | 4.6                               |
|                                      | Gamma                                  | 15    | 12.44                           | 3.5                    | 0.8                               |
|                                      | Total                                  | 16.5  | 19.40                           | 2.3                    | 1.2                               |

*The results show that MCNP predicts conservatively higher total (neutron plus gamma) dose rates compared to the measured data. For those two points (neutron dose on the roof bird screens for HSM No. 1 and gamma dose rate on the door for HSM No. 2) where the measured*

*data is higher than the calculated data, it should be noted that the magnitude of these dose rates is small. However, at these two locations the calculated total dose rate is still higher than the measured dose rates. Therefore, a ratio of 0.8 for calculated/measured dose rates for the aforementioned two points is regarded as a fairly accurate estimate. Some conservatism still exists in the methodology used to calculate the source terms, and this is why the calculated dose rates are, in general, higher than the measured dose rates.*

#### **5.5.2.3     Summary of 2-D versus 3-D Shielding Analysis**

*As shown in Section 5.5.2.2, MCNP produces a conservative estimate of the dose rates compared to measured data. Section 5.5.2.1 provides a supportive 3-D analysis of the Advanced NUHOMS® System using MCNP. Also, it is demonstrated here that the 2-D DORT analysis bounds the 3-D results.*

## 6. CRITICALITY EVALUATION

The Advanced NUHOMS® System is designed to meet 10CFR 72.124 [6.1] criticality safety limits during worst case wet loading/unloading operations with the use of fixed neutron absorbing materials (poisons) in the flooded Dry Shielded Canister (24PT1-DSC). The design assures criticality safety under all normal, off-normal and accident conditions associated with fuel handling, 24PT1-DSC handling, 24PT1-DSC storage and off-site transportation.

The results of the detailed analyses demonstrate that the Advanced NUHOMS® System is criticality safe under normal, off normal and accident conditions considering a variety of mechanical uncertainties.

The bounding criticality model used in the SAR analysis is a fully flooded 24PT1-DSC loaded into a flooded NUHOMS®-MP187 transportation cask. Specular boundary conditions are specified on all four sides of a square enveloping the outer cask diameter. This provides for an infinite array of MP187 casks. The AHSM storage configuration is bounded by this configuration. The canister is dry under all conditions of storage. The reactivity of this system is highly dependent on the internal moderator density, with the maximum reactivity occurring at maximum internal moderator density. The reactivity of an array of AHSMs is much less than 0.5 as demonstrated by the internal moderator density varying cases documented in Tables 6.4-1 through 6.4-3. All actual conditions of loading and unloading are bounded because an infinite array of casks is more reactive than a single flooded canister and cask.

The cask used in the criticality analysis is the NUHOMS®-MP187 cask [6.12]. The MP187 transportation cask accident configuration also bounds an infinite array of damaged OS197 transfer casks. A comparison of the pertinent dimensions for the MP187 and OS197 casks are presented below.

|   | MP187  | OS197  |
|---|--------|--------|
| DSC Shell Outer Radius (in)                   | 33.625 | 33.625 |
| H <sub>2</sub> O Gap Thickness, (in)          | 0.375  | 0.375  |
| SS-304 Inner Shell Thickness, (in)            | 1.25   | 0.5    |
| Lead Gamma Shield Radius Thickness, (in)      | 4.0    | 3.56   |
| SS-304 Structural Shell Thickness, (in)       | 2.5    | 1.5    |
| Neutron Shield <sup>(1)</sup> Thickness, (in) | 4.31   | 3 0    |
| SS-304 Neutron Shield Skin Thickness, (in)    | 0.188  | 1.88   |

(1) NS-3 for the MP187, Water for the OS197

As shown in the comparisons above there are only minor differences between the two casks. The differences in the material thickness are insufficient to cause a statistically significant variation in the system  $k_{eff}$ . Also, the neutron shield and neutron shield skin are assumed to be stripped away and replaced by water for the more reactive accident scenarios, therefore for the bounding analysis there is very little physical difference between the cask designs for criticality purposes.

## 6.1 Discussion and Results

Criticality control in the 24PT1-DSC is provided by the basket structural components that maintain the relative position of the spent fuel assemblies under all normal, off-normal and accident conditions and by fixed neutron absorbing materials. The structural analysis of the basket is presented in Chapter 3.

The 24PT1-DSC is designed to ensure nuclear criticality safety during worst case wet loading operations. There is no credible scenario for fresh water inleakage during transfer or storage. However, the wet loading scenario, assuming fresh water (unborated) in the 24PT1-DSC is used to envelope all storage and transfer scenarios including dry 24PT1-DSC and non-mechanistic loss of confinement scenarios, as required by 10CFR 71 [6.2]. A high integrity confinement boundary tested to demonstrate it is leaktight per ANSI N14.5 [6.11] is provided to exclude the possibility of flooding the 24PT1-DSC cavity during the transfer operations and storage period. Prior to these operations, the 24PT1-DSC is vacuum dried, backfilled with helium, double seal welded, and helium leak tested to assure weld integrity. Under these dry conditions, there is no possibility of exceeding criticality safety limits.

Control methods for the prevention of criticality for the 24PT1-DSC consist of administrative procedures (i.e., a plant-specific system using records or tests to document initial enrichment of the selected fuel assemblies), fixed neutron absorbing materials, and the geometrical arrangement of the basket.

The 24PT1-DSC contents are limited to the fuel designs listed in Section 6.2. Computer models of the 24PT1-DSC are discussed in Section 6.3. The criticality evaluation is presented in Section 6.4. The 24PT1-DSC was evaluated for the following conditions that bound normal conditions and the off-normal and accident events listed in Chapter 11:

varied water density including flooding of the basket, with fresh water (water density evaluated includes steam which may be generated during loading and unloading operations),  
variations in material tolerances,  
variations in fuel assembly position in guidesleeves,  
fresh water in the fuel pellet - cladding annulus,  
postulated change of pin pitch due to fuel grid crushing in a drop accident,  
postulated failures for damaged fuel payloads.

The various effects are evaluated individually, and are combined as required to demonstrate compliance with the requirement of 10CFR 72.124 that "before a criticality accident is possible, at least two unlikely, independent, and concurrent or sequential changes have occurred in the conditions essential to nuclear criticality safety."

A series of benchmark calculations were performed with the SCALE 4.4 PC/CSAS25 [6.3] package using the 44-group cross-section library as presented in Section 6.5. The minimum value of the Upper Subcritical Limit (USL) was determined to be 0.9401.

The results of the limiting criticality configurations are summarized in Table 6.1-1. The maximum  $k_{\text{eff}}$  for the normal Westinghouse 14x14 (WE 14x14) Stainless Steel Clad (SC) fuel

geometry is  $0.8677 (k_{eff}+2\sigma)$ . The maximum  $k_{eff}$  for the damaged fuel geometry for WE 14x14 SC fuel is  $0.9392 (k_{eff}+2\sigma)$ . The maximum  $k_{eff}$  for the WE 14x14 Mixed Oxide (MOX) fuel assembly is  $0.9111 (k_{eff}+2\sigma)$ .

**Table 6.1-1**  
**Summary of Limiting Criticality Evaluations for the WE 14x14 SC Fuel Assemblies and**  
**the WE MOX Fuel Assemblies**

| WE 14x14 SC Fuel Assembly   |                     |          |                     |        |
|---|---------------------|----------|---------------------|--------|
| Case  | $K_{eff}$           | $\sigma$ | $K_{eff} + 2\sigma$ | USL    |
| Limiting Assembly Position- The fuel assembly is located in the corner of each guidesleeve closest to the 24PT1-DSC centerline. | 0.8679 <sup>1</sup> | 0.0011   | 0.8702 <sup>1</sup> | 0.9401 |
| NOC-Internal moderator density at 1.0 g/cc  | 0.8679 <sup>1</sup> | 0.0011   | 0.8702 <sup>1</sup> | 0.9401 |
| NOC-External moderator density at 1.0 g/cc  | 0.8684 <sup>1</sup> | 0.0012   | 0.8709 <sup>1</sup> | 0.9401 |
| HAC-Internal moderator density at 1.0 g/cc  | 0.8674 <sup>1</sup> | 0.0010   | 0.8694 <sup>1</sup> | 0.9401 |
| HAC-External moderator at 0.8 g/cc  | 0.8693 <sup>1</sup> | 0.0014   | 0.8720 <sup>1</sup> | 0.9401 |
| Damaged Fuel case with the pin pitch at 0.652 inches and the external moderator density at 0.8 g/cc (4.05% U-235 enrichment)    | 0.9368              | 0.0012   | 0.9392              | 0.9401 |
| WE 14x14 MOX Fuel Assembly  |                     |          |                     |        |
| Case  | $K_{eff}$           | $\sigma$ | $K_{eff} + 2\sigma$ | USL    |
| Limiting Assembly Position- The fuel assembly is located in the corner of each guidesleeve closest to the 24PT1-DSC centerline. | 0.9104 <sup>1</sup> | 0.0014   | 0.9132 <sup>1</sup> | 0.9401 |
| NOC-Internal moderator density at 1.0 g/cc  | 0.9104 <sup>1</sup> | 0.0014   | 0.9132 <sup>1</sup> | 0.9401 |
| NOC-External moderator density at 0.0 g/cc  | 0.9130 <sup>1</sup> | 0.0012   | 0.9154 <sup>1</sup> | 0.9401 |
| HAC-Internal moderator density at 1.0 g/cc  | 0.9113 <sup>1</sup> | 0.0011   | 0.9135 <sup>1</sup> | 0.9401 |
| HAC-External moderator at 0.5 g/cc  | 0.9129 <sup>1</sup> | 0.0011   | 0.9151 <sup>1</sup> | 0.9401 |

<sup>1</sup> Results shown are based on analysis results plus 0.0043 to incorporate sensitivity analysis for fuel clad ID (nominal vs maximum fuel clad ID), Section 6.4.5, Table 6.4-6.

## 6.2 Spent Fuel Loading

This section provides a summary of the maximum spent fuel loading and spent fuel parameters for the 24PT1-DSC.

The allowable contents are listed in Chapter 2 and in the Functional and Operating Limits (Chapter 12) of the Technical Specifications. Each of the fuel assembly types listed in the Technical Specifications has been evaluated in Section 6.4.

Rod Cluster Control Assemblies (RCCAs), Neutron Source Assemblies (NSAs), and Thimble Plug Assemblies (TPAs) can be stored in the canisters with no more than one per fuel assembly. Integral fuel burnable absorber (IFBA, ZrB<sub>2</sub> coating on fuel pellets) fuel assemblies may also be stored.

Each 24PT1-DSC is designed to accommodate four UO<sub>2</sub> damaged fuel assemblies or one MOX damaged fuel assembly (see Section 6.4.3) in lieu of intact assemblies. The required placement of the damaged fuel assemblies is defined in Chapter 12. Damaged fuel includes assemblies with known or suspected cladding defects greater than hairline cracks or pinhole leaks. Damaged fuel assemblies shall be placed in failed fuel cans inside the basket guidesleeves.

### 6.2.1 WE 14x14 SC Fuel Assemblies

The fuel parameters used in the criticality calculations for WE 14x14 SC fuel assemblies are listed in Table 6.2-1.

### 6.2.2 WE 14x14 MOX Fuel Assemblies

The fuel parameters used in the criticality calculations for WE 14x14 MOX fuel assemblies are listed in Table 6.2-2. The mechanical design of the MOX assemblies, for the purpose of handling and storage, is similar to the design of the uranium dioxide assemblies. These assemblies have only minor structural modifications to accommodate the Zircaloy-4 clad fuel rods.




**Table 6.2-1**  
**Design Parameters for Criticality Analysis of the**  
**WE 14x14 SC Fuel Assemblies [6.8]**

| Maximum Initial Enrichment           | 4.05 weight % U-235   |
|--------------------------------------|-----------------------|
| Number of rods:                      | 180 fuel rods (14x14) |
|                                      | 16 guide tubes        |
| Fuel Rod Material (sintered pellet): | UO <sub>2</sub>       |
| Pellet Diameter (inches):            | 0.3835                |
|                                      |                       |
| Pellet Density (% theoretical):      | 95                    |
| Clad Material:                       | Type 304 SS           |
| Clad OD (nominal, inches):           | 0.422                 |
|                                      |                       |
| Active Fuel Length (inches):         | 120                   |
| Rod Pitch (inches)                   | 0.556                 |

**Table 6.2-2**  
**Design Parameters for Criticality Analysis of the**  
**WE 14x14 MOX Fuel Assemblies [6.8]**



|  |                                   |
|--|-----------------------------------|
| Number of rods:  | 180 fuel rods (14x14)             |
|  | 16 guide tubes                    |
| Fuel Rod Material (sintered pellet):   | PuO <sub>2</sub> -UO <sub>2</sub> |
| Pellet Diameter (inches):  | 0.3659                            |
|  |                                   |
| Clad-OD (nominal, inches):   | 0.422                             |
| Clad Thickness (nominal, inches):  | 0.0243                            |
| Active Length (inches):  | 120                               |
| Rod Pitch (inches):  | 0.556                             |

### 6.3 Model Specification

#### 6.3.1 Description of Criticality Analysis Model

Criticality analyses were performed using the microcomputer application KENO-Va and the 44 neutron group library based on ENDF-B Version 5 cross-section data that are part of the SCALE 4.4 code package [6.3]. Validation and benchmarking of these codes is performed in accordance with applicable QA program requirements (see Chapter 13) and is discussed in Section 6.5.

SCALE 4.4 [6.3] is an extensive computer package which has many applications including cross section processing, criticality studies, and heat transfer analyses among others. The package is comprised of many functional modules, which can be run independently of each other. Control Modules were created to combine certain functional modules in order to make the input requirements less complex. For the purpose of criticality analysis, only four functional modules are used and one control module. These Modules are CSAS25, which includes the three dimensional criticality code KENO-Va and the preprocessing codes BONAMI-S, NITAWL-II and XSDRNPM-S.

KENO-Va, in conjunction with a suitable working library of nuclear cross section data, is used to calculate the multiplication factor,  $k_{\text{eff}}$ , of systems of fissile material. It can also compute lifetime and generation time, energy dependent leakages, energy and region-dependent absorptions, fissions, fluxes, and fission densities. KENO-Va utilizes a three-dimensional Monte-Carlo computation scheme. KENO-Va is capable of modeling complex geometries including facilities for handling arrays, arrays of arrays, and holes.

SCALE 4.4 is set up so that any number of cross-section libraries may be used with the preprocessing functional and control modules. For the purpose of this analysis, only the 44-group ENDF/B Version 5 library is used.

The preprocessing codes used for this analysis are the functional modules BONAMI-S, NITAWL-II and XSDRNPM-S. They are consolidated into the control module CSAS25. BONAMI-S has the function of performing Bondarenko calculations for resonance self-shielding. The cross sections and Bondarenko factor data are pulled from an AMPX master library. The output is placed into a master library as well. Dancoff approximations allow for different fuel lattice cell geometries. The main function of NITAWL-II is to change the format of the master cross-section libraries to one which the criticality code (KENO-Va) can access. It also provides the Nordheim Integral Treatment for resonance self-shielding. XSDRNPM-S provides cell-weighted cross sections based on the specified unit cell.

The criticality analysis, using the above computer codes, is performed in compliance with 10CFR 71 [6.2] and bounds the 10CFR 72 [6.1] requirements. Transportation regulations (10CFR 71) distinguish between "damaged" and "undamaged" packages. The undamaged condition is denoted "NOC" for Normal Operating Condition and the damaged condition is denoted "HAC" for Hypothetical Accident Condition. The conditions of a damaged package are established by tests that simulate the effects of a cask drop during handling, fire, extremes of summer heat, winter cold and rain. Specifically for criticality analysis, the HAC case eliminates the neutron shield and fills the space with moderator.

The KENO models consist of 560 axial layers stacked into an array. The layers consist of partial spacer disc or partial moderator regions inside and outside of the active fuel region. The very top and bottom layers of the model are the 24PT1-DSC cover plates. The length of the active fuel is 120 inches. The center to center spacing of the consecutive spacer discs intervals varies from 5.0 to 6.75 inches in increments of 0.25 inches. An axially finite model is shown in Figure 6.3-1.

An infinite array of casks is created by specifying specular reflection on the  $\pm x$  and  $\pm y$  axes and is conservatively used for all normal operation cases. A 12-inch (30.48-cm) water differential albedo is used for hypothetical accident cases which involve loss of transfer cask neutron shield due to a fire or a drop. This accident scenario can only impact one canister at a time since transfer operations of multiple canisters is not probable.

Figure 6.3-2 is an exploded view of the KENO model. UNIT 33 is a slice through the cask at the 24PT1-DSC spacer disc level. UNIT 34 is a slice through the moderator region between consecutive spacer discs.

Figure 6.3-3 shows the structure of the cask at the 24PT1-DSC spacer disc level (UNIT 33) and Figure 6.3-4 shows the structure of the cask at the moderator region between spacer discs (UNIT 34). Note that the difference between the two is that UNIT 33 has a spacer disc (steel surrounding fuel assemblies) and UNIT 34 has steel support rods in addition to water surrounding fuel assemblies. The fuel assemblies are identified in Figure 6.3-3 and Figure 6.3-4 by the position numbers 1 through 24. UNIT numbers 1-8 are used to represent the active fuel in both the spacer disc region and in the moderator region. The fuel assemblies are inserted into the model using KENO's HOLE capability.

Figure 6.3-5 is a cross section of the design basis WE 14x14 SC fuel assembly. Shown is the placement of the individual fuel rods and guide tubes. The width of the fuel assembly is modeled as 7.784 inches. The physical description of the MOX fueled 14x14 Zircaloy-4 clad fuel assembly is similar to that of the WE 14x14 SC fuel assembly. Figure 6.3-6 is a cross section of the design basis WE MOX fueled 14x14 Zircaloy-4 clad fuel assembly.

A detail of the guidesleeve and fuel assembly is shown in Figure 6.3-7. The KENO cases model the square tubes, neutron absorber (Boral™) sheets (4 per tube), and a stainless steel oversleeve wrapper, not shown, which holds the Boral™ sheets in place. Note that the absorber sheets on the outer periphery of the basket (12 locations total) are not needed due to neutron leakage through the cask walls.

Figure 6.3-8 shows the fuel assembly location within the guidesleeves for the "Assembly In Position" runs. Figure 6.3-9 shows the fuel assembly location within the guidesleeves for the "Assembly Out Position" runs. Figure 6.3-10 shows the fuel assembly location within the guidesleeves for the "Assembly Upper Left Position" runs.

The analyses performed are based on a completely flooded 24PT1-DSC. Slots are provided at the bottom of the guidesleeves and openings are provided at the bottom and sides (near the bottom) of the failed fuel cans to ensure uniform draining and filling of all areas of the 24PT1-DSC. The failed fuel can openings are screened to contain potentially loose pellets or debris.

The 6x6 mesh size and 0.047" wire diameter used for these screens will not obstruct uniform draining and filling.

No credit is taken for fuel depletion, fission products, burnable poisons, or axial and radial variations in initial fuel enrichment. Hence, the fuel assemblies are modeled as unirradiated fuel. This assumption results in a considerable conservatism in the calculated  $k_{\text{eff}}$ . Other conservatisms in the computational models include:

1. All neutron absorber panels are assumed to have the minimum width, maximum thickness, and minimum specified areal boron density. The assumption of maximum thickness is conservative because aluminum, which is a weak absorber, displaces water in the flux trap while providing relatively little moderation. Only 75% credit for the boron in the neutron absorber panels is taken in the criticality evaluation.
2. The worst case position tolerance was assumed for all spacer disc cutout locations. This effectively moves all guidesleeve assembly units inward in the x- and y-directions simultaneously, down to the minimum ligament size and minimum spacer disc cutout dimensions. The ligaments are the steel region between spacer disc cutouts. The tolerance in the spacer disc hole dimensions results in a smaller effective inward positioning of the assemblies. This is the worst case condition for criticality since inter-assembly moderation is minimized, thereby reducing the effectiveness of the neutron absorber plates.

The major assumptions made in the intact fuel models are:

1. Unirradiated fuel – no credit is taken for fissile depletion, fuel burnable poisons or fission product poisoning.
2. No credit is taken for soluble boron in the spent fuel pool. All moderation is assumed to be from pure water. No credit is taken for neutron absorption in water impurities.
3. No credit is taken for fuel control components or non fuel assembly hardware such as RCCAs, TPAs, NSAs and IFBA coatings in the 24PT1-DSC. The presence of these components displaces moderator material and/or provides neutron poison reducing  $k_{\text{eff}}$ .
4. All fuel rods are filled with 100% moderator density in the fuel/cladding gap. Moderator density in the range of 0 to 100% is used for water in the 24PT1-DSC cavity to account for any steam generated during loading/unloading operations.
5. 3-D modeling is implemented in all KENO models.
6. Only the active fuel length, 120 inches, is explicitly modeled. The presence of fuel assembly components above and below the active fuel

region displaces moderating material reducing keff, therefore, these regions are conservatively modeled as water. The maximum uranium content is therefore; 375, 200 grams U/assembly or 375 MTU/assembly.

7. For the NOC and HAC storage and transportation conditions, fuel is assumed to be intact with no gross damage or missing rods.
8. It is assumed for the criticality analyses for all HAC cases that the neutron shield and stainless steel shells in the neutron shield cavity of the cask are stripped away and replaced with moderator.
9. The least material condition (LMC) is assumed for the guidesleeves and wrappers. The neutron absorption lost in the thinner steel sheets is offset by the increased moderation.
10. Neutron absorber panel boron content is assumed to be 75% of the minimum specified boron content.
11. The most material condition (MMC) was assumed for the neutron absorber panels (at 75% of the minimum boron content), which is conservative because the maximum amount of moderator is displaced in the flux trap while maintaining the minimum allowable boron content.
12. Impact limiters on the cask ends are not included because they have negligible effect on the keff of the system.
13. Both the bottom of the bottom spacer disc and the bottom of the guidesleeve and Boral™ sheet start at the same axial level. The fuel assembly is completely covered by the Boral™ sheet over the entire active fuel length.



Table 6.3-1, Table 6.3-2, and Table 6.3-3 summarize the 24PT1-DSC materials and dimensions that were assumed in these analyses.

The fuel parameters used in the criticality calculations for WE 14x14 SC Fuel Assemblies are listed in Table 6.2-1. The fuel parameters used in the criticality calculation for WE 14x14 MOX fuel assemblies are listed in Table 6.2-2. The assembly fuel pin loading pattern is given in Figure 6.3-5. Each MOX fuel assembly has 3 types of MOX fuel rods. The fuel rod types are given below with the assembly fuel pin loading pattern given in Figure 6.3-6.

| No. of Fuel Rods | Fissile Pu, weight % | Total Pu, weight % |
|------------------|----------------------|--------------------|
| 64               | 2.84                 | 3.30               |
| 92               | 3.10                 | 3.65               |
| 24               | 3.31                 | 3.85               |

The nominal isotopic composition for the fresh fuel MOX assemblies are:

| Isotope | Atom Density, atom % | Weight Density, weight % |
|---------|----------------------|--------------------------|
| Pu-239  | 80.6                 | 80.51                    |
| Pu-240  | 13.4                 | 13.44                    |
| Pu-241  | 5.2                  | 5.24                     |
| Pu-242  | 0.8                  | 0.81                     |

The analysis methodology and modeling provide an accurate representation of actual cask configurations with the exception of conservatism employed and the use of conservative simplifying assumptions.

### 6.3.2 Neutron Absorber Panel Material Efficacy

The absorber panel material used in the 24PT1-DSC was chosen due to its desirable neutron attenuation, low density, and minimal thickness. It has been used for applications and in environments comparable to those found in spent fuel storage and transportation since the early 1950s (the U.S. Atomic Energy Commission's AE-6 Water-Boiler Reactor). In the 1960s, it was used as a poison material to ship irradiated fuel rods from Canada's Chalk River laboratories to Savannah River. More than 12,000 British Nuclear Fuels, Ltd. (BNFL) flasks containing the material have been used to transport fuel to BNFL's reprocessing plant in Sellafield.

The neutron absorber panels are composed of boron carbide and 1100 alloy aluminum. Boron carbide provides the necessary content of the neutron absorbing B<sup>10</sup> isotope in a chemically inert, heat resistant, highly crystalline and extremely hard form. Boron carbide contained in the panels does not react under these conditions. The boron carbide core is tightly held within an 1100 aluminum alloy matrix and further protected by solid 1100 aluminum alloy cladding plates. Although 1100 alloy aluminum is a chemically reactive material; it behaves much like an inert material when properly applied. Proper application includes due consideration to the formation of a highly protective aluminum oxide layer and allowance for creation of the reaction by-product hydrogen.



Aluminum reacts with water to produce hydrogen (H<sub>2</sub>) and an impervious tightly adhering layer of hydrated aluminum oxide (Al<sub>2</sub>O<sub>3</sub>•3H<sub>2</sub>O) called bayerite which protects the surface from further attack.

When the 24PT1-DSC basket is initially submerged in the spent fuel pool, aluminum in the panels will react with water to form a small amount of hydrogen gas and a stable bayerite layer on all surfaces of the panel. The bayerite layer formed on the panel during pool immersion persists through 24PT1-DSC drying, sealing, storage, and eventual shipping; preventing further corrosion or hydrogen production.

Leaching of the boron carbide along the unsealed edges of the panels is expected to occur to an insignificant degree. There are three reasons why this is anticipated to be insignificant. First, the panel core is a sintered Al/B<sub>4</sub>C material. Only the boron carbide particles exposed by saw cut are available for leaching. Second, the immersion environment is relatively benign and the time is brief (a few hours or days). The material has been commonly used in the United States spent fuel racks for many years and in fact, has gained a reputation for not leaching. And third, direct experimental observations of accelerated aging tests performed at the University of Michigan [6.10] showed no indications of boron degradation. The test specimens were exposed to high neutron and gamma irradiation in a reactor pool environment for over nine years. Subsequent neutron radiography showed no signs of reduced neutron attenuation anywhere on the test specimens.

Depletion of the B<sup>10</sup> in the neutron poison plates is evaluated below. Although the license period of the cask is 20 years, actual storage time could be much longer. Using the total calculated scalar flux of  $5.0 \times 10^5$  n/cm<sup>2</sup>-s at the center of the basket, and the thermal neutron cross section for B<sup>10</sup> is 3837 barn [6.9] the fraction of the original B<sup>10</sup> depleted after 1000 years would be:

$$5 \times 10^5 \text{ n/cm}^2\text{-s} \times (3837 \times 10^{-24} \text{ cm}^2) \times 3.156 \times 10^7 \text{ s/year} \times (1000 \text{ year}) = 1.1 \times 10^{-6}$$

which is negligible. Therefore, the continued efficacy of the neutron poison is assured.

**Table 6.3-1**  
**Geometrical Parameters Used in the Criticality Analysis**

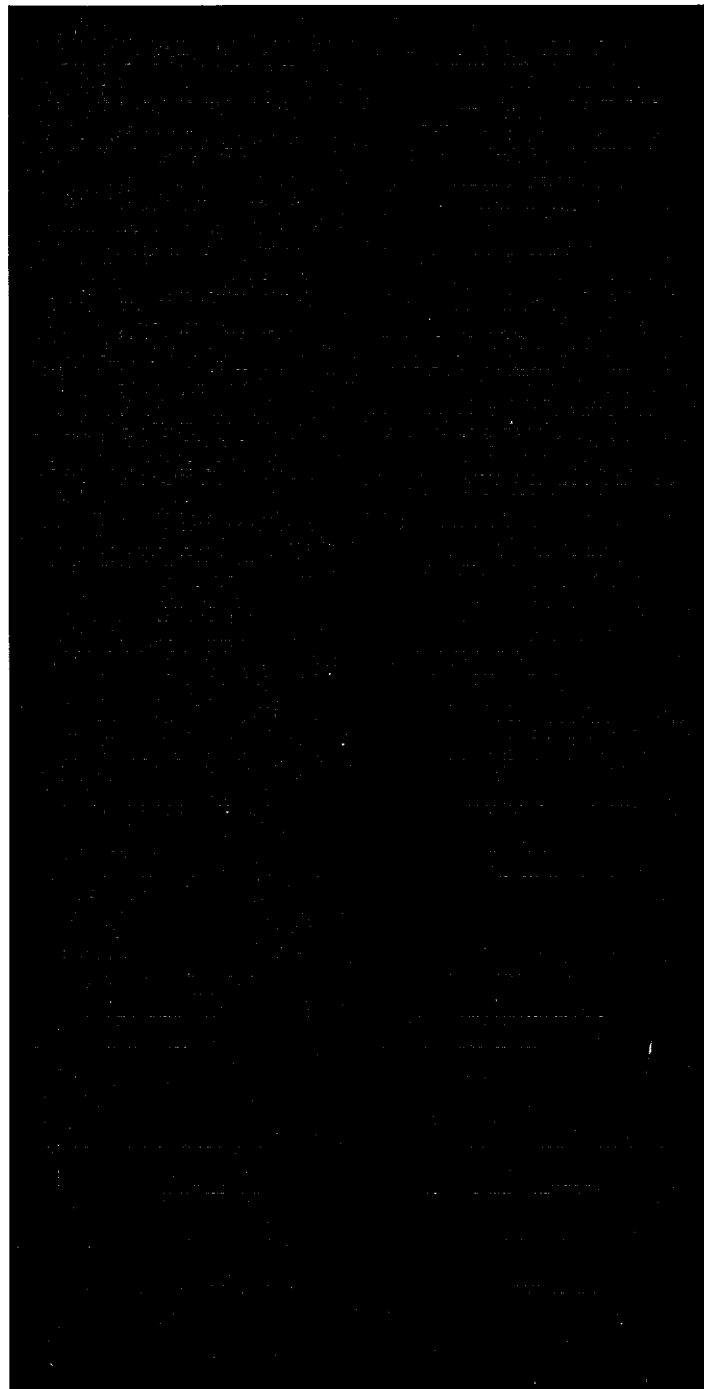


**Table 6.3-1**  
**Geometrical Parameters Used in the Criticality Analysis**

(Continued)

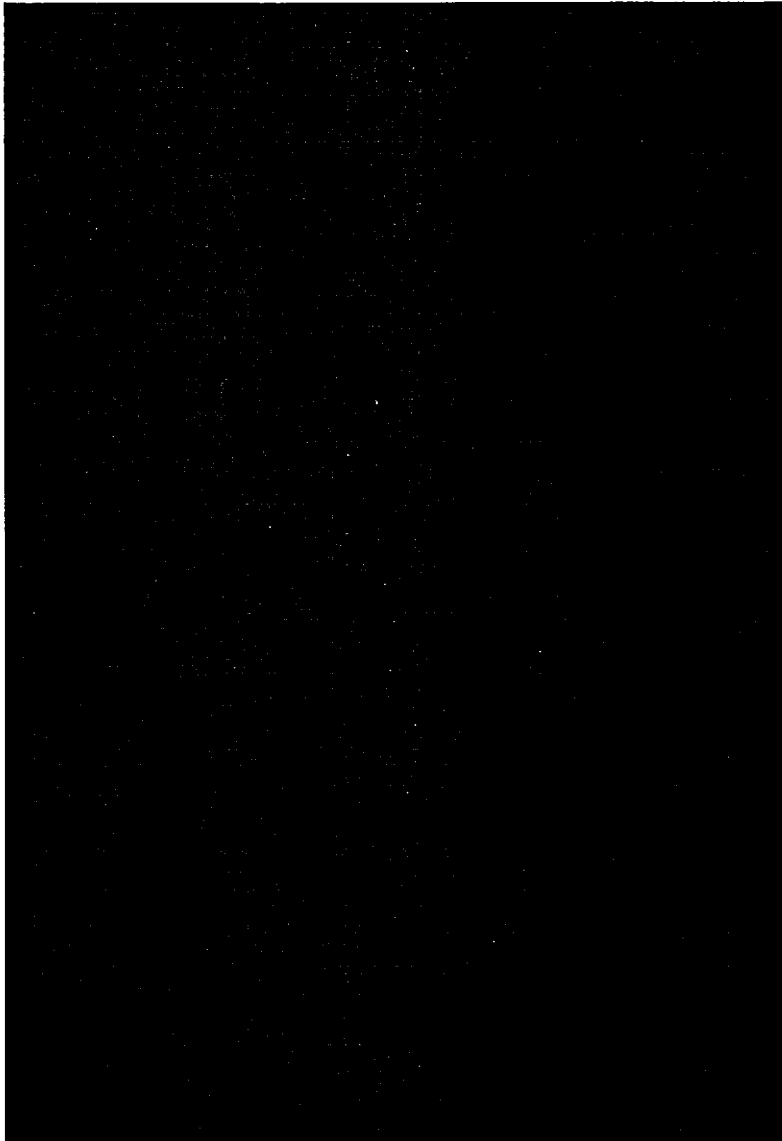


**Table 6.3-1**  
**Design Inputs Used in the Criticality Analysis**

(Concluded)



**Table 6.3-2**  
**Design Parameters for WE 14x14 SC Fuel Assembly Criticality Analysis**

| <b>Boral™ (75%) Material Density*</b>            |                       |
|--|-----------------------|
| Aluminum   | 3.9268E-02 atms/bn-cm |
| Boron  | 2.4879E-02 atms/bn-cm |
| Carbon   | 7.6705E-03 atms/bn-cm |
| <b>NS3 Material Density</b>                      |                       |
| Aluminum   | 7.0275E-03 atms/bn-cm |
| Calcium  | 1.4835E-03 atms/bn-cm |
| Carbon   | 8.2505E-03 atms/bn-cm |
| Hydrogen   | 5.0996E-02 atms/bn-cm |
| Iron   | 1.0628E-04 atms/bn-cm |
| Oxygen   | 3.7793E-02 atms/bn-cm |
| Silicon  | 1.2680E-03 atms/bn-cm |
| <b>WE 14x14 SC Clad Fuel Parameters</b>          |                       |
| Fuel OD (in)                                     | 0.3835                |
| Clad OD (in)                                     | 0.422                 |
| Clad Thickness (nominal)                         | 0.01650               |
| Clad Material                                    | Stainless Steel       |
|  |                       |
| Active Fuel Height (in)                          | 120.0                 |
| Rod Pitch (in)                                   | 0.556                 |
| Fuel Theoretical Density                         | 0.95                  |
| <b>Fuel Pellet Material Density (atms/bn-cm)</b> |                       |
| $U^{235}$  | 9.4064E-04            |
| $U^{238}$  | 2.2290E-02            |
| O  | 4.6462E-02            |

\* Boral™ is modeled as a homogenous material. The Boral™ material, however, is manufactured with an aluminum clad Boron Carbide matrix. Analyses have been performed modeling the aluminum clad and the Boral™ core separately. The results of these analyses demonstrate that the affect of the homogenization of the Boral™ on  $k_{eff}$  is within the statistical uncertainty ( $2\sigma$ ) of the analyses.

**Table 6.3-3**  
**Design Parameters for WE 14x14 MOX Fuel Assembly Criticality Analysis**

| <b>Boral™ (75%) Material Density*</b>                                 |                       |
|---|-----------------------|
| Aluminum  | 3.9268E-02 atms/bn-cm |
| Boron   | 2.4879E-02 atms/bn-cm |
| Carbon  | 7.6705E-03 atms/bn-cm |
| <b>NS3 Material Density</b>   |                       |
| Aluminum  | 7.0275E-03 atms/bn-cm |
| Calcium   | 1.4835E-03 atms/bn-cm |
| Carbon  | 8.2505E-03 atms/bn-cm |
| Hydrogen  | 5.0996E-02 atms/bn-cm |
| Iron  | 1.0628E-04 atms/bn-cm |
| Oxygen  | 3.7793E-02 atms/bn-cm |
| Silicon   | 1.2680E-03 atms/bn-cm |
| <b>WE 14x14 MOX Zr-4 Clad Fuel Parameters</b>                         |                       |
| Fuel OD (in)  | 0.3659                |
| Clad OD (in)  | 0.422                 |
|   |                       |
| Active Fuel Height (in)   | 120.0                 |
| Rod Pitch (in)  | 0.556                 |
|   |                       |
| <b>Fuel Pellet Material Density 3.85% Total Weight % Pu (24 Rods)</b> |                       |
| U <sup>234</sup>  | 1.22345E-06           |
| U <sup>235</sup>  | 1.60161E-04           |
| U <sup>238</sup>  | 2.20831E-02           |
| O   | 4.65088E-02           |
| Pu <sup>239</sup>   | 8.13970E-04           |
| Pu <sup>240</sup>   | 1.35314E-04           |
| Pu <sup>241</sup>   | 5.25386E-05           |
| Pu <sup>242</sup>   | 8.08755E-06           |
| <b>Fuel Pellet Material Density 3.30% Total Weight % Pu (64 Rods)</b> |                       |
| U <sup>234</sup>  | 1.22345E-06           |
| U <sup>235</sup>  | 1.60161E-04           |
| U <sup>238</sup>  | 2.20831E-02           |
| O   | 4.62086E-02           |
| Pu <sup>239</sup>   | 6.93002E-04           |
| Pu <sup>240</sup>   | 1.15204E-04           |
| Pu <sup>241</sup>   | 4.47306E-05           |
| Pu <sup>242</sup>   | 6.88562E-06           |
| <b>Fuel Pellet Material Density 3.65% Total Weight % (92 Rods)</b>    |                       |
| U <sup>234</sup>  | 1.22345E-06           |
| U <sup>235</sup>  | 1.60161E-04           |
| U <sup>238</sup>  | 2.20831E-02           |
| O   | 4.64019E-02           |
| Pu <sup>239</sup>   | 7.70913E-04           |
| Pu <sup>240</sup>   | 1.28156E-04           |
| Pu <sup>241</sup>   | 4.97595E-05           |
| Pu <sup>242</sup>   | 7.65974E-06           |

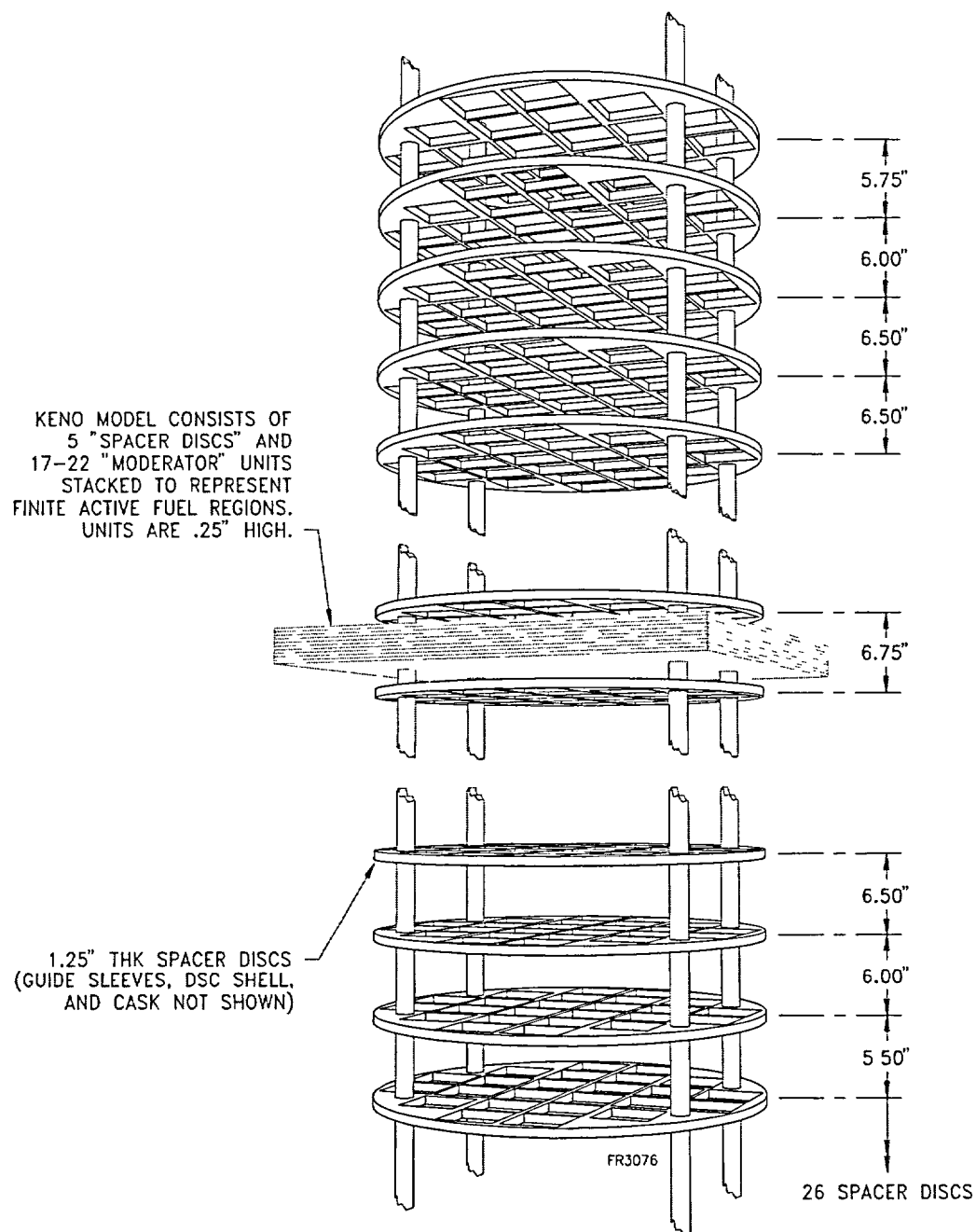


**Figure 6.3-1**  
**KENO Model of the 24PT1-DSC Basket**

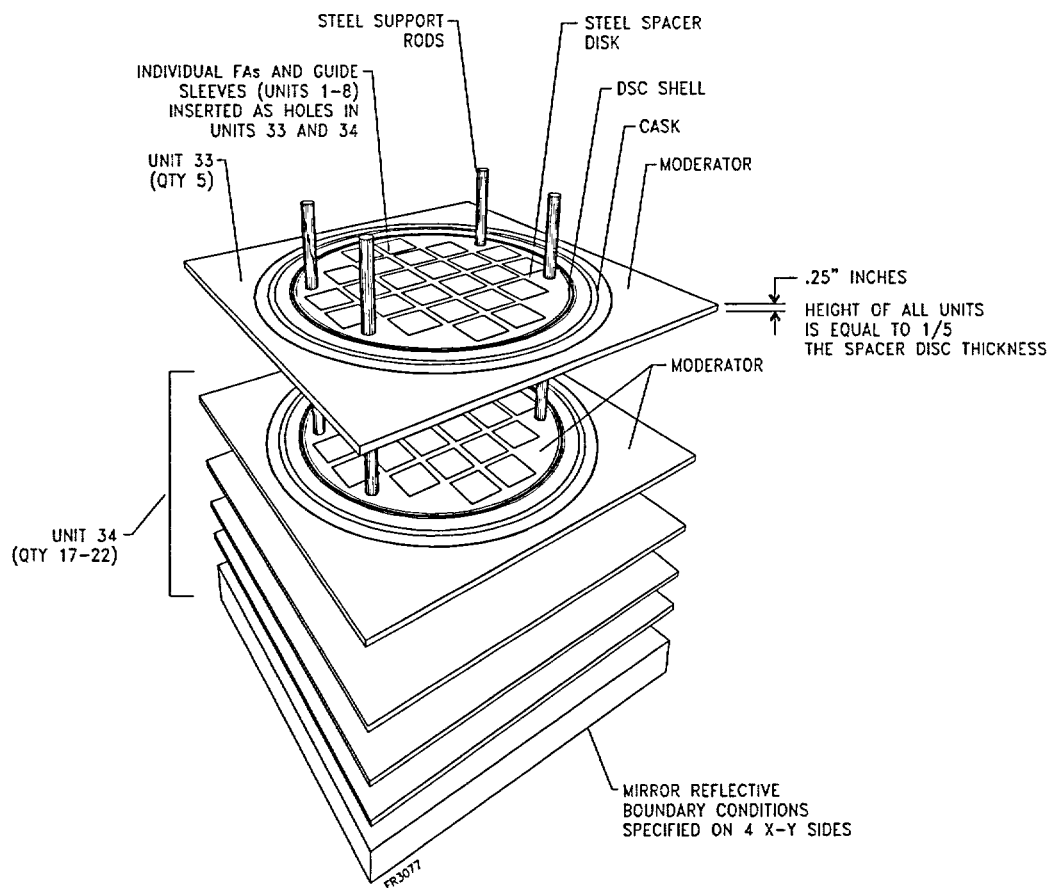


**Figure 6.3-2**  
**Exploded View of KENO Model**



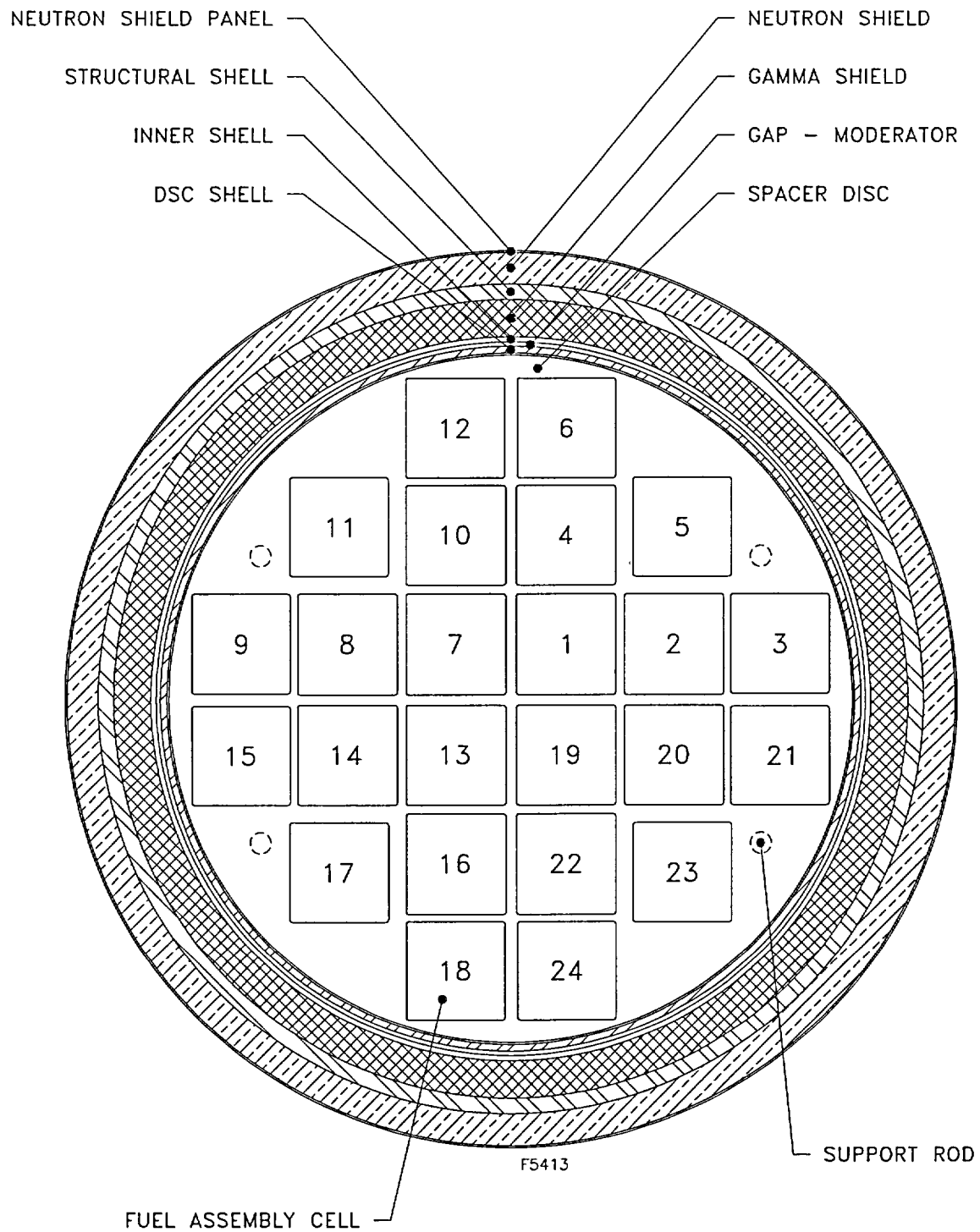


**Figure 6.3-3**  
**Structure of KENO Model – UNIT 33**

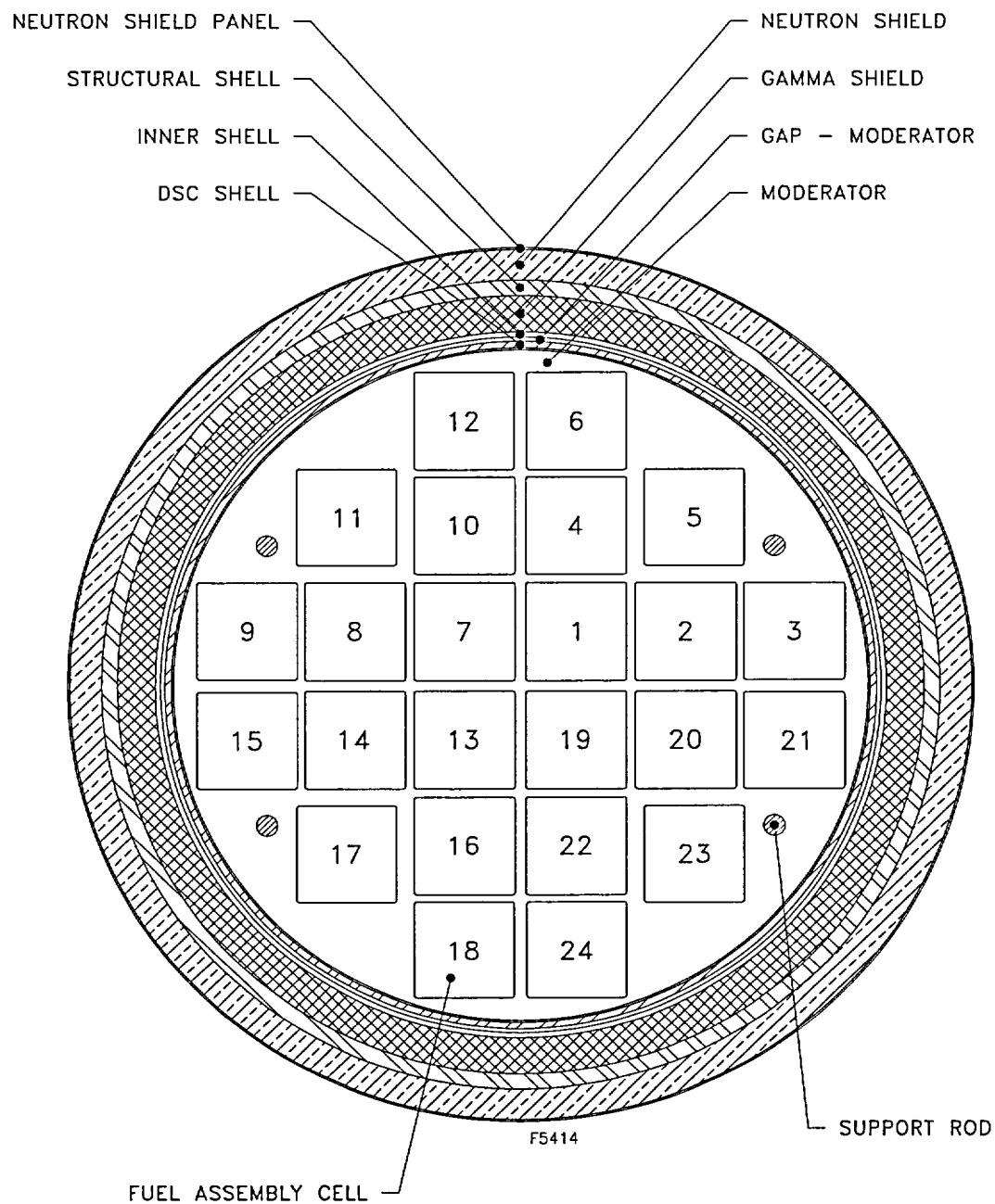


**Figure 6.3-4**  
**Structure of KENO Model – UNIT 34**

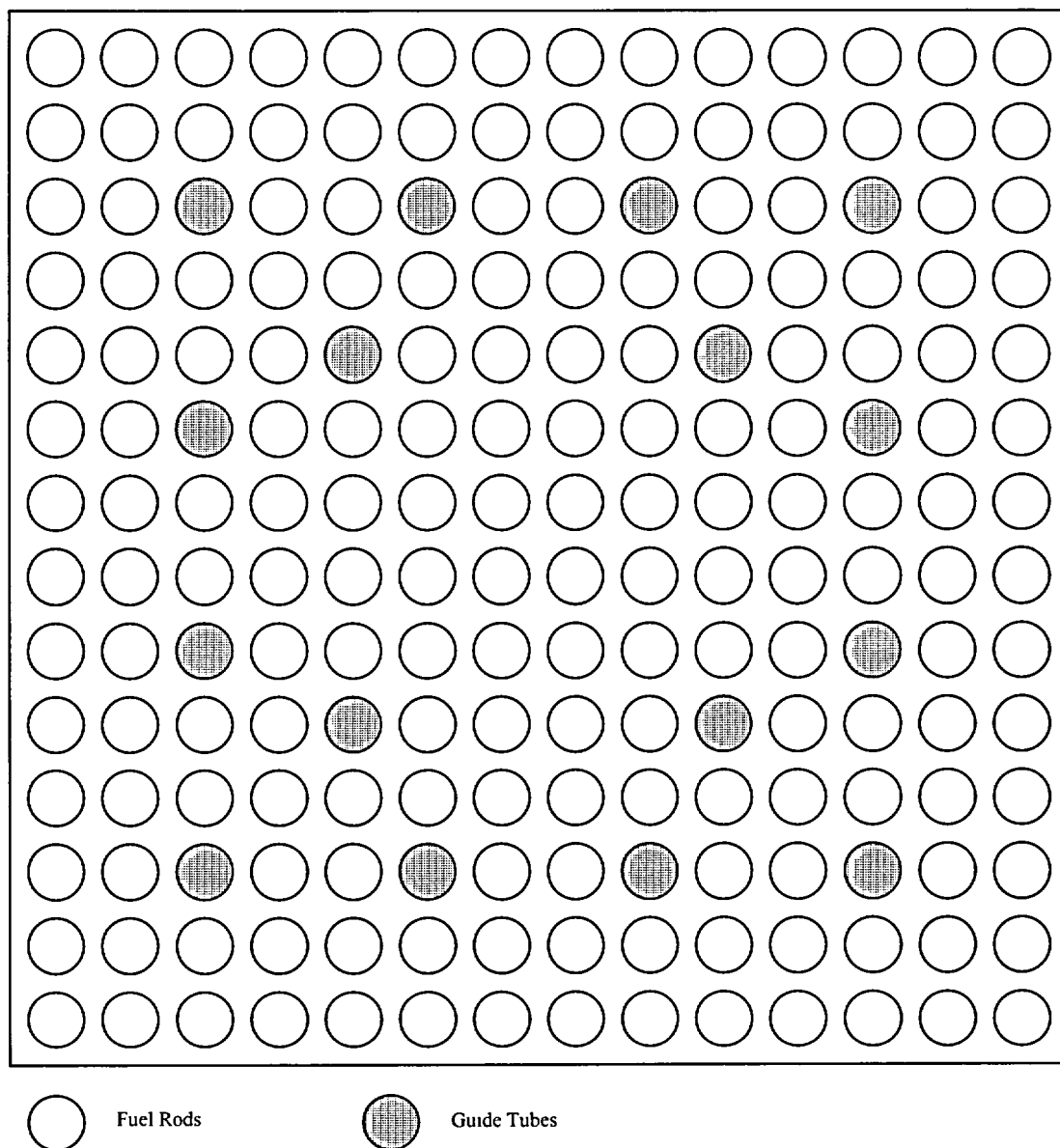


**Figure 6.3-5**  
**Cross Section of the Design Basis WE 14x14 SC Fuel Assembly**

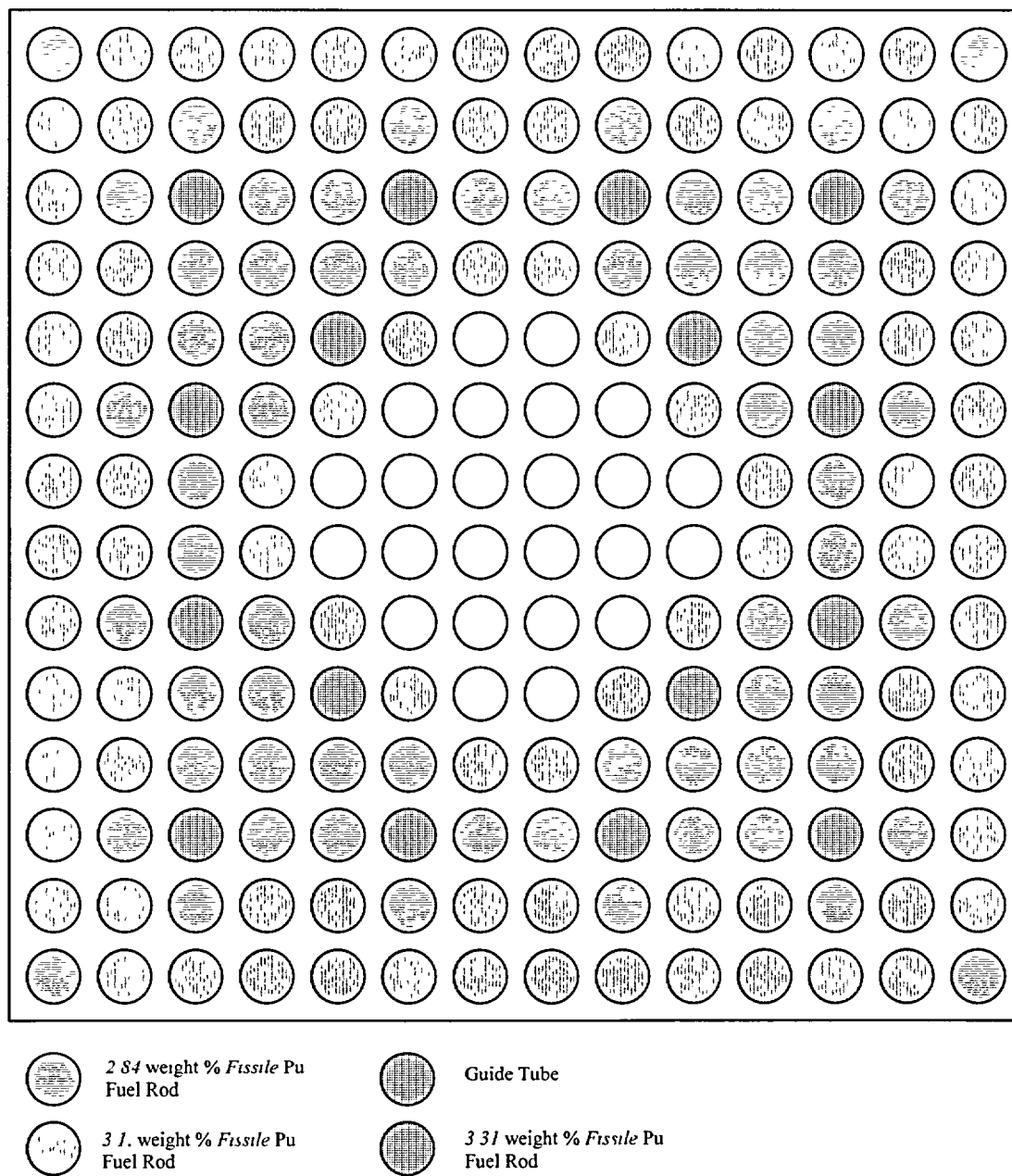


**Figure 6.3-6**  
**Cross Section of the Design Basis WE 14x14 MOX Fuel Assembly**

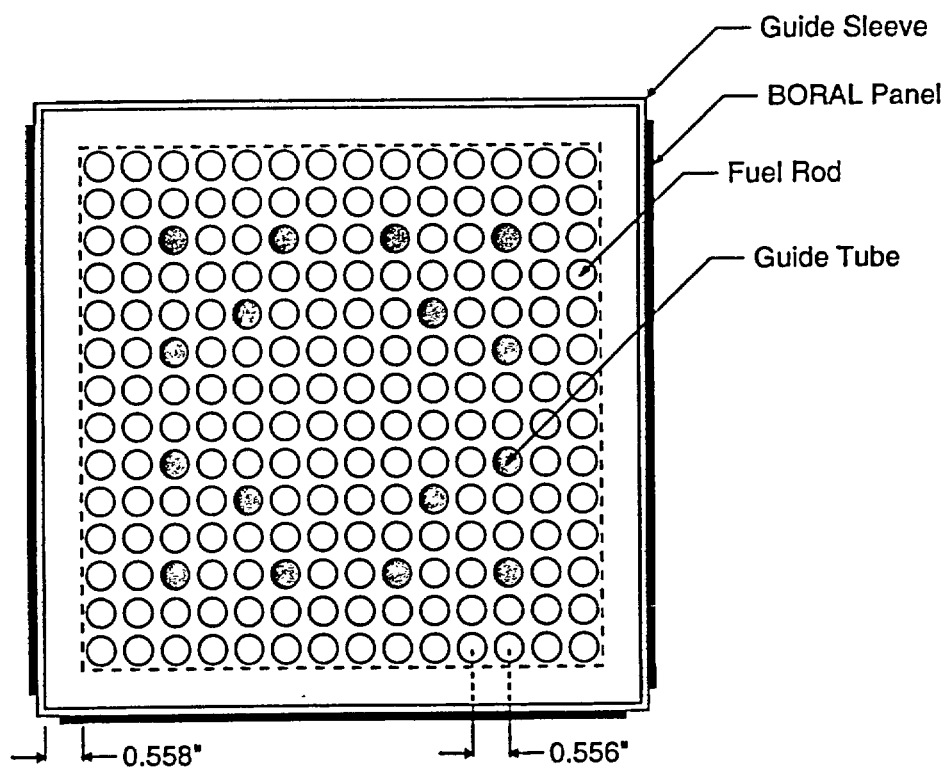


**Figure 6.3-7**  
**Guidesleeve and Fuel Assembly Cross Section**

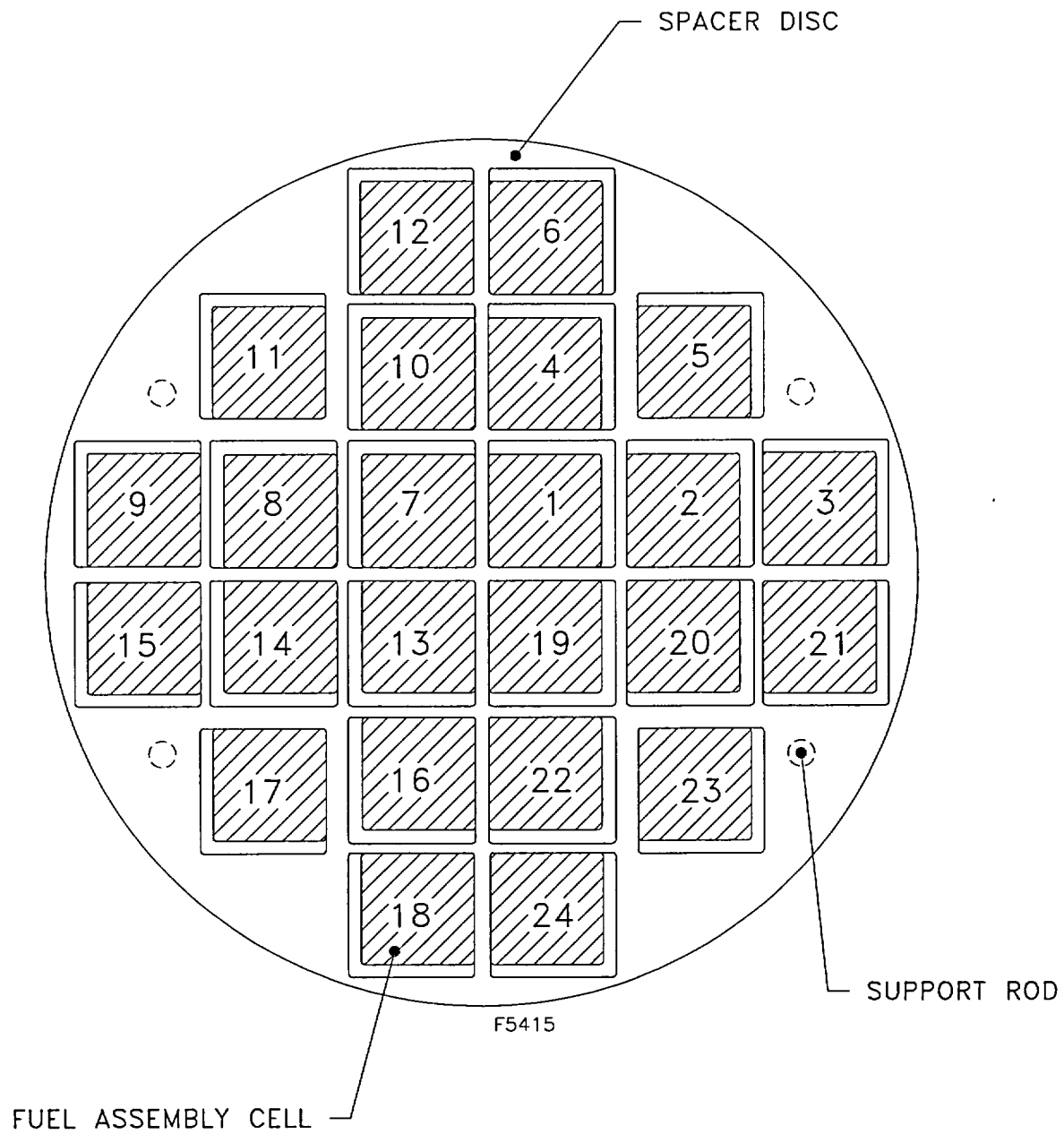


**Figure 6.3-8**  
**Fuel Assemblies Located in the Inner Guidesleeve Corner Closest to the DSC Centerline (Assembly in Case)**

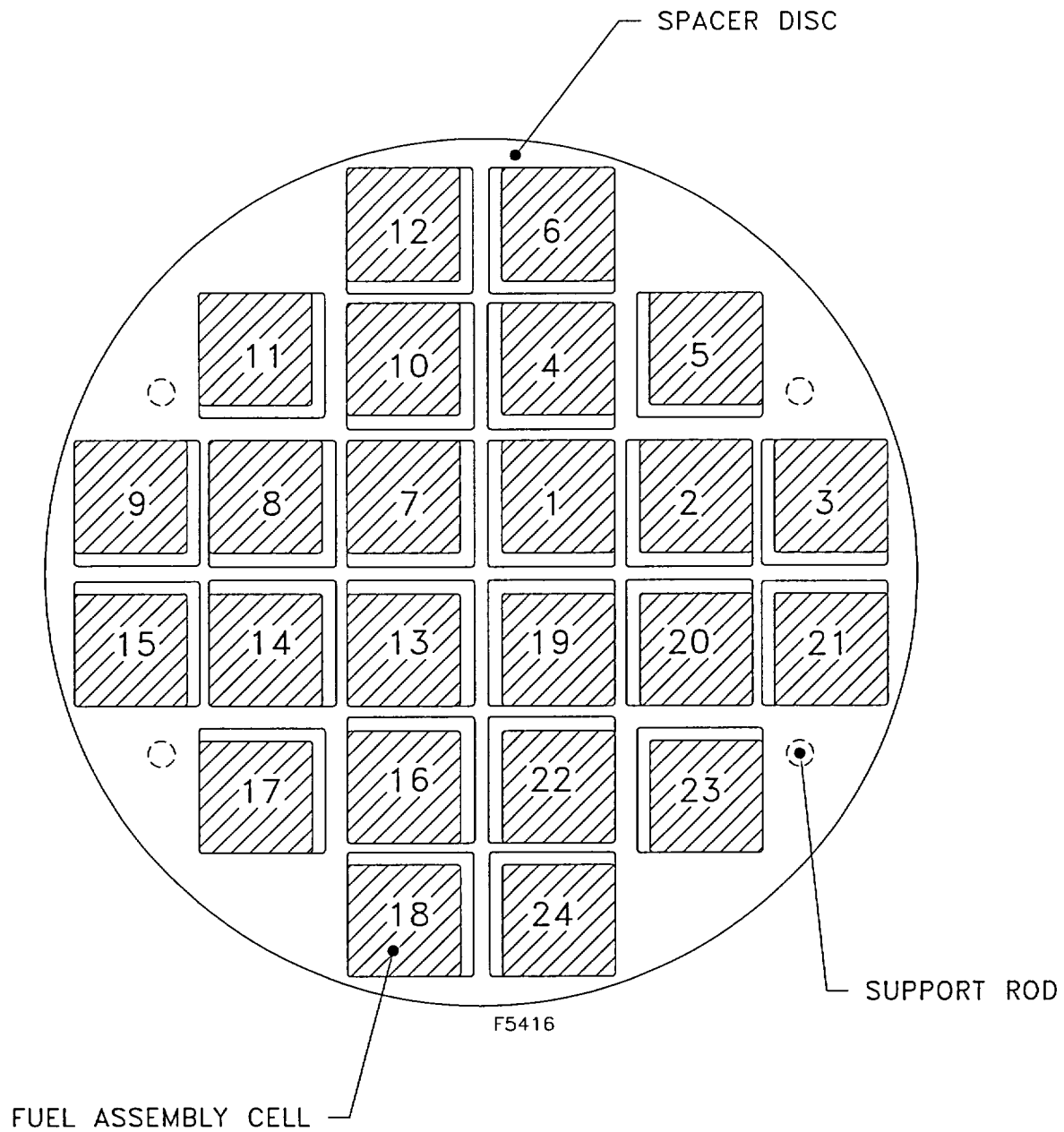


**Figure 6.3-9**  
**The Fuel Assemblies Moved Radially Outwards from the Center**  
**of the DSC (Assembly Out Case)**

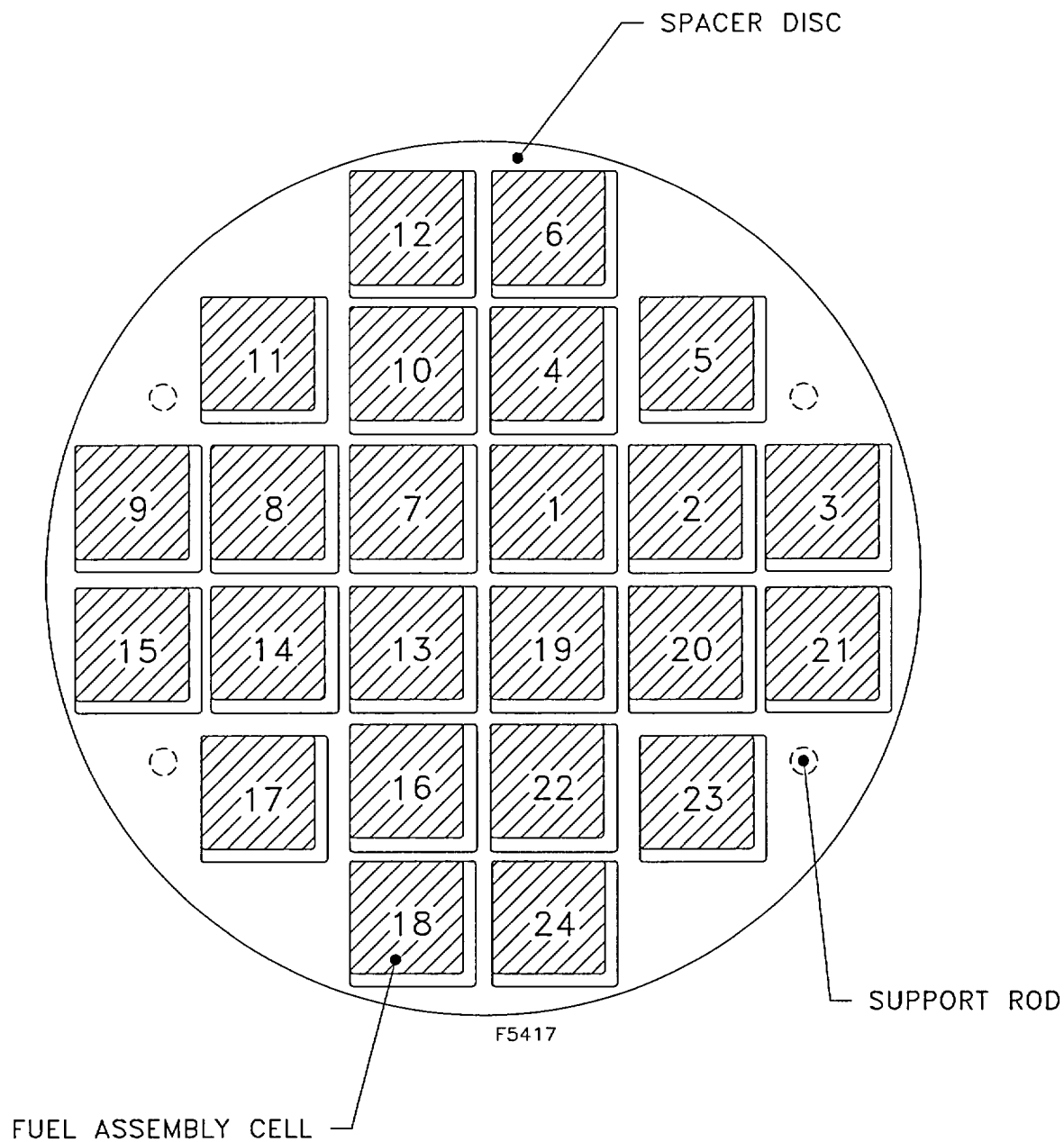


**Figure 6.3-10**  
**The Fuel Assemblies Are Moved Towards the Upper Left Corner of Each**  
**Guidesleeve Assembly Upper Left Corner Case**



## 6.4 Criticality Calculation

This section contains descriptions of the calculational methods used to determine the nuclear reactivity for the maximum fuel loading intended to be stored in the 24PT1-DSC.

### 6.4.1 Calculational Method

The effective neutron multiplication factor ( $k_{\text{eff}}$ ) was calculated using the CSAS25 module of the SCALE 4.4 Code with the 44-group ENDF/B-V cross-section library [6.3]. The control module CSAS25 includes the three dimensional criticality code KENO-Va and the preprocessing codes BONAMI-S, NITAWL-II and XSDRNPM-S.

KENO-Va, in conjunction with a suitable working library of nuclear cross section data, is used to calculate the  $k_{\text{eff}}$  of systems of fissile material. It can also compute lifetime and generation time, energy dependent leakages, energy and region-dependent absorptions, fissions, fluxes, and fission densities. KENO-Va utilizes a three-dimensional Monte-Carlo computation scheme. BONAMI-S has the function of performing Bondarenko calculations for resonance self-shielding. The main function of NITAWL-II is to change the format of the master cross-section libraries to one that the criticality code (KENO-Va) can access. It also provides the Nordheim Integral Treatment for resonance self-shielding. XSDRNPM-S provides cell-weighted cross sections based on the specified unit cell.

Analyses provided vary both internal (inside DSC shell) and external (outside cask) moderator density.

### 6.4.2 Fuel Loading Optimization

The criticality analysis is performed for the 24PT1-DSC loaded with 24 WE 14x14 SC fuel assemblies, 24 WE 14x14 MOX fuel assemblies, or 24 damaged fuel assemblies. A 4.0 weight percent enriched fuel was used for the WE 14x14 SC fuel assemblies and the damaged fuel assemblies. The loading pattern considered in the criticality analysis also bounds all possible loading configurations including the addition of dummy assemblies and/or leaving assembly locations open.

The criticality analyses for the MOX fuel assemblies assumed the 24PT1-DSC was entirely loaded with twenty four MOX fuel assemblies for the purposes of determining the most reactive fuel configuration. This configuration bounds the possible loading configurations including mixtures of MOX and UO<sub>2</sub> fuel assemblies.

The KENO models were specified with either 100% specular reflection or infinite water boundary conditions on all four sides. All models were specified with the specular reflective conditions on top and bottom. Further discussion regarding the models can be found in Section 6.3.





### 6.4.3 Criticality Results

This section presents the results of the analyses used to demonstrate the acceptability of storing qualified fuel in the 24PT1-DSC under normal, off-normal, and accident conditions for fuel loading, handling, and storage. Uncertainties are addressed and are applied to the nominal calculated  $k_{\text{eff}}$  value.

ANS/ANSI-8.1 [6.5] recommends that calculational methods used in determining criticality safety limits for applications outside reactors be validated by comparison with appropriate critical experiments. An Upper Subcritical Limit (USL) provides a high degree of confidence that a given system is subcritical if a criticality calculation based on the system yields a  $k_{\text{eff}}$  below the USL. In Section 6.5, the minimum USL is determined to be 0.9401. The criticality analysis verifies that in normal, off-normal, and accident conditions,  $k_{\text{eff}} + 2\sigma \leq \text{USL}$ . Therefore, the fuel will remain subcritical. Conclusions regarding specific aspects of the methods used or the analyses presented can be drawn from the quantitative results presented in the associated tables.

Reactivity calculations were performed in *three* sets of parametric studies for the 24PT1-DSC loaded with WE 14x14 SC assemblies, WE 14x14 MOX fuel assemblies, and WE 14x14 SC assemblies containing damaged fuel rods. The results are summarized in Table 6.4-1, Table 6.4-2, and Table 6.4-3, respectively.

The maximum  $k_{\text{eff}}$  for the 24PT1-DSC with intact WE 14x14 SC fuel assemblies was determined to be  $0.8650 \pm 0.0014$  for HAC conditions with internal moderation at 1.0 g/cc and external moderation at 0.8 g/cc interspersed between an infinite array of packages. The  $k_{\text{eff}} + 2\sigma$  is less than the USL,  $0.8677 < 0.9401$ .

The maximum  $k_{\text{eff}}$  for the 24PT1-DSC with intact WE 14x14 MOX fuel assemblies was determined to be  $0.9087 \pm 0.0012$  for HOC conditions with internal moderation at 1.0 g/cc and external moderation at 0.0001 g/cc in an infinite array of packages. The  $k_{\text{eff}} + 2\sigma$  is less than the USL,  $0.9111 < 0.9401$ .

The maximum  $k_{\text{eff}}$  for the 24PT1-DSC loaded with 24 WE 14x14 SC failed fuel assemblies was determined to be  $0.9340 \pm 0.0014$  for HAC conditions with a rod pitch of 0.652 inches, internal moderation at 1.0 g/cc, and external moderation at 0.8 g/cc in an infinite array of packages. The  $k_{\text{eff}} + 2\sigma$  is less than the USL,  $0.9392 < 0.9401$ . This is close to the USL; however, it should be noted that it was conservatively assumed in the modeling of the damaged fuel geometry that the entire 24PT1-DSC was filled with damaged fuel assemblies. There will be significantly more margin to the USL if less than 24 damaged fuel assemblies are loaded in the 24PT1-DSC (a maximum of four damaged fuel assemblies are allowed, see Chapter 12). This analysis, although performed specifically for the WE 14x14 SC damaged fuel assemblies will bound the payload condition of one damaged MOX assembly with no other damaged assemblies in the 24PT1-DSC. The conservatism of the analyzed canister with 24 WE 14x14 SC damaged fuel assemblies bounds the condition of only one MOX damaged fuel assembly at one of the corner locations in the 24PT1-DSC (outermost fuel assembly locations at 45, 135, 225, or 315 degree azimuths). The MOX damaged fuel assembly at this location is also bounded by the 24PT1-DSC analysis for 24 undamaged MOX assemblies. The increase in reactivity of one damaged MOX assembly

at a location with significant neutron leakage (adjacent undamaged, non-MOX assemblies on only 2 sides with the remaining two sides facing the 24PT1-DSC shell without intervening fuel) will have little effect on the low  $k_{eff}$  calculated for the WE 14x14 SC intact fuel case.

#### 6.4.4 Evaluation of Effect of Uncertainty in Maximum Initial Enrichment

The maximum initial enrichment used in the criticality analyses for  $UO_2$  fuel (4.0%) does not include uncertainties (manufacturing tolerance) in maximum initial enrichment. Also, the maximum initial enrichment for MOX fuel used in the criticality analysis does account for potential uncertainty in Pu maximum initial enrichment.

To address the effect of potential  $UO_2$  fuel assembly initial enrichment uncertainty, an evaluation of the effect of an increased initial enrichment from 4.0 weight % to 4.05 weight %, has been performed. The results of this analysis are presented in Table 6.4-4. These results when compared to the equivalent case analyzed for 4.0 weight %, Table 6.4-3, show that the increase in enrichment from 4.0 weight % to 4.05 weight % results in an increase in  $k_{eff}$  (incl.  $2\sigma$ ) from .9368 to .9392. The increased  $k_{eff}$  remains less than the USL of .9401. Based on these results, storage of fuel of up to 4.05 weight % enrichment is acceptable. Chapter 12 therefore uses a maximum enrichment of 4.05 weight % for  $UO_2$  fuel.

#### 6.4.5 Effect of Fuel Parameter Tolerances on Reactivity

To evaluate the effect of fuel parameter tolerances on reactivity, the fuel parameters used in the criticality analyses have been reviewed to identify sensitivity studies needed to evaluate these effects. A review of fuel parameters identified in Tables 6.2-1 and 6.2-2 indicates that all parameters listed with the exception of pellet diameter, clad outer diameter (OD) and clad thickness are enveloped by the criticality analyses performed. To evaluate the effect of tolerances in clad OD, clad thickness and fuel pellet diameter on reactivity, sensitivity analyses are performed to evaluate system reactivity as a function of these parameters. These analyses are performed for the SC fuel assemblies since the damaged SC assembly analysis is the bounding analysis. In addition, changes in the configuration of the stainless steel cladding have a more significant effect on reactivity than the zirconium cladding used in the MOX fuel. The CSAS25 models used to perform this sensitivity analysis are based on the model used to calculate  $k_{eff}$  for the fuel assemblies centered in the guidesleeves, the results of which are reported in Table 6.4-1. This model is revised to include 4.05 wt. % enriched fuel and the revised clad and pellet dimensions. The results of the evaluation are presented in Tables 6.4-5, 6.4-6 and 6.4-7. The results demonstrate that the calculated changes in reactivity between the various cladding and pellet dimensions are not significant. *The increase in reactivity between nominal and maximum clad ID is added to the normal conditions  $k_{eff}$  in Table 6.1-1. This increase in reactivity is not included for the damaged fuel analysis since it is enveloped by the analysis assumptions of a larger number of damaged fuel assemblies than allowed by the Technical Specifications (Chapter 12).*

**Table 6.4-1**  
**Results for the WE 14x14 SC Fuel Assembly**

| Normal Operating Condition: Assembly Position Case Results |               |                     |   |
|--|---------------|---------------------|---|
| $K_{eff}$  | $\pm 1\sigma$ | $K_{eff} + 2\sigma$ | Description   |
| 0.8636   | 0.0011        | 0.8659              | The fuel assembly is located in the corner of each guidesleeve closest to the 24PT1-DSC centerline. |
| 0.8581   | 0.0013        | 0.8608              | The fuel assemblies are centered in each guidesleeve.   |
| 0.8382   | 0.0011        | 0.8404              | The fuel assemblies are moved radially outwards from the center of the 24PT1-DSC                    |
| 0.8475   | 0.0011        | 0.8497              | The fuel assemblies are moved towards the upper left corner of each guidesleeve.                    |

| Normal Operating Condition: Internal Moderator Density Varying Assuming the Inward Assembly Position |               |                     |   |
|--|---------------|---------------------|---|
| $K_{eff}$  | $\pm 1\sigma$ | $K_{eff} + 2\sigma$ | Internal Moderator (H <sub>2</sub> O) Density, g/cc |
| 0.4122   | 0.0006        | 0.4133              | 0.0001  |
| 0.4762   | 0.0006        | 0.4774              | 0.05  |
| 0.5101   | 0.0007        | 0.5114              | 0.1   |
| 0.5660   | 0.0009        | 0.5678              | 0.2   |
| 0.6161   | 0.0010        | 0.6181              | 0.3   |
| 0.6634   | 0.0010        | 0.6655              | 0.4   |
| 0.7055   | 0.0012        | 0.7078              | 0.5   |
| 0.7424   | 0.0011        | 0.7446              | 0.6   |
| 0.7767   | 0.0013        | 0.7792              | 0.7   |
| 0.8088   | 0.0011        | 0.8111              | 0.8   |
| 0.8379   | 0.0013        | 0.8406              | 0.9   |
| 0.8636   | 0.0011        | 0.8659              | 1.0   |

**Table 6.4-1**  
**Results for the WE 14x14 SC Fuel Assembly**  
 (Continued)

| Normal Operating Condition: External Moderator Density Varying Assuming the Inward Assembly Position |               |                     |   |
|--|---------------|---------------------|---|
| $K_{eff}$  | $\pm 1\sigma$ | $K_{eff} + 2\sigma$ | External Moderator (H <sub>2</sub> O) Density, g/cc |
| 0.8605   | 0.0011        | 0.8628              | 0.0001  |
| 0.8623   | 0.0013        | 0.8649              | 0.05  |
| 0.8629   | 0.0013        | 0.8654              | 0.1   |
| 0.8644   | 0.0011        | 0.8665              | 0.2   |
| 0.8633   | 0.0010        | 0.8653              | 0.3   |
| 0.8639   | 0.0011        | 0.8661              | 0.4   |
| 0.8625   | 0.0014        | 0.8652              | 0.5   |
| 0.8617   | 0.0011        | 0.8640              | 0.6   |
| 0.8620   | 0.0012        | 0.8643              | 0.7   |
| 0.8593   | 0.0012        | 0.8618              | 0.8   |
| 0.8616   | 0.0013        | 0.8641              | 0.9   |
| 0.8641   | 0.0012        | 0.8666              | 1.0   |

| Hypothetical Accident Condition: Internal Moderator Density Varying Assuming the Inward Assembly Position |               |                     |   |
|---|---------------|---------------------|---|
| $K_{eff}$   | $\pm 1\sigma$ | $K_{eff} + 2\sigma$ | Internal Moderator (H <sub>2</sub> O) Density, g/cc |
| 0.4118  | 0.0005        | 0.4128              | 0.0001  |
| 0.4764  | 0.0007        | 0.4777              | 0.05  |
| 0.5111  | 0.0006        | 0.5124              | 0.1   |
| 0.5644  | 0.0008        | 0.5661              | 0.2   |
| 0.6160  | 0.0011        | 0.6182              | 0.3   |
| 0.6623  | 0.0011        | 0.6646              | 0.4   |
| 0.7058  | 0.0010        | 0.7077              | 0.5   |
| 0.7429  | 0.0010        | 0.7449              | 0.6   |
| 0.7782  | 0.0012        | 0.7805              | 0.7   |
| 0.8088  | 0.0012        | 0.8113              | 0.8   |
| 0.8360  | 0.0012        | 0.8385              | 0.9   |
| 0.8631  | 0.0010        | 0.8651              | 1.0   |

**Table 6.4-1**  
**Results for the WE 14x14 SC Fuel Assembly**  
(Concluded)

| Hypothetical Accident Condition: External Moderator Density Varying Assuming the Inward Assembly Position |               |                     |   |
|---|---------------|---------------------|---|
| $K_{eff}$   | $\pm 1\sigma$ | $K_{eff} + 2\sigma$ | External Moderator (H <sub>2</sub> O) Density, g/cc |
| 0.8625  | 0.0013        | 0.8651              | 0.0001  |
| 0.8622  | 0.0013        | 0.8647              | 0.05  |
| 0.8640  | 0.0013        | 0.8665              | 0.1   |
| 0.8635  | 0.0011        | 0.8657              | 0.2   |
| 0.8620  | 0.0011        | 0.8642              | 0.3   |
| 0.8626  | 0.0011        | 0.8647              | 0.4   |
| 0.8621  | 0.0012        | 0.8645              | 0.5   |
| 0.8622  | 0.0012        | 0.8647              | 0.6   |
| 0.8624  | 0.0011        | 0.8645              | 0.7   |
| 0.8650  | 0.0014        | 0.8677              | 0.8   |
| 0.8635  | 0.0011        | 0.8658              | 0.9   |
| 0.8599  | 0.0011        | 0.8621              | 1.0   |



**Table 6.4-2**  
**Results for the WE 14x14 MOX Fuel Assembly**

| Normal Operating Condition: Assembly Position Study |               |                     |   |
|---|---------------|---------------------|---|
| $K_{eff}$   | $\pm 1\sigma$ | $K_{eff} + 2\sigma$ | Description   |
| 0.9061  | 0.0014        | 0.9089              | The fuel assembly is located in the corner of each guidesleeve closest to the 24PT1-DSC centerline. |
| 0.8952  | 0.0012        | 0.8976              | The fuel assemblies are centered in each guidesleeve.   |
| 0.8771  | 0.0012        | 0.8795              | The fuel assemblies are moved radially outwards from the center of the 24PT1-DSC                    |
| 0.8875  | 0.0018        | 0.8911              | The fuel assemblies are moved towards the upper left corner of each guidesleeve.                    |

| Normal Operating Condition: Internal Moderator Density Varying Assuming the Inward Assembly Position |               |                     |   |
|--|---------------|---------------------|---|
| $K_{eff}$  | $\pm 1\sigma$ | $K_{eff} + 2\sigma$ | Internal Moderator (H <sub>2</sub> O) Density, g/cc |
| 0.4269   | 0.0005        | 0.4279              | 0.0001  |
| 0.5223   | 0.0008        | 0.5239              | 0.1   |
| 0.5799   | 0.0009        | 0.5817              | 0.2   |
| 0.6339   | 0.0011        | 0.6361              | 0.3   |
| 0.6819   | 0.0011        | 0.6841              | 0.4   |
| 0.7272   | 0.0011        | 0.7294              | 0.5   |
| 0.7694   | 0.0011        | 0.7716              | 0.6   |
| 0.8067   | 0.0012        | 0.8091              | 0.7   |
| 0.8461   | 0.0011        | 0.8483              | 0.8   |
| 0.8764   | 0.0013        | 0.8790              | 0.9   |
| 0.9061   | 0.0014        | 0.9089              | 1.0   |

**Table 6.4-2**  
**Results for the WE 14x14 MOX Fuel Assembly**  
 (Continued)

| Normal Operating Condition: External Moderator Density Varying Assuming the Inward Assembly Position |               |                     |   |
|--|---------------|---------------------|---|
| $K_{eff}$  | $\pm 1\sigma$ | $K_{eff} + 2\sigma$ | External Moderator (H <sub>2</sub> O) Density, (g/cc) |
| 0.9087   | 0.0012        | 0.9111              | 0.0001 g/cc   |
| 0.9068   | 0.0013        | 0.9094              | 0.05 g/cc   |
| 0.9058   | 0.0013        | 0.9084              | 0.1 g/cc  |
| 0.9062   | 0.0013        | 0.9088              | 0.2 g/cc  |
| 0.9065   | 0.0012        | 0.9089              | 0.3 g/cc  |
| 0.9071   | 0.0013        | 0.9097              | 0.4 g/cc  |
| 0.9047   | 0.0012        | 0.9071              | 0.5 g/cc  |
| 0.9077   | 0.0013        | 0.9103              | 0.6 g/cc  |
| 0.9067   | 0.0012        | 0.9091              | 0.7 g/cc  |
| 0.9052   | 0.0012        | 0.9076              | 0.8 g/cc  |
| 0.9073   | 0.0012        | 0.9097              | 0.9 g/cc  |
| 0.9069   | 0.0014        | 0.9097              | 1.0 g/cc  |

| Hypothetical Accident Condition: Internal Moderator Density Varying Assuming the Inward Assembly Position |               |                     |   |
|---|---------------|---------------------|---|
| $K_{eff}$   | $\pm 1\sigma$ | $K_{eff} + 2\sigma$ | Internal Moderator (H <sub>2</sub> O) Density, (g/cc) |
| 0.4276  | 0.0005        | 0.4286              | 0.0001  |
| 0.4856  | 0.0005        | 0.4866              | 0.05  |
| 0.5217  | 0.0007        | 0.5231              | 0.1   |
| 0.5792  | 0.0009        | 0.5810              | 0.2   |
| 0.6326  | 0.0009        | 0.6344              | 0.3   |
| 0.6836  | 0.0011        | 0.6858              | 0.4   |
| 0.7290  | 0.0010        | 0.7310              | 0.5   |
| 0.7691  | 0.0012        | 0.7715              | 0.6   |
| 0.8086  | 0.0012        | 0.8110              | 0.7   |
| 0.8426  | 0.0011        | 0.8448              | 0.8   |
| 0.8775  | 0.0011        | 0.8797              | 0.9   |
| 0.9070  | 0.0011        | 0.9092              | 1.0   |

**Table 6.4-2**  
**Results for the WE 14x14 MOX Fuel Assembly**  
(Concluded)

| Hypothetical Accident Condition: External Moderator Density Varying Assuming the Inward Assembly Position |               |                     |   |
|---|---------------|---------------------|---|
| $K_{eff}$   | $\pm 1\sigma$ | $K_{eff} + 2\sigma$ | External Moderator ( $H_2O$ ) Density, (g/cc) |
| 0.9054  | 0.0014        | 0.9082              | 0.0001  |
| 0.9071  | 0.0012        | 0.9095              | 0.05  |
| 0.9061  | 0.0014        | 0.9089              | 0.1   |
| 0.9056  | 0.0013        | 0.9082              | 0.2   |
| 0.9071  | 0.0011        | 0.9093              | 0.3   |
| 0.9057  | 0.0012        | 0.9081              | 0.4   |
| 0.9086  | 0.0011        | 0.9108              | 0.5   |
| 0.9065  | 0.0011        | 0.9087              | 0.6   |
| 0.9047  | 0.0012        | 0.9071              | 0.7   |
| 0.9072  | 0.0012        | 0.9096              | 0.8   |
| 0.9063  | 0.0011        | 0.9085              | 0.9   |
| 0.9070  | 0.0011        | 0.9092              | 1.0   |

**Table 6.4-3**  
**Results for the Damaged Fuel Assemblies**

**Variation of the Rod Pitch Study**

| $K_{eff}$ | 1 sigma | $K_{eff} + 2 \text{ sigma}$ | Rod Pitch (inches) |
|-----------|---------|-----------------------------|--------------------|
| 0.6366    | 0 0010  | 0.6385                      | 0.422              |
| 0.6719    | 0.0013  | 0.6744                      | 0.440              |
| 0.7462    | 0.0010  | 0.7482                      | 0.480              |
| 0.8101    | 0.0012  | 0.8126                      | 0.520              |
| 0.8571    | 0.0011  | 0.8593                      | 0.556              |
| 0.8843    | 0 0011  | 0.8865                      | 0.580              |
| 0.9118    | 0.0011  | 0.9139                      | 0.610              |
| 0.9332    | 0.0011  | 0.9354                      | 0.652              |

| $K_{eff}$ | 1 sigma | $K_{eff} + 2 \text{ sigma}$ |  |
|-----------|---------|-----------------------------|--|
| 0.8559    | 0.0011  | 0 8580                      |  |
| 0.8608    | 0.0014  | 0.8635                      |  |
| 0.8647    | 0.0013  | 0.8673                      |  |
| 0.8642    | 0.0012  | 0 8665                      |  |
| 0.8576    | 0.0010  | 0.8597                      |  |

| $K_{eff}$ | 1 sigma | $K_{eff} + 2 \text{ sigma}$ |  |
|-----------|---------|-----------------------------|--|
| 0.8562    | 0.0012  | 0.8585                      |  |
| 0.8584    | 0.0011  | 0.8607                      |  |
| 0.8594    | 0.0013  | 0.8620                      |  |

**Table 6.4-3**  
**Results for the Damaged Fuel Assemblies**

(Concluded)

**Internal Moderator Density Varying for Most Reactive Rod Pitch Case**

| $K_{eff}$ | 1 sigma | $K_{eff} + 2 \text{ sigma}$ | Internal Moderator (H <sub>2</sub> O)<br>Density, g/cc |
|-----------|---------|-----------------------------|--|
| 0.4061    | 0.0004  | 0.4070                      | 0.0001   |
| 0.4821    | 0.0008  | 0.4836                      | 0.05   |
| 0.5285    | 0.0007  | 0.5298                      | 0.10   |
| 0.6097    | 0.0010  | 0.6116                      | 0.20   |
| 0.6786    | 0.0010  | 0.6805                      | 0.30   |
| 0.7363    | 0.0010  | 0.7383                      | 0.40   |
| 0.7852    | 0.0012  | 0.7875                      | 0.50   |
| 0.8236    | 0.0011  | 0.8257                      | 0.60   |
| 0.8583    | 0.0013  | 0.8610                      | 0.70   |
| 0.8872    | 0.0011  | 0.8895                      | 0.80   |
| 0.9119    | 0.0012  | 0.9143                      | 0.90   |
| 0.9332    | 0.0011  | 0.9354                      | 1.00   |

**External Moderator Density Varying for Most Reactive Rod Pitch Case**

| $K_{eff}$ | 1 sigma | $K_{eff} + 2 \text{ sigma}$ | External Moderator (H <sub>2</sub> O)<br>Density, g/cc |
|-----------|---------|-----------------------------|--|
| 0.9333    | 0.0012  | 0.9356                      | 0.0001   |
| 0.9319    | 0.0011  | 0.9340                      | 0.05   |
| 0.9336    | 0.0011  | 0.9358                      | 0.10   |
| 0.9305    | 0.0011  | 0.9327                      | 0.20   |
| 0.9329    | 0.0013  | 0.9355                      | 0.30   |
| 0.9323    | 0.0012  | 0.9347                      | 0.40   |
| 0.9316    | 0.0012  | 0.9340                      | 0.50   |
| 0.9328    | 0.0010  | 0.9348                      | 0.60   |
| 0.9319    | 0.0013  | 0.9345                      | 0.70   |
| 0.9340    | 0.0014  | 0.9368                      | 0.80   |
| 0.9340    | 0.0012  | 0.9365                      | 0.90   |
| 0.9330    | 0.0014  | 0.9358                      | 1.00   |

**Table 6.4-4**  
**Bounding Criticality Analysis Analyzed for 4.05 weight % <sup>235</sup>U**

**Damaged Fuel Assemblies with External Moderator Density Varying for  
Most Reactive Rod Pitch Case**

| $K_{eff}$ | +/- 1 $\sigma$ | $K_{eff} + 2\sigma$ | External Moderator (H <sub>2</sub> O)<br>Density, g/cc |
|-----------|----------------|---------------------|--|
| 0.9348    | 0.0013         | 0.9374              | 0.0001   |
| 0.9364    | 0.0012         | 0.9389              | 0.05   |
| 0.9341    | 0.0012         | 0.9365              | 0.10   |
| 0.9365    | 0.0012         | 0.9389              | 0.20   |
| 0.9348    | 0.0013         | 0.9374              | 0.30   |
| 0.9364    | 0.0013         | 0.9390              | 0.40   |
| 0.9338    | 0.0011         | 0.9360              | 0.50   |
| 0.9362    | 0.0012         | 0.9386              | 0.60   |
| 0.9368    | 0.0012         | 0.9392              | 0.70   |
| 0.9365    | 0.0012         | 0.9389              | 0.80   |
| 0.9345    | 0.0012         | 0.9369              | 0.90   |
| 0.9354    | 0.0011         | 0.9376              | 1.00   |

**Table 6.4-5**  
**Clad OD Sensitivity Evaluation**

| Fuel Clad OD: 4.05 wt.% U-235 Fuel Centered In Guide Tube |                |                     |                                  |
|---|----------------|---------------------|----------------------------------|
| $K_{eff}$   | +/- 1 $\sigma$ | $K_{eff} + 2\sigma$ | Clad OD<br>(inches) <sup>1</sup> |
| 0.8645  | 0.0011         | 0.8667              | 0.415                            |
| 0.8653  | 0.0013         | 0.8679              | 0.418                            |
| 0.8640  | 0.0013         | 0.8666              | 0.420                            |
| 0.8625  | 0.0013         | 0.8651              | 0.422                            |
| 0.8646  | 0.0012         | 0.8670              | 0.424                            |
| 0.8642  | 0.0012         | 0.8666              | 0.426                            |
| 0.8631  | 0.0012         | 0.8655              | 0.429                            |

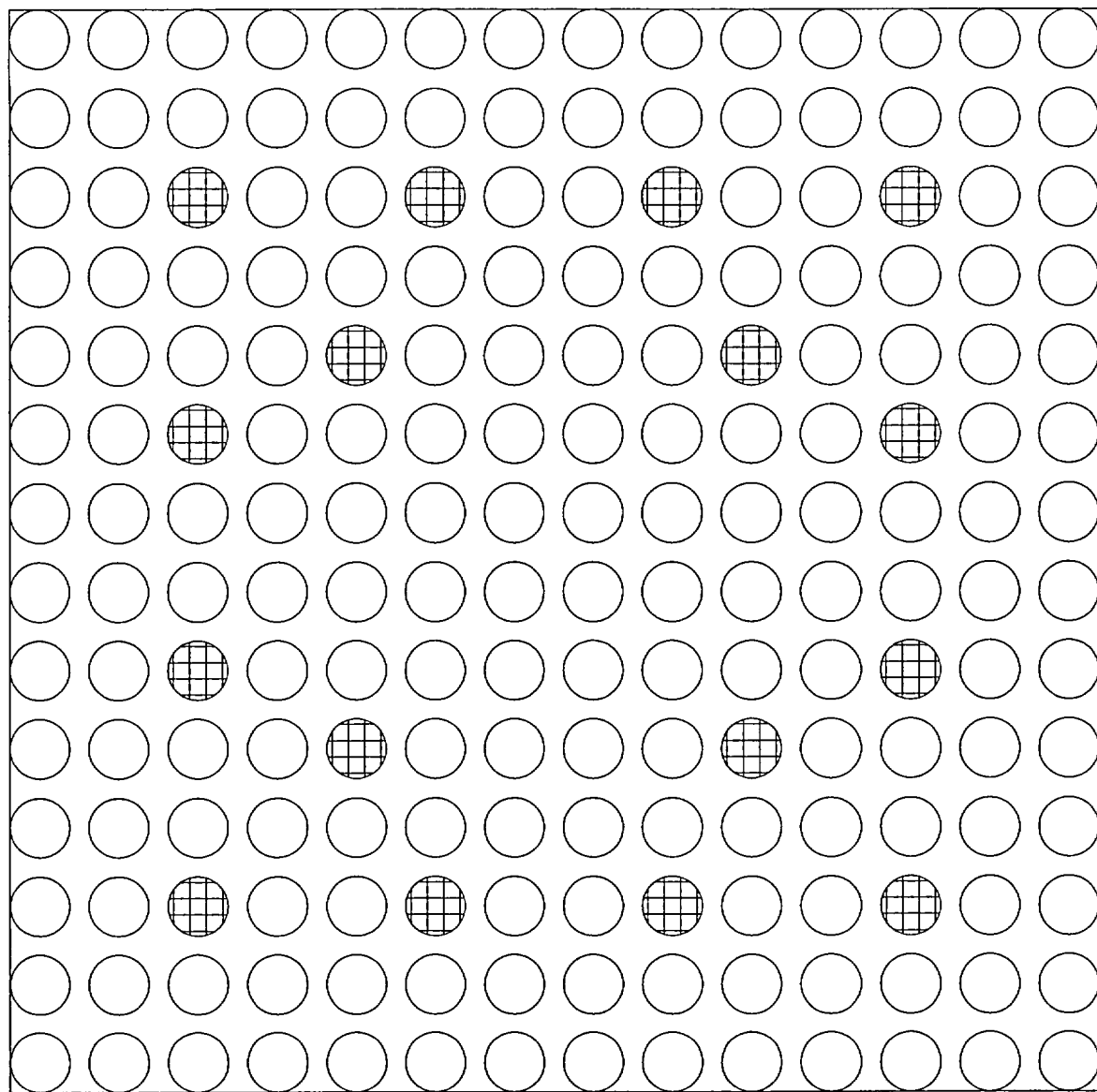
1. Min. clad thickness is used for this evaluation.

**Table 6.4-6**  
**Clad Thickness Sensitivity Evaluation**

| $K_{eff}$ | $\pm 1\sigma$ | $K_{eff} + 2\sigma$ | Clad OD (inches) | Clad ID |
|-----------|---------------|---------------------|------------------|---------|
| 0.8631    | 0.0012        | 0.8654              | 0.429            | .3976   |
| 0.8599    | 0.0012        | 0.8623              | 0.429            | .3970   |
| 0.8591    | 0.0013        | 0.8617              | 0.429            | .3964   |
| 0.8588    | 0.0011        | 0.8610              | 0.429            | .3960   |
| 0.8575    | 0.0013        | 0.8602              | 0.429            | .3954   |
| 0.8563    | 0.0011        | 0.8584              | 0.429            | .3948   |
| 0.8559    | 0.0012        | 0.8583              | 0.429            | .3944   |

**Table 6.4-7**  
**Pellet Diameter Sensitivity Evaluation**

| $K_{eff}$ | $\pm 1\sigma$ | $K_{eff} + 2\sigma$ | Pellet OD (inches) |
|-----------|---------------|---------------------|--------------------|
| 0.8626    | 0.0010        | 0.8646              | 0.3831             |
| 0.8610    | 0.0010        | 0.8631              | 0.3833             |
| 0.8619    | 0.0012        | 0.8642              | 0.3834             |
| 0.8630    | 0.0012        | 0.8653              | 0.3836             |
| 0.8628    | 0.0013        | 0.8655              | 0.3838             |
| 0.8621    | 0.0013        | 0.8647              | 0.3839             |
| 0.8615    | 0.0011        | 0.8638              | 0.3841             |



F5412

*Guide Tube**4.0 Weight % Fuel*

**Figure 6.4-1**  
**Rod Pitch Study: Figure Shows Maximum Rod Pitch Allowed**



**Figure 6.4-2**  
**Single-Ended Rod Shear Example**

**Figure 6.4-3**  
**Double-Ended Rod Shear Example**

## 6.5 Critical Benchmark Experiments

### 6.5.1 Benchmark Experiments and Applicability

A series of 122 benchmark experiments were simulated in calculations with the SCALE 4.4 PC/CSAS25 package [6.3] using the 44-group cross-section library. 110 of these calculations were with uranium oxide fuel, while twelve were with mixed uranium/plutonium MOX fuel.

The benchmark problems used in this verification are representative of benchmarks of commercial light water reactor (LWR) fuels with the following characteristics:

- A. water moderation
- B. boron neutron absorbers
- C. unirradiated light water reactor type fuel (no fission products or “burnup credit”)
- D. close reflection
- E. near room temperature (vs. reactor operating temperature)
- F. Uranium oxide and MOX fuels.

Verification and validation (V&V) of the software is performed in accordance with QA program requirements (see Chapter 13). Sample cases are defined in the V&V report which are run prior to performance of an analysis on a new computer hardware configuration to assure consistency with the hardware used for V&V and benchmarking.

Criticality codes are verified by comparing benchmark calculations to actual critical benchmark experiments. The difference between the calculated reactivity and the experimental reactivity is referred to as ‘calculational’ bias. This bias may be a function of system parameters such as fuel lattice separation, fuel enrichment, neutron absorber properties, reflector properties, or fuel/moderator volume ratio; or, there may be no specific correlation with system parameters. The benchmark data used for determination of the USL is provided in Table 6.5-1. The set of criticality experiments used as benchmarks are representative of the composition, configuration, and nuclear characteristics of the system modeled. Eight parameters were selected in order to demonstrate the applicability of the SCALE 44-group ENDF/B-V cross-section library for the range of conditions spanned by the calculation models. The results of these evaluations are provided in Table 6.5-2. Only those experiments with the parameter in question were used to determine the USL for that parameter. The methodology used to calculate the USL is based on NUREG/CR-6361 [6.6], USL method 1. USL-1 applies a statistical calculation of the bias and its uncertainty plus an administrative margin ( $0.05 \Delta k$ ) to the linear fit of results of the experimental benchmark data developed. The USL from the data set with the best correlation is used as the acceptance criteria for subsequent criticality evaluations. Since there was not a strong correlation for any of the data sets, i.e., the correlation was essentially random and the lowest possible USL-1 result was used as the USL.

The uncertainty due to modeling approximations does not impact the calculated  $k_{eff}$ . Worst case tolerances (as specified in the design drawings presented in Chapter 1) are used in the analysis to

maximize  $k_{\text{eff}}$ . Only the tolerances of those dimensions that had a positive effect on  $K_{\text{eff}}$  were included in the SCALE geometry models.

#### 6.5.1.1 Uranium Oxide Fuel Assemblies

The 110 uranium oxide experiments were chosen to model a wide range of uranium enrichments, fuel pin pitches, assembly separation, concentration of soluble boron and control elements in order to test the codes ability to accurately calculate  $k_{\text{eff}}$ . These experiments are discussed in detail in Reference [6.6]. The input decks were in general taken from Reference [6.6], however each input deck was modified to be consistent with use of CSAS25. The case ID names are identical to those used in Reference [6.6].

#### 6.5.1.2 MOX Fuel Assemblies

In order to verify and validate the CSAS25 module for MOX fuel; twelve additional critical benchmark experiments were included in the evaluation. These experiments are discussed in Reference [6.6]. The input decks for the twelve MOX cases were in general taken from Reference [6.6], however each input deck was modified to be consistent with use of CSAS25. The case ID names are identical to those used in Reference [6.6].

The MOX experiments include variations on fuel rod arrangement, fuel enrichment (both uranium and plutonium), fuel rod pitch, fuel rod diameter, fuel-to-moderator ratio, absorber materials and soluble boron concentration.

#### 6.5.2 Results of the Benchmark Calculations

A summary of all of the pertinent parameters for each experiment along with the results of each case is included in Table 6.5-1. The best correlation (linear regression correlation for each parameter vs.  $k_{\text{eff}}$ ) is observed for fuel assembly separation distance, with a correlation of 0.67. All other parameters show much lower correlation ratios indicating no real correlation. All parameters were evaluated for trends and to determine the most conservative USL. Since there was no observable correlation, the worst case USL was selected for the identified parameters.

The USL is calculated in accordance to NUREG/CR-6361 [6.6]. USL Method 1 (USL-1) applies a statistical calculation of the bias and its uncertainty plus an administrative margin (0.05) to the linear fit of results of the experimental benchmark data. The basis for the administrative margin is from Reference [6.7]. Results from the USL evaluation are presented in Table 6.5-2.

The criticality evaluation presented here used the same cross section library, fuel materials and similar material/geometry options that were used in the 122 benchmark calculations as shown in Table 6.5-3. The modeling techniques and the applicable parameters listed in Table 6.5-3 for the actual criticality evaluations fall within the range of those addressed by the benchmarks in Table 6.5-2. The results from the comparisons of physical parameters of each of the fuel assembly types to the applicable USL value are presented in Table 6.5-4. The minimum value of the USL-1 was determined to be 0.9401 based on comparisons to the most limiting assembly parameters.

**Table 6.5-1**  
**Benchmark Results**

| Run ID   | U Enrich<br>Wt% | Pu Enrich<br>Wt% | Pitch (cm) | H <sub>2</sub> O/fuel<br>volume | Separation of<br>assemblies<br>(cm) | AEG     | Boron Wt% | B-10 Areal<br>Density<br>(g/cm <sup>2</sup> ) | k <sub>eff</sub> | 1σ     |
|----------|-----------------|------------------|------------|---------------------------------|-------------------------------------|---------|-----------|---|------------------|--------|
| B1645SO1 | 2.46            |                  | 1.41       | 1.015                           |                                     | 32.8194 |           |   | 0.9967           | 0.0009 |
| B1645SO2 | 2.46            |                  | 1.41       | 1.015                           |                                     | 32.7584 |           |   | 1.0002           | 0.0011 |
| BW1231B1 | 4.02            |                  | 1.511      | 1.139                           |                                     | 31.1427 |           |   | 0.9966           | 0.0012 |
| BW1231B2 | 4.02            |                  | 1.511      | 1.139                           |                                     | 29.8854 |           |   | 0.9972           | 0.0009 |
| BW1273M  | 2.46            |                  | 1.511      | 1.376                           |                                     | 32.2106 |           |   | 0.9965           | 0.0009 |
| BW1484A1 | 2.46            |                  | 1.636      | 1.841                           | 1.636                               | 34.5304 | 1.6140    |   | 0.9962           | 0.0010 |
| BW1484A2 | 2.46            |                  | 1.636      | 1.841                           | 4.908                               | 35.1629 | 0.1000    |   | 0.9931           | 0.0010 |
| BW1484B1 | 2.46            |                  | 1.636      | 1.841                           |                                     | 33.9421 |           |   | 0.9979           | 0.0010 |
| BW1484B2 | 2.46            |                  | 1.636      | 1.841                           | 1.636                               | 34.5820 |           |   | 0.9955           | 0.0012 |
| BW1484B3 | 2.46            |                  | 1.636      | 1.841                           | 4.908                               | 35.2609 |           |   | 0.9969           | 0.0011 |
| BW1484C1 | 2.46            |                  | 1.636      | 1.841                           | 1.636                               | 34.6463 |           |   | 0.9931           | 0.0011 |
| BW1484C2 | 2.46            |                  | 1.636      | 1.841                           | 4.908                               | 35.2422 |           |   | 0.9939           | 0.0012 |
| BW1484S1 | 2.46            |                  | 1.636      | 1.841                           | 1.636                               | 34.5105 |           |   | 1.0001           | 0.0010 |
| BW1484S2 | 2.46            |                  | 1.636      | 1.841                           | 1.636                               | 34.5569 |           |   | 0.9992           | 0.0010 |
| BW1484SL | 2.46            |                  | 1.636      | 1.841                           | 6.544                               | 35.4151 |           |   | 0.9935           | 0.0011 |
| BW1645S1 | 2.46            |                  | 1.209      | 0.383                           | 1.778                               | 30.1040 |           |   | 0.9990           | 0.0010 |
| BW1645S2 | 2.46            |                  | 1.209      | 0.383                           | 1.778                               | 29.9961 |           |   | 1.0037           | 0.0011 |
| BW1810F  | 2.46            |                  | 1.636      | 1.841                           |                                     | 33.9556 |           |   | 1.0031           | 0.0011 |
| BW1810G  | 2.46            |                  | 1.636      | 1.841                           |                                     | 32.9409 |           |   | 0.9973           | 0.0011 |
| BW1810H  | 2.46            |                  | 1.636      | 1.841                           |                                     | 32.9420 |           |   | 0.9972           | 0.0011 |
| BW1810J  | 2.46            |                  | 1.636      | 1.841                           |                                     | 33.1403 |           |   | 0.9983           | 0.0011 |
| EPRU65   | 2.35            |                  | 1.562      | 1.196                           |                                     | 33.9106 |           |   | 0.9960           | 0.0011 |
| EPRU65B  | 2.35            |                  | 1.562      | 1.196                           |                                     | 33.4013 |           |   | 0.9993           | 0.0012 |
| EPRU75   | 2.35            |                  | 1.905      | 2.408                           |                                     | 35.8671 |           |   | 0.9958           | 0.0010 |
| EPRU75B  | 2.35            |                  | 1.905      | 2.408                           |                                     | 35.3043 |           |   | 0.9996           | 0.0010 |
| EPRU87   | 2.35            |                  | 2.21       | 3.687                           |                                     | 36.6129 |           |   | 1.0007           | 0.0011 |
| EPRU87B  | 2.35            |                  | 2.21       | 3.687                           |                                     | 36.3499 |           |   | 1.0007           | 0.0011 |
| NSE71SQ  | 4.74            |                  | 1.26       | 1.823                           |                                     | 33.7610 |           |   | 0.9979           | 0.0012 |
| NSE71W1  | 4.74            |                  | 1.26       | 1.823                           |                                     | 34.0129 |           |   | 0.9988           | 0.0013 |
| NSE71W2  | 4.74            |                  | 1.26       | 1.823                           |                                     | 36.3037 |           |   | 0.9957           | 0.0010 |
| P2438BA  | 2.35            |                  | 2.032      | 2.918                           | 5.05                                | 36.2277 | 28.7000   | 0.0670  | 0.9979           | 0.0013 |
| P2438SLG | 2.35            |                  | 2.032      | 2.918                           | 8.39                                | 36.2889 |           |   | 0.9986           | 0.0012 |
| P2438SS  | 2.35            |                  | 2.032      | 2.918                           | 6.88                                | 36.2705 |           |   | 0.9974           | 0.0011 |
| P2438ZR  | 2.35            |                  | 2.032      | 2.918                           | 8.79                                | 36.2840 |           |   | 0.9987           | 0.0010 |
| P2615BA  | 4.31            |                  | 2.54       | 3.883                           | 6.72                                | 35.7286 | 28.7000   | 0.0670  | 1.0019           | 0.0014 |
| P2615SS  | 4.31            |                  | 2.54       | 3.883                           | 8.58                                | 35.7495 |           |   | 0.9952           | 0.0015 |
| P2615ZR  | 4.31            |                  | 2.54       | 3.883                           | 10.92                               | 35.7700 |           |   | 0.9977           | 0.0014 |
| P2827L1  | 2.35            |                  | 2.032      | 2.918                           | 13.27                               | 36.2526 |           |   | 1.0057           | 0.0011 |
| P2827L2  | 2.35            |                  | 2.032      | 2.918                           | 11.25                               | 36.2908 |           |   | 0.9999           | 0.0012 |

**Table 6.5-1**  
**Benchmark Results**

(Continued)

| Run ID   | U Enrich<br>Wt% | Pu Enrich<br>Wt% | Pitch (cm) | H <sub>2</sub> O/fuel<br>volume | Separation of<br>assemblies<br>(cm) | AEG     | Boron Wt% | B-10 Areal<br>Density<br>(g/cm <sup>2</sup> ) | k <sub>eff</sub> | 1σ     |
|----------|-----------------|------------------|------------|---------------------------------|-------------------------------------|---------|-----------|---|------------------|--------|
| P2827L3  | 4 31            |                  | 2 54       | 3 883                           | 20 78                               | 35 6766 |           |   | 1 0092           | 0 0012 |
| P2827L4  | 4 31            |                  | 2 54       | 3 883                           | 19 04                               | 35 7131 |           |   | 1 0073           | 0 0012 |
| P2827SLG | 2 35            |                  | 2 032      | 2 918                           | 8 31                                | 36 3037 |           |   | 0 9957           | 0 0010 |
| P3314BA  | 4 31            |                  | 1 892      | 1 6                             | 2 83                                | 33 1881 | 28 7000   | 0 0669  | 0 9988           | 0 0012 |
| P3314BC  | 4 31            |                  | 1 892      | 1 6                             | 2 83                                | 33 2284 | 31 8800   | 0 0262  | 0 9992           | 0 0012 |
| P3314BF1 | 4 31            |                  | 1 892      | 1 6                             | 2 83                                | 33 2505 | 32 7400   | 0 0236  | 1 0037           | 0 0013 |
| P3314BF2 | 4 31            |                  | 1 892      | 1 6                             | 2 83                                | 33 2184 | 32 7400   | 0 0471  | 1 0009           | 0 0013 |
| P3314BS1 | 2 35            |                  | 1 684      | 1 6                             | 3 86                                | 34 8594 | 1 0500    | 0 0045  | 0 9956           | 0 0013 |
| P3314BS2 | 2 35            |                  | 1 684      | 1 6                             | 3 46                                | 34 8356 | 1 6200    | 0 0069  | 0 9949           | 0 0010 |
| P3314BS3 | 4 31            |                  | 1 892      | 1 6                             | 7 23                                | 33 4247 | 1 0500    | 0 0045  | 0 9970           | 0 0013 |
| P3314BS4 | 4 31            |                  | 1 892      | 1 6                             | 6 63                                | 33 4162 | 1 6200    | 0 0069  | 0 9998           | 0 0012 |
| P3314SLG | 4 31            |                  | 1 892      | 1 6                             | 2 83                                | 34 0198 |           |   | 0 9974           | 0 0012 |
| P3314SS1 | 4 31            |                  | 1 892      | 1 6                             | 2 83                                | 33 9601 |           |   | 0 9999           | 0 0012 |
| P3314SS2 | 4 31            |                  | 1 892      | 1 6                             | 2 83                                | 33 7755 |           |   | 1 0022           | 0 0012 |
| P3314SS3 | 4 31            |                  | 1 892      | 1 6                             | 2 83                                | 33 8904 |           |   | 0 9992           | 0 0013 |
| P3314SS4 | 4 31            |                  | 1 892      | 1 6                             | 2 83                                | 33 7625 |           |   | 0 9958           | 0 0011 |
| P3314SS5 | 2 35            |                  | 1 684      | 1 6                             | 7 8                                 | 34 9531 |           |   | 0 9949           | 0 0013 |
| P3314SS6 | 4 31            |                  | 1 892      | 1 6                             | 10 52                               | 33 5333 |           |   | 1 0020           | 0 0011 |
| P3314W1  | 4 31            |                  | 1 892      | 1 6                             |                                     | 34 3994 |           |   | 1 0024           | 0 0013 |
| P3314W2  | 2 35            |                  | 1 684      | 1 6                             |                                     | 35 2167 |           |   | 0 9969           | 0 0011 |
| P3314ZR  | 4 31            |                  | 1 892      | 1 6                             | 2 83                                | 33 9954 |           |   | 0 9971           | 0 0013 |
| P3602BB  | 4 31            |                  | 1 892      | 1 6                             | 8 3                                 | 33 3221 | 30 3600   | 0 0408  | 1 0029           | 0 0013 |
| P3602BS1 | 2 35            |                  | 1 684      | 1 6                             | 4 8                                 | 34 7750 | 1.0500    | 0 0045  | 1 0027           | 0 0012 |
| P3602BS2 | 4 31            |                  | 1 892      | 1 6                             | 9 83                                | 33 3679 | 1.0500    | 0 0045  | 1 0039           | 0 0012 |
| P3602N11 | 2 35            |                  | 1 684      | 1 6                             | 8 98                                | 34 7438 |           |   | 1 0023           | 0 0012 |
| P3602N12 | 2 35            |                  | 1 684      | 1 6                             | 9 58                                | 34 8391 |           |   | 1 0030           | 0 0012 |
| P3602N13 | 2 35            |                  | 1 684      | 1 6                             | 9 66                                | 34 9337 |           |   | 1 0013           | 0 0012 |
| P3602N14 | 2 35            |                  | 1 684      | 1 6                             | 8 54                                | 35 0282 |           |   | 0 9974           | 0 0013 |
| P3602N21 | 2 35            |                  | 2 032      | 2 918                           | 11 2                                | 36 2821 |           |   | 0 9987           | 0 0011 |
| P3602N22 | 2 35            |                  | 2 032      | 2 918                           | 10 36                               | 36 1896 |           |   | 1.0025           | 0 0011 |
| P3602N31 | 4 31            |                  | 1 892      | 1 6                             | 14 87                               | 33 2094 |           |   | 1 0057           | 0 0013 |
| P3602N32 | 4 31            |                  | 1 892      | 1 6                             | 15 74                               | 33 3067 |           |   | 1 0093           | 0 0012 |
| P3602N33 | 4 31            |                  | 1 892      | 1 6                             | 15 87                               | 33 4174 |           |   | 1.0107           | 0 0012 |
| P3602N34 | 4 31            |                  | 1 892      | 1 6                             | 15 84                               | 33 4683 |           |   | 1 0045           | 0 0013 |
| P3602N35 | 4 31            |                  | 1 892      | 1 6                             | 15 45                               | 33 5185 |           |   | 1.0013           | 0 0012 |
| P3602N36 | 4 31            |                  | 1 892      | 1 6                             | 13 82                               | 33 5855 |           |   | 1 0004           | 0 0014 |
| P3602N41 | 4 31            |                  | 2 54       | 3 883                           | 12 89                               | 35 5276 |           |   | 1 0109           | 0 0013 |
| P3602N42 | 4 31            |                  | 2 54       | 3 883                           | 14 12                               | 35 6695 |           |   | 1 0071           | 0 0014 |
| P3602N43 | 4 31            |                  | 2 54       | 3 883                           | 12 44                               | 35 7542 |           |   | 1 0053           | 0 0015 |
| P3602SS1 | 2 35            |                  | 1 684      | 1 6                             | 8 28                                | 34 8701 |           |   | 1 0025           | 0 0013 |
| P3602SS2 | 4 31            |                  | 1 892      | 1 6                             | 13 75                               | 33 4202 |           |   | 1 0035           | 0 0012 |
| P3926L1  | 2 35            |                  | 1 684      | 1 6                             | 10 06                               | 34 8519 |           |   | 1 0000           | 0 0011 |
| P3926L2  | 2 35            |                  | 1 684      | 1 6                             | 10 11                               | 34 9324 |           |   | 1 0017           | 0 0011 |
| P3926L3  | 2 35            |                  | 1 684      | 1 6                             | 8 5                                 | 35 0641 |           |   | 0 9949           | 0 0012 |
| P3926L4  | 4 31            |                  | 1 892      | 1 6                             | 17 74                               | 33 3243 |           |   | 1 0074           | 0 0014 |
| P3926L5  | 4 31            |                  | 1 892      | 1 6                             | 18.18                               | 33 4074 |           |   | 1 0057           | 0 0013 |
| P3926L6  | 4 31            |                  | 1 892      | 1 6                             | 17 43                               | 33 5246 |           |   | 1 0046           | 0 0013 |
| P3926SL1 | 2 35            |                  | 1 684      | 1 6                             | 6 59                                | 33 4737 |           |   | 0 9995           | 0 0012 |
| P3926SL2 | 4 31            |                  | 1 892      | 1 6                             | 12.79                               | 33 5776 |           |   | 1 0007           | 0 0012 |

**Table 6.5-1**  
**Benchmark Results**  
(Concluded)


| Run ID      | U Enrich<br>Wt% | Pu Enrich<br>Wt% | Pitch (cm) | H <sub>2</sub> O/fuel<br>volume | Separation of<br>assemblies<br>(cm) | AEG     | Boron Wt% | B-10 Areal<br>Density<br>(g/cm <sup>2</sup> ) | k <sub>eff</sub> | 1σ     |
|-------------|-----------------|------------------|------------|---------------------------------|-------------------------------------|---------|-----------|---|------------------|--------|
| P4267B1     | 4.31            |                  | 1.8901     | 1.59                            |                                     | 31.8075 |           |   | 0.9990           | 0.0010 |
| P4267B2     | 4.31            |                  | 0.89       | 1.59                            |                                     | 31.5323 |           |   | 1.0033           | 0.0010 |
| P4267B3     | 4.31            |                  | 1.715      | 1.09                            |                                     | 30.9905 |           |   | 1.0050           | 0.0011 |
| P4267B4     | 4.31            |                  | 1.715      | 1.09                            |                                     | 30.5061 |           |   | 0.9996           | 0.0011 |
| P4267B5     | 4.31            |                  | 1.715      | 1.09                            |                                     | 30.1011 |           |   | 1.0004           | 0.0011 |
| P4267SL1    | 4.31            |                  | 1.89       | 1.59                            |                                     | 33.4737 |           |   | 0.9995           | 0.0012 |
| P4267SL2    | 4.31            |                  | 1.715      | 1.09                            |                                     | 31.9460 |           |   | 0.9988           | 0.0016 |
| P62FT231    | 4.31            |                  | 1.891      | 1.6                             | 5.19                                | 32.9196 | 35.6300   |   | 1.0012           | 0.0013 |
| P71F14F3    | 4.31            |                  | 1.891      | 1.6                             | 5.19                                | 32.8237 | 29.2200   |   | 1.0009           | 0.0014 |
| P71F14V3    | 4.31            |                  | 1.891      | 1.6                             | 5.19                                | 32.8597 | 29.2200   |   | 0.9972           | 0.0014 |
| P71F14V5    | 4.31            |                  | 1.891      | 1.6                             | 5.19                                | 32.8609 | 29.2200   |   | 0.9993           | 0.0013 |
| P71F214R    | 4.31            |                  | 1.891      | 1.6                             | 5.19                                | 32.8778 | 29.2200   |   | 0.9969           | 0.0012 |
| PAT80L1     | 4.74            |                  | 1.6        | 3.807                           | 4.9                                 | 35.0253 | 22.2000   | 0.0460  | 1.0012           | 0.0012 |
| PAT80L2     | 4.74            |                  | 1.6        | 3.807                           | 4.9                                 | 35.1136 | 22.2000   | 0.0460  | 0.9993           | 0.0015 |
| PAT80SS1    | 4.74            |                  | 1.6        | 3.807                           | 4.9                                 | 35.0045 | 22.2000   | 0.0460  | 0.9988           | 0.0013 |
| PAT80SS2    | 4.74            |                  | 1.6        | 3.807                           | 4.9                                 | 35.1072 | 22.2000   | 0.0460  | 0.9960           | 0.0013 |
| W3269SL1    | 2.72            |                  | 1.524      | 1.494                           |                                     | 33.3850 |           |   | 0.9981           | 0.0014 |
| W3269SL2    | 5.7             |                  | 1.422      | 1.93                            |                                     | 33.0910 |           |   | 1.0005           | 0.0013 |
| W3269W1     | 2.72            |                  | 1.524      | 1.494                           |                                     | 33.5114 |           |   | 0.9966           | 0.0014 |
| W3269W2     | 5.7             |                  | 1.422      | 1.93                            |                                     | 33.1680 |           |   | 1.0014           | 0.0014 |
| W3385SL1    | 5.74            |                  | 1.422      | 1.932                           |                                     | 33.2387 |           |   | 1.0009           | 0.0012 |
| W3385SL2    | 5.74            |                  | 2.012      | 5.067                           |                                     | 35.8818 |           |   | 0.9997           | 0.0013 |
| EPRI70UN    | 0.71            | 2                | 1.778      | 1.2                             |                                     | 31.6775 |           |   | 0.9983           | 0.0012 |
| EPRI70B     | 0.71            | 2                | 1.778      | 1.2                             |                                     | 30.9021 |           |   | 1.0009           | 0.0012 |
| EPRI87UN    | 0.71            | 2                | 2.2098     | 2.53                            |                                     | 33.3230 |           |   | 1.0096           | 0.0011 |
| EPRI87B     | 0.71            | 2                | 2.2098     | 2.53                            |                                     | 31.6775 |           |   | 0.9983           | 0.0012 |
| EPRI99UN    | 0.71            | 2                | 2.5146     | 3.64                            |                                     | 35.1817 |           |   | 1.0063           | 0.0011 |
| EPRI99B     | 0.71            | 2                | 2.5146     | 3.64                            |                                     | 34.4098 |           |   | 1.0095           | 0.0011 |
| SAXTON52    | 0.71            | 6.6              | 1.3208     | 1.68                            |                                     | 30.2980 |           |   | 1.0020           | 0.0014 |
| SAXTON56    | 0.71            | 6.6              | 1.4224     | 2.16                            |                                     | 31.4724 |           |   | 1.0010           | 0.0014 |
| SAXTON56B   | 0.71            | 6.6              | 1.4224     | 2.16                            |                                     | 31.0038 |           |   | 0.9994           | 0.0013 |
| SAXTN735    | 0.71            | 6.6              | 1.8669     | 4.7                             |                                     | 34.1848 |           |   | 1.0007           | 0.0016 |
| SATN792     | 0.71            | 6.6              | 2.01168    | 5.67                            |                                     | 34.6401 |           |   | 1.0026           | 0.0013 |
| SAXTN104    | 0.71            | 6.6              | 2.6416     | 10.75                           |                                     | 35.8333 |           |   | 1.0054           | 0.0014 |
| Correlation | 0.34            | -0.26            | 0.41       | 0.24                            | 0.67                                | -0.04   | 0.36      | 0.05  | N/A              | N/A    |

**Table 6.5-2**  
**USL-1 Results**

| Parameter                                  | Range of Applicability | USL-1  |
|--|------------------------|--------|
| U Enrichment (wt% U-235)                   | 2.4                    | 0.9422 |
|  | 2.8                    | 0.9428 |
|  | 3.3                    | 0.9434 |
|  | 3.8 – 5.7              | 0.9436 |
| Pu Enrichment (wt% Pu)                     | 2.0 – 6.6              | 0.9417 |
| Fuel Rod Pitch (cm)                        | 1.07                   | 0.9401 |
|  | 1.1                    | 0.9405 |
|  | 1.4                    | 0.9418 |
|  | 1.6                    | 0.9430 |
|  | 1.9 – 2.6              | 0.9436 |
| Water/Fuel Volume Ratio                    | 0.38                   | 0.9412 |
|  | 1.9                    | 0.9423 |
|  | 3.3 – 11               | 0.9423 |
| Assembly Separation (cm)                   | 1.6                    | 0.9409 |
|  | 4.4                    | 0.9425 |
|  | 7.1                    | 0.9440 |
|  | 9.8 – 21               | 0.9441 |
| Average Energy Group Causing Fission (AEG) | 30 – 37                | 0.9431 |
| B-10 Areal Density (g/cm <sup>2</sup> )    | 4.50E-3                | 0.9434 |
|  | 1.34E-2 – 2.23E-2      | 0.9435 |
|  | 3.12E-2                | 0.9436 |
|  | 4.02E-2 – 4.91E-2      | 0.9437 |
|  | 5.80E-2 – 6.69E-2      | 0.9438 |
| Boron Content (wt% B)                      | 0.1                    | 0.9421 |
|  | 5.2                    | 0.9425 |
|  | 10                     | 0.9429 |
|  | 15                     | 0.9433 |
|  | 20                     | 0.9437 |
|  | 25                     | 0.9441 |
|  | 31 – 36                | 0.9445 |



**Table 6.5-3**  
**Fuel Assembly Design Parameters Used in Criticality Benchmarks**

| Parameter                                  | WE 14x14           | MOX 14x14   |
|--|--------------------|---|
| Fuel Material -                            | UO <sub>2</sub>    | MOX   |
| U-enrichment (wt% U-235)                   | 4.05               |  |
| Pu-enrichment (wt% Pu)                     | 0.00               |   |
| Clad Material                              | Type 304 SS        |   |
| Fuel Rod Pitch (cm)                        | 1.4 (1.07 - 1.66)* | 1.4   |
| Water/Fuel Volume Ratio                    | 1.5 (0.3 - 2.5)*   | 1.6   |
| Assembly Separation (cm)                   | 2.5-4.2            | 2.5-4.2   |
| Average Energy Group Causing Fission (AEG) | 33 (34)*           | 32  |
| B-10 Areal Density (g/cm <sup>2</sup> )    | 0.019              | 0.019   |
| Absorber Material - B (wt %)               | 18.9               | 18.9  |

\* (Damaged fuel)

**Table 6.5-4**  
**Limiting Upper Subcritical Limit Based on Method 1 for the WE 14x14 SC Fuel**  
**Assemblies and the WE 14x14 MOX Fuel Assemblies**

| Parameter                               | WE 14x14 SC        | WE 14x14 MOX | Most Limiting USL-1 |
|---|--------------------|--------------|---------------------|
| U-Enrichment (weight % U-235)           | 4.05               |              | 0.9436              |
| Pu-enrichment (weight % Pu)             | 0.00               |              | 0.9417              |
| Fuel Rod Pitch (cm)                     | 1.4 (1.07 - 1.66)* | 1.4          | 0.9401              |
| Water/Fuel Volume Ratio                 | 1.5 (0.3 - 2.5)*   | 1.6          | 0.9412              |
| Assembly Separation (cm)                | 2.5 - 4.2          | 2.5 - 4.2    | 0.9409              |
| Average Energy Group Fission (AEG)      | 33 (34)*           | 32           | 0.9431              |
| B-10 Areal Density (g/cm <sup>2</sup> ) | 0.019              | 0.019        | 0.9434              |
| Absorber Material – B (wt. %)           | 18.9               | 18.9         | 0.9433              |

\*(Damaged fuel)

## 6.6 Supplemental Information

### 6.6.1 References

- [6.1] Code of Federal Regulations, Title 10, Part 72, "Licensing Requirements for the Independent Storage of Spent Nuclear Fuel and High-Level Radioactive Waste."
- [6.2] Code of Federal Regulations, Title 10, Part 71, "Packaging and Transportation of Radioactive Material."
- [6.3] "SCALE, A Modular Code System for Performing Standardized Computer Analyses for Licensing Evaluation", NUREG/CR-0200, Rev. 6 (ORNL/NUREG/CSD-2/R6), Vol. I-III, September 1998.
- [6.4] ANSI/ANS 57.2, Design Requirements for Light Water Reactor Spent Fuel Storage Facilities at Nuclear Power Plants, 1983.
- [6.5] ANS/ANSI-8.1, American National Standard for Nuclear Criticality Safety in Operations with Fissionable Materials Outside Reactors, 1983.
- [6.6] U.S. Nuclear Regulatory Commission, "Criticality Benchmark Guide for Light-Water-Reactor fuel in Transportation and Storage Packages," NUREG/CR-6361, ORNL-TM-13211, March 1997.
- [6.7] U.S. Nuclear Regulatory Commission, "Recommendations for Preparing the Criticality Safety Evaluation of Transportation Packages," NUREG/CR-5661, ORNL/TM-11936, April 1997.
- [6.8] Southern California Edison Specification S01-207-01.
- [6.9] J. J. Duderstadt and L. J. Hamilton, "Nuclear Reactor Analysis," John Wiley and Sons, 1976.
- [6.10] Burn, Reed R., "Boral™ Accelerated Radiation Aging Tests", Nuclear Reactor Laboratory, University of Michigan, Ann Arbor, Michigan, May 9, 1990.
- [6.11] American National Standards Institute, ANSI N14.5-1997, Leakage Tests on Packages for Shipment of Radioactive Materials.
- [6.12] *TN*, Safety Analysis Report for the NUHOMS® MP187 Multi-Purpose Cask, NUH-005, Revision 16, July 2002, USNRC Docket No. 71-9255.

## 6.6.2 KENO Input Files